AD_____

Award Number:
W81XWH-09-1-0457

TITLE:
Predicting the Toxicity of Adjuvant Breast Cancer Drug Combination Therapy

PRINCIPAL INVESTIGATOR:
Susan F Hudachek, MS, PhD

CONTRACTING ORGANIZATION:
Colorado State University
Fort Collins, CO 80523-0001

REPORT DATE:
September 2012

TYPE OF REPORT:
Revised Annual Summary

PREPARED FOR:
U.S. Army Medical Research and Materiel Command Fort Detrick, Maryland 21702-5012

DISTRIBUTION STATEMENT: **Approved for Public Release;**
Distribution Unlimited

The views, opinions and/or findings contained in this report are those of the author(s) and should not be construed as an official Department of the Army position, policy or decision unless so designated by other documentation.

REPORT DOCUMENTATION PAGE

Form Approved
OMB No. 0704-0188

1. REPORT DATE	**2. REPORT TYPE**	**3. DATES COVERED**
September 2012	Revised Annual Summary	1 September 2011 - 31 August 2012

4. TITLE AND SUBTITLE
Predicting the toxicity of adjuvant breast cancer drug combination therapy

5a. CONTRACT NUMBER

5b. GRANT NUMBER
W81XWH-09-1-0457

5c. PROGRAM ELEMENT NUMBER

6. AUTHOR(S)
Susan F Hudachek

5d. PROJECT NUMBER

5e. TASK NUMBER

5f. WORK UNIT NUMBER

7. PERFORMING ORGANIZATION NAME(S) AND ADDRESS(ES)
Colorado State University
Fort Collins, CO 80523-0001

8. PERFORMING ORGANIZATION REPORT NUMBER

9. SPONSORING / MONITORING AGENCY NAME(S) AND ADDRESS(ES)
U.S. Army Medical Research and Materiel Command
Fort Detrick, Maryland 21702-5012

10. SPONSOR/MONITOR'S ACRONYM(S)

11. SPONSOR/MONITOR'S REPORT NUMBER(S)

12. DISTRIBUTION / AVAILABILITY STATEMENT
Approved for Public Release; Distribution Unlimited

13. SUPPLEMENTARY NOTES

14. ABSTRACT
Purpose: Combination therapy is increasingly utilized for the treatment of metastatic breast cancer. However, co-administration of drugs, particularly agents that are substrates for or inhibitors of p-glycoprotein, can result in increased toxicity. As adverse tissue drug concentrations are not always exposed by plasma drug concentrations, we performed studies in mice to assess both the plasma and tissue levels of the cytotoxics docetaxel and doxorubicin when administered concomitantly with the p-glycoprotein substrate/inhibitor lapatinib. Both combinations are currently being investigated in clinical trials. Materials and Methods: Time course plasma and tissue distribution studies of concomitant lapatinib and docetaxel or doxorubicin were conducted in mice. Intravenous chemotherapy was administered one hour after the first intraperitoneal lapatinib dose. Both single and multiple dose lapatinib were evaluated. Samples were collected up to 12 and 48 hrs post docetaxel and doxorubicin administration, respectively, and drug concentrations were determined.
Results: In toxicologically significant tissues, combination lapatinib and docetaxel resulted in a 32.8% and 44.6% increase in intestinal docetaxel exposure after single and multiple dose lapatinib, respectively. The causative drug-drug interaction was likely mediated more by competitive inhibition of CYP3A4 metabolism than p-glycoprotein efflux.
Conclusion: Our mouse studies of combination dosing demonstrate that lapatinib, when dosed to achieve human equivalent plasma exposure in mice, did not significantly alter the plasma or tissue pharmacokinetics of doxorubicin but did increase exposure to docetaxel in the intestine, likely leading to enhanced toxicity. Thus, caution should be taken when docetaxel and lapatinib are administered together, particularly to patients with compromised CYP3A activity.

15. SUBJECT TERMS- lapatinib, doxorubicin, docetaxel, p-glycoprotein

16. SECURITY CLASSIFICATION OF:			**17. LIMITATION OF ABSTRACT**	**18. NUMBER OF PAGES**	**19a. NAME OF RESPONSIBLE PERSON**
					USAMRMC
a. REPORT	**b. ABSTRACT**	**c. THIS PAGE**			**19b. TELEPHONE NUMBER** *(include area code)*
U	U	U	UU		

Table Of Contents

Introduction

When drugs are given in combination, which is common practice in adjuvant breast cancer treatment, interactions can occur that alter an agent's pharmacokinetics (PKs) and pharmacodynamics (PDs) and potentiate the toxicity of the anti-cancer therapies. This is especially true for drugs that are substrates or inhibitors of P-glycoprotein (PGP), including docetaxel (DTX), doxorubicin (DOX) and lapatinib (LAP). The purpose of the subsequent work is to use physiologically-based pharmacokinetic (PBPK) modeling to determine the changes in both plasma and tissue PKs of DTX and DOX when administered in combination with LAP. PBPK models mathematically incorporate biochemical and physiological principles to determine the pharmacologic disposition of drugs in the body using compartments that represent specific organs or tissue groups. Once the PBPK models have been optimized in humans, variability in patient covariates and PBPK model parameters will be incorporated using Monte Carlo simulation and a virtual population will be created and validated. This population will then be used for population PK analyses to identify the patient covariates that contribute to the variability in the PK data when agents are given in combination. Once these sources of variability are determined, dosing adjustments can be made that will ultimately maximize efficacy and minimize toxicity of combination therapies.

Body

Specific Aim 1. Determine the PKs of LAP, DTX, DOX, combination LAP and DTX, and combination LAP and DOX in mice.

Task 1b. Obtain samples for PK analysis. Dose FVB mice with LAP, DTX, DOX, combination LAP and DTX, and combination DOX and LAP, sacrifice at pre-specified time points, and collect and store plasma and tissue samples. For this study, there will be a total of 600 FVB mice divided into 20 cohorts. In each cohort, there will be a total of 30 mice, as three mice will be sacrificed at each of ten time points.

Time course plasma and tissue distribution studies of concomitant lapatinib with docetaxel or doxorubicin were conducted in mice. Intravenous chemotherapy was administered one hour after the first intraperitoneal lapatinib dose. Both single and multiple dose lapatinib were evaluated. Samples were collected up to 12 and 48 hrs post docetaxel and doxorubicin administration, respectively. A detailed description of the pharmacokinetic study methodology can be found in the appended manuscript titled "Co-administration of lapatinib increases exposure to docetaxel but not doxorubicin in the small intestine of mice".

Task 1f. Analyze drug levels in collected samples. Using the samples from Task 1b and Task 1c, the concentration of drugs in the plasma and tissue samples will be determined. LAP and DTX levels will be analyzed using LC/MS/MS and DOX levels will be analyzed using HPLC with fluorescence detection.

Samples from the time course plasma and tissue distribution studies of concomitant lapatinib with docetaxel or doxorubicin conducted in mice were analyzed and drug concentrations were determined. A detailed description of the drug analysis methodology can be found in the appended manuscript titled "Co-administration of lapatinib increases exposure to docetaxel but not doxorubicin in the small intestine of mice".

Task 1g. Using the data from Task 1f, plasma and tissue drug concentration versus time data will be modeled by compartmental analysis and PK parameters will be calculated using SAAM II software, version 1.2.1 (Saam Institute, University of Washington).

Doxorubicin and docetaxel plasma and tissue concentrations were modeled by noncompartmental analysis. A detailed description of the modeling methodology can be found in the appended manuscript draft titled "Co-administration of lapatinib increases exposure to docetaxel but not doxorubicin in the small intestine of mice".

Research Results and Discussion

We have submitted a manuscript to the Journal of Pharmacokinetics and Pharmacodynamics (which has been accepted contingent on revisions) that includes the lapatinib biodistribution studies from Tasks 1b, 1f and 1g. A detailed description of the methods, results and analysis of these studies can be found in the appended manuscript draft titled "Physiologically based pharmacokinetic model of lapatinib developed in mice and scaled to humans".

Additionally, we have submitted a manuscript to Molecular Cancer Therapeutics regarding our mouse studies that investigated the combination dosing of lapatinib with docetaxel or doxorubicin. A detailed description of the methods, results and analysis of this work can be found in the appended manuscript titled "Co-administration of lapatinib increases exposure to docetaxel but not doxorubicin in the small intestine of mice".

Based on the work from the latter manuscript, lapatinib did not alter the pharmacokinetics of doxorubicin and docetaxel to the extent that we hypothesized this PGP substrate/inhibitor would. As detailed in the manuscript, the plasma and tissue pharmacokinetics of doxorubicin were unchanged by co-administration with lapatinib. However, concomitant lapatinib did increase docetaxel exposure in the intestine but not in plasma or any of the seven other tissues evaluated. Moving forward with this data to Specific Aim 2 was not feasible because we proposed to model differences seen when either docetaxel or doxorubicin was administered with a PGP substrate and/or inhibitor. Thus, to continue with Aim 2 and the

subsequent Aims that are dependent upon Aim 2, PGP needed to be altered such that there was a resultant PK difference in docetaxel or doxorubicin. To accomplish this, we could have used a more potent PGP inhibitor, like cyclosporin A, but this had the potential to be problematic because many compounds that are PGP inhibitors also inhibit other pathways important for drug disposition. For example, cyclosporin A also inhibits CYP3A4, the major metabolic enzyme responsible for docetaxel elimination. Therefore, it would be impossible to determine if the altered PK was the result of PGP and/or CYP3A4 inhibition. Consequently, as an alternative to pharmacologic inhibition, we used genetic inhibition. Specifically, we utilized PGP (mdr1a/b) knockout mice as proposed in Task 1c and dosed them with docetaxel to directly evaluate the effect of PGP on docetaxel PK. The plasma and tissue docetaxel concentration profiles in PGP knockout and wild-type mice are presented in Figure 1. Mice without PGP showed significant increases in docetaxel concentrations in intestine, kidney, brain, heart, lung and muscle. With this data, we have subsequently begun work on Specific Aim 2.

Key Research Accomplishments

▪Further elucidated the plasma and tissue pharmacokinetics of lapatinib
▪Determined that co-administration of lapatinib with doxorubicin did not alter the plasma or tissue pharmacokinetics of doxorubicin.
▪Determined that co-administration of lapatinib with docetaxel substantially increased intestinal exposure to docetaxel.
▪Determined that docetaxel concentrations are significantly increased in intestine, kidney, brain, heart, lung and muscle when PGP is absent.

Reportable Outcomes

Manuscripts

1. Physiologically based pharmacokinetic model of lapatinib developed in mice and scaled to humans
Journal of Pharmacokinetics and Pharmacodynamics (accepted contingent on revisions)

2. Co-administration of lapatinib increases exposure to docetaxel but not doxorubicin in the small intestine of mice
Molecular Cancer Therapeutics (submitted)

Abstracts

The following abstract was submitted for the University of Colorado Cancer Center Retreat's Poster Session at the Anschutz Medical Campus in Aurora, Colorado, on October 30th, 2012.

Title: Physiologically-Based Pharmacokinetic Model of Lapatinib Developed in Mice and Scaled to Humans

Authors: Susan F. Hudachek and Daniel L. Gustafson

Program: Animal Cancer Center, Department of Clinical Sciences, Colorado State University

Background: Lapatinib is an oral 4-anilinoquinazoline derivative that dually inhibits epidermal growth factor receptor (EGFR, ErbB1) and human epidermal growth factor receptor 2 (HER2/neu, ErbB2). This drug is a mere decade old and has only been approved by the FDA for the treatment of breast cancer since 2007. Consequently, the intricacies of the pharmacokinetics are still being elucidated.

Material and Methods: In the work presented herein, we determined the biodistribution of orally-administered lapatinib in mouse plasma, brain, heart, lung, kidney, intestine, liver, muscle and adipose tissue. Using this data, we subsequently developed a physiologically based pharmacokinetic (PBPK) model of lapatinib in mice and, by taking into account interspecies differences in physiology and physiochemistry, we then extrapolated the mouse PBPK model to humans.

Results: Our mouse PBPK model accurately predicted plasma and tissue concentrations after doses of 30, 60 and 90 mg/kg. In humans, our model predictions closely reflected lapatinib plasma pharmacokinetics in healthy subjects. Additionally, we were also able to simulate the pharmacokinetics of this drug in the plasma of patients with solid malignancies by incorporating a decrease in liver metabolism into the model. Finally, our human PBPK model also facilitated the estimation of various tissue exposures to lapatinib, which harmonized with the organ-specific toxicities observed in clinical trials.

Conclusions: We have successfully developed a first-generation PBPK model of lapatinib that accurately predicts the pharmacokinetics of this drug in mice, healthy subjects and cancer patients. Additionally, this model improves our understanding of the absorption, distribution, metabolism and elimination of lapatinib in both mouse and man. Potential applications of this model include the prediction of drug interactions with lapatanib as well as determining the sources and magnitudes of exposure variability in specific human populations.

Acknowledgements: This work was supported in part by grant number W81XWH-09-1-0457 from the Department of Defense (DOD) Breast Cancer Research Program (BCRP) of the Office of the Congressionally Directed Medical Research Programs (CDMRP).

Conclusion

A discussion of the conclusions of the work conducted during the third year of this award can be found in the amended manuscripts titled " Physiologically based pharmacokinetic model of lapatinib developed in mice and scaled to humans" and " Co-administration of lapatinib increases exposure to docetaxel but not doxorubicin in the small intestine of mice". To reiterate the most clinically significant findings, our mouse studies involving co-administration of the PGP substrate/inhibitor lapatinib at doses that resulted in human-equivalent exposure demonstrated that this tyrosine kinase inhibitor does not alter the PK of doxorubicin. In contrast, lapatinib did increase exposure to docetaxel in the intestine, likely leading to enhanced toxicity. The significant lapatinib-docetaxel interaction is likely CYP3A4-mediated and thus, our study suggests that caution should be taken when this combination is administered, particularly to patients with compromised CYP3A activity. As co-administration of these two agents is protocol for clinical trials that are either recruiting or active, we recommend closely monitoring the recipients of combined lapatinib and docetaxel for enhanced toxicity, particularly for adverse effects on the intestine.

Supporting Data

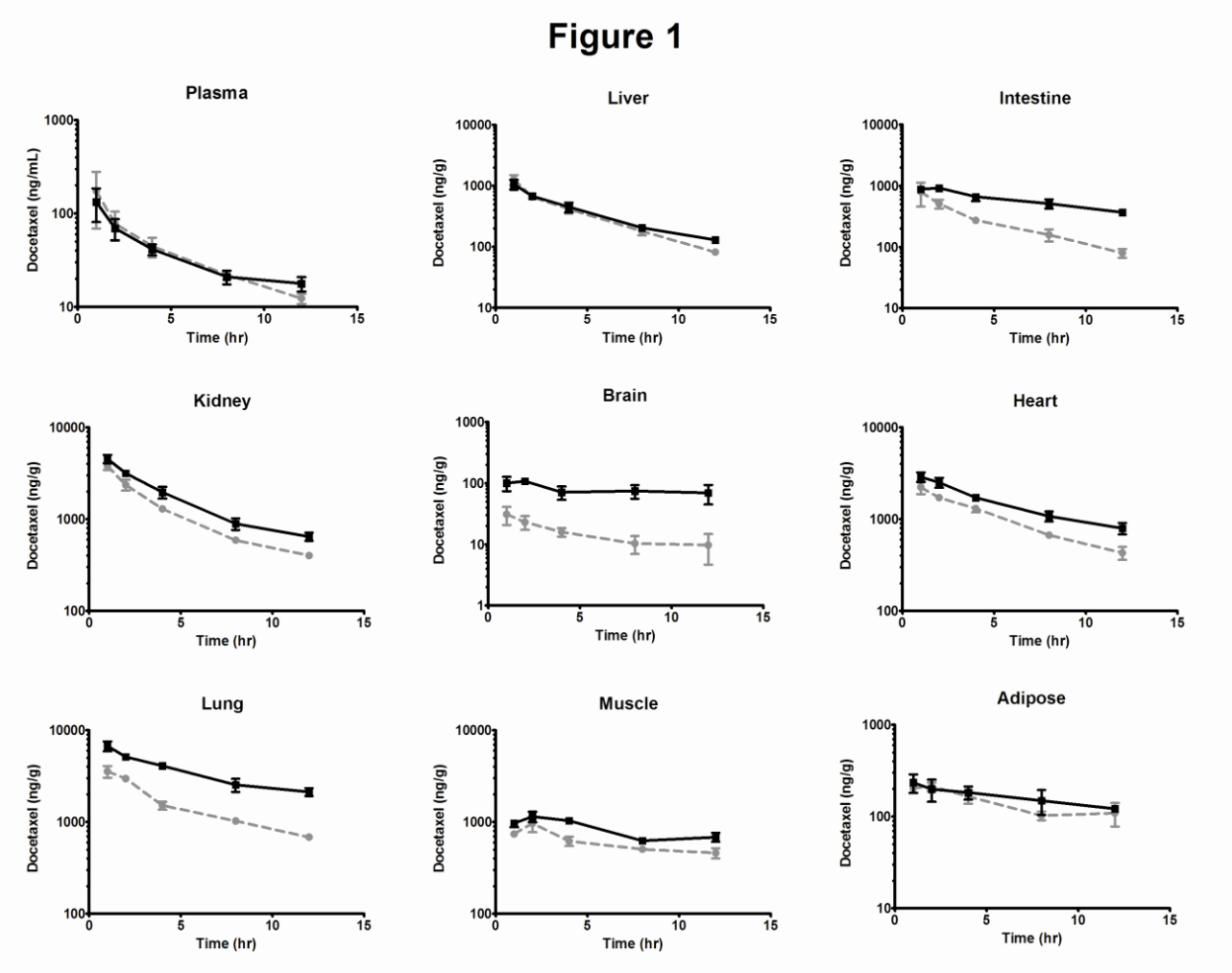

Figure 1: Mean ± standard deviation of plasma and tissue concentrations of docetaxel after an intravenous doses of 3 mg/kg to FVB wild-type (gray circles and dashed gray lines) and mdr1a/b (-/-) mice (black squares and solid black lines). n = 3 per timepoint.

J Pharmacokinet Pharmacodyn
DOI 10.1007/s10928-012-9295-8

ORIGINAL PAPER

Physiologically based pharmacokinetic model of lapatinib developed in mice and scaled to humans

Susan F. Hudachek · Daniel L. Gustafson

Received: 19 July 2012 / Accepted: 22 December 2012

Abstract Lapatinib is an oral 4-anilinoquinazoline derivative that dually inhibits epidermal growth factor receptor and human epidermal growth factor receptor 2 (HER2). This drug is a mere decade old and has only been approved by the FDA for the treatment of breast cancer since 2007. Consequently, the intricacies of the pharmacokinetics are still being elucidated. In the work presented herein, we determined the biodistribution of orally administered lapatinib in mouse plasma, brain, heart, lung, kidney, intestine, liver, muscle and adipose tissue. Using this data, we subsequently developed a physiologically based pharmacokinetic (PBPK) model of lapatinib in mice that accurately predicted the tissue concentrations after doses of 30, 60 and 90 mg/kg. By taking into account interspecies differences in physiology and physiochemistry, we then extrapolated the mouse PBPK model to humans. Our model predictions closely reflected lapatinib plasma pharmacokinetics in healthy subjects. Additionally, we were also able to simulate the pharmacokinetics of this drug in the plasma of patients with solid malignancies by incorporating a decrease in liver metabolism into the model. Finally, our PBPK model also facilitated the estimation of various human tissue exposures to lapatinib, which harmonize with the organ-specific toxicities observed in clinical trials. This first-generation PBPK model of lapatinib can be further improved with a greater understanding of lapatinib absorption, distribution, metabolism and excretion garnered from subsequent in vitro and in vivo studies and expanded to include other pharmacokinetic determinants, including efflux transporters, metabolite generation, combination dosing, etc., to better predict lapatinib disposition in both mouse and man.

Keywords Breast cancer · Lapatinib · Physiologically based pharmacokinetic modeling · Tyrosine kinase inhibitor

Introduction

Lapatinib is an oral 4-anilinoquinazoline derivative that dually inhibits epidermal growth factor receptor (EGFR) and human epidermal growth factor receptor 2 (HER2) (estimated K_i^{app} values of 3 and 13 nM, respectively) by competing with ATP [1]. Aberrant signaling of these tyrosine kinases is prevalent in various types of solid tumors, thus making them attractive therapeutic targets. Presently, lapatinib is approved by the US Food and Drug Administration (FDA) in combination with capecitabine for the treatment of HER2 positive metastatic breast cancer and in combination with letrozole for the treatment of hormone receptor positive, HER2 positive metastatic breast cancer. In addition, there are approximately 250 current clinical trials in cancer patients involving this drug [2].

Numerous preclinical studies and clinical trials have investigated the plasma pharmacokinetics of lapatinib [3–15]. However, none have elucidated the biodistribution of this compound in tissues other than blood. Based on adverse reactions reported in humans (including cardiac, hepatic, gastrointestinal and lung toxicities), it can be presumed that there are significant levels of drug in these organs.

Electronic supplementary material The online version of this article (doi:10.1007/s10928-012-9295-8) contains supplementary material, which is available to authorized users.

S. F. Hudachek (✉) · D. L. Gustafson
Department of Clinical Sciences, Animal Cancer Center, Colorado State University, Fort Collins, CO, USA
e-mail: Susan.Hudachek@colostate.edu

Published online: 12 January 2013

To empirically determine both plasma and organ exposure to lapatinib, we developed a physiologically based pharmacokinetic (PBPK) model in mice and then scaled this model to humans. This type of pharmacologic modeling is a useful tool that facilitates the prediction of target tissue drug concentrations by incorporating mathematical descriptions of the uptake and disposition of chemicals based on quantitative interrelations among the critical determinants of physiological processes (i.e., absorption, metabolism, excretion and tissue solubility phenomena) [16]. Accordingly, PBPK models are comprised of compartments corresponding to discrete tissues or groupings of tissues with appropriate volumes, blood flows, and pathways for xenobiotic clearance including pertinent biochemical and physiochemical constants [17]. Each compartment in the model is described with a mass-balance differential equation whose terms mathematically represent biological processes; the set of equations is then solved by numerical integration to simulate tissue time-course concentrations of chemicals and their metabolites [17]. The PBPK model of lapatinib presented herein consisted of eight tissue compartments (plasma, brain, heart, lung, kidney, intestine, liver and slowly perfused tissues) and incorporated drug absorption, intestinal and hepatic metabolism and fecal elimination in both mouse and man.

Materials and methods

Chemicals

Lapatinib (GW572016) and GW572016AH were generously provided by GlaxoSmithKline. Hydroxypropyl methylcellulose and Tween® 80 were purchased from Sigma-Aldrich. All other reagents were of analytical grade.

Lapatinib pharmacokinetic studies in mice

Five to six-week-old female FVB mice were purchased from Taconic. Animals were housed in polycarbonate cages and kept on a 12 h light/dark cycle. Food and water were given ad libitum. All experimental procedures were approved by Colorado State University's Animal Care and Use Committee and the Department of Defense US Army Medical Research and Material Command (USAMRMC) Animal Care and Use Review Office (ACURO).

Upon arrival, mice acclimated for a minimum of seven days prior to any experimentation. After acclimation, a time course distribution study of lapatinib was conducted at doses of 30, 60 and 90 mg/kg. Lapatinib was formulated as a suspension in 0.5 % hydroxypropyl methylcellulose: 0.1 % Tween® 80 in Milli-Q water and was administered via oral gavage as a single bolus dose. Subsequently, three mice were sacrificed at 0.25, 0.5, 1, 2, 4, 8, 12 and 16 h by cardiac stick exsanguination under isoflurane anesthesia. Plasma, brain, liver, proximal small intestine, kidney, heart, lung, muscle and adipose tissue were immediately collected, rinsed with phosphate buffered saline, frozen in liquid nitrogen and stored at -80 °C until analysis.

Lapatinib high-pressure liquid chromatography-tandem mass spectrometry analysis

Analysis of lapatinib in plasma and tissue was done using high-pressure liquid chromatography-tandem mass spectrometry (LC/MS/MS) analysis based on the method of Bai et al. [18], modified as follows. Briefly, lapatinib was extracted from plasma by adding 210 μL of acetonitrile and 10 μL of internal standard (17.2 pmol GW572016AH) to 100 μL of unknown sample plasma, vortexing for 10 min and centrifuging at 18,000×*g* for 10 min at 4 °C. An aliquot of 20 μL of the supernatant was injected into the LC/MS/MS system for analysis. Tissues (brain, liver, proximal small intestine, kidney, heart, lung, muscle and adipose) were homogenized at 100 mg/mL in water and 100 μL of the homogenates were extracted using the method for plasma detailed above. Standards and quality control samples were prepared in the appropriate matrix and analyzed as described above.

The HPLC system consisted of an Agilent 1200 Series binary pump SL, vacuum degasser, thermostatted column compartment SL (Agilent Technologies, Santa Clara, CA, USA) and a CTC Analytics HTC PAL System autosampler (Leap Technologies, Carrboro, NC, USA). The HPLC column was a Waters Sunfire C8 column (4.6 × 50 mm I.D., 2.5 μm bead size) (Waters Corporation, Milford, MA, USA) protected by a SecurityGuard™ C18 cartridge (4 × 2.0 mm I.D.) (Phenomenex, Torrance, CA, USA) and maintained at room temperature. The mobile phase consisted of an aqueous component (A) of 20 mM ammonium formate in MilliQ water, pH 2.2 (with formic acid) and an organic component (B) of acetonitrile with 1 % formic acid. The 3.5 min run consisted of the following linear gradient elution: 95 % A and 5 % B at 0 min, 95 % A and 5 % B at 0.25 min, 25 % A and 75 % B at 0.35 min, 25 % A and 75 % B at 3.0 min, 95 % A and 5 % B at 3.1 min and 95 % A and 5 % B at 3.5 min. The system operated at a flow-rate of 0.75 mL/min.

Mass spectrometric detection was performed on an API 3200™ triple quadrupole instrument (Applied Biosystems Inc., Foster City, CA, USA) using multiple reaction monitoring (MRM). Ions were generated in positive ionization mode using an electrospray interface. Lapatinib compound-dependent parameters were as follows: declustering potential (DP): 60 V; entrance potential (EP): 10 V; collision cell entrance potential (CEP): 21 V; collision energy (CE): 51 V and collision cell exit potential (CXP): 5.8 V. GW572016AH

(internal standard) compound-dependent parameters were as follows: DP: 67 V; EP: 7.5 V; CEP: 23 V; CE: 49 V and CXP: 5.5 V. Source-dependent parameters were as follows: nebulizer gas (GS1): 50 psi; auxiliary (turbo) gas (GS2): 60 psi; turbo gas temperature (TEM): 500 °C; curtain gas [7]: 10 psi; collision-activated dissociation (CAD) gas (nitrogen): 6 psi; ionspray voltage (IS): 5,000 V and interface heater (IH): 500 °C. Peak areas ratios obtained from MRM of lapatinib (*m/z* 581 → 365.1) and GW572016AH (*m/z* 587 → 367) were used for quantification.

The lower limit of quantitation for this assay was 1 ng/mL for plasma and 5 ng/g for tissues. The accuracy for the assay was 95.61 ± 4.60 % in plasma and 95.83 ± 3.47 % in tissues. The precision of the assay was 1.97 % in plasma and 3.75 % in tissues.

PBPK model development

A PBPK model for lapatinib was developed incorporating absorption, intestinal and hepatic metabolism and fecal elimination. This flow-limited model was comprised of eight tissue compartments: plasma, brain, heart, lung, kidney, intestine, liver and slowly perfused tissue (Fig. 1). Physiological parameters (tissue volumes and tissue blood flows) were obtained from Brown et al. [19] and are shown in Table 1.

The unbound fraction of drug in the plasma was set at 0.01 (1 %), as lapatinib is highly bound (>99 %) to albumin and alpha-1 acid glycoprotein [1]. The arterial blood drug concentration available to all tissues except liver was considered to be the unbound lapatinib concentration in the blood. Both unbound and bound lapatinib were available for uptake into the liver.

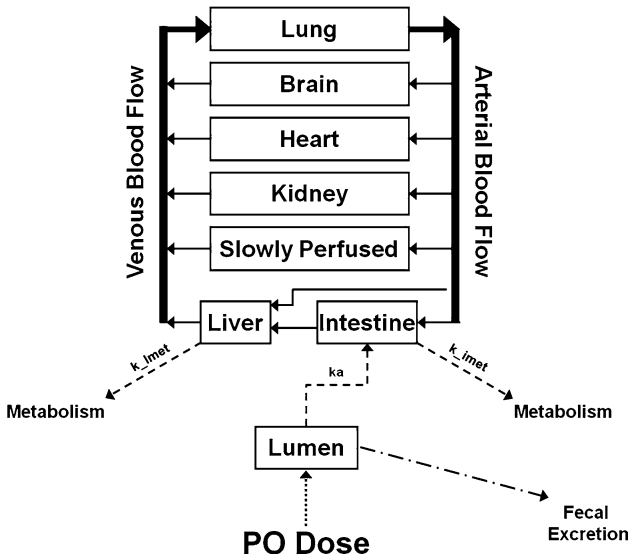

Fig. 1 Schematic representation of a physiologically based pharmacokinetic (PBPK) model of lapatinib. *Solid arrows* represent blood flow. *Dashed lines* represent first-order rate constants for absorption from intestinal lumen (*ka*), hepatic metabolism (*k_lmet*) and intestinal metabolism (k_imet). The *dotted line* represents lapatinib input into the system via per os (*p.o.*) dosing. Drug remaining in the lumen is eliminated via fecal excretion

Table 1 PBPK model parameter values

Parameter	Units	Mouse	Human
Lapatinib properties			
Molecular weight		581.06 g/mol	
Percent unbound		1 %	
Tissue volume[a]	% of body weight		
Blood		4.90	7.9
Brain		1.65	2.0
Heart		0.50	0.5
Lung		0.73	0.8
Kidney		1.67	0.4
Intestine		4.22	1.7
Liver		5.49	2.6
Slowly perfused[b]		80.84	84.1
Tissue blood flow[a]	% of cardiac output		
Brain		3.3	11.4
Heart		6.6	4.0
Lung		100	100
Kidney		9.1	17.5
Intestine		14.1	18.1
Liver		2.0	4.6
Slowly perfused[b]		64.9	44.4
Partition coefficients[c]	Ratio		
Brain:plasma		10 (19)	10
Heart:plasma		215 (22)	215
Lung:plasma		1,643 (19)	1,643
Kidney:plasma		1,064 (18)	1,064
Intestine:plasma		531 (31)	531
Liver:plasma		12 (20)	12
Slowly perfused:plasma		65 (20)	65
Absorption rate constants[d]	h^{-1}		
Lumen → Intestine		0.237 (2)	0.07 (6)
Metabolism rate constants	h^{-1}		
Liver[d]		127 (13)	75 (5)
Intestine		2.5[e]	0.975[f]

[a] Physiological parameters obtained from Brown et al. [19]

[b] Slowly perfused tissue parameters calculated as the remaining percent

[c] Determined by parameter estimation optimized for observed plasma and tissue concentrations from mouse 60 mg/kg dose cohort. Data is parameter estimate (CV%)

[d] First-order rate constants determined by parameter estimation optimized for observed plasma and tissue concentrations from mouse 60 mg/kg dose cohort for mouse model and observed plasma concentrations from healthy subject human data for human model. Data is parameter estimate (CV%)

[e] Calculated as 2 % of liver metabolism

[f] Calculated as 1.3 % of liver metabolism

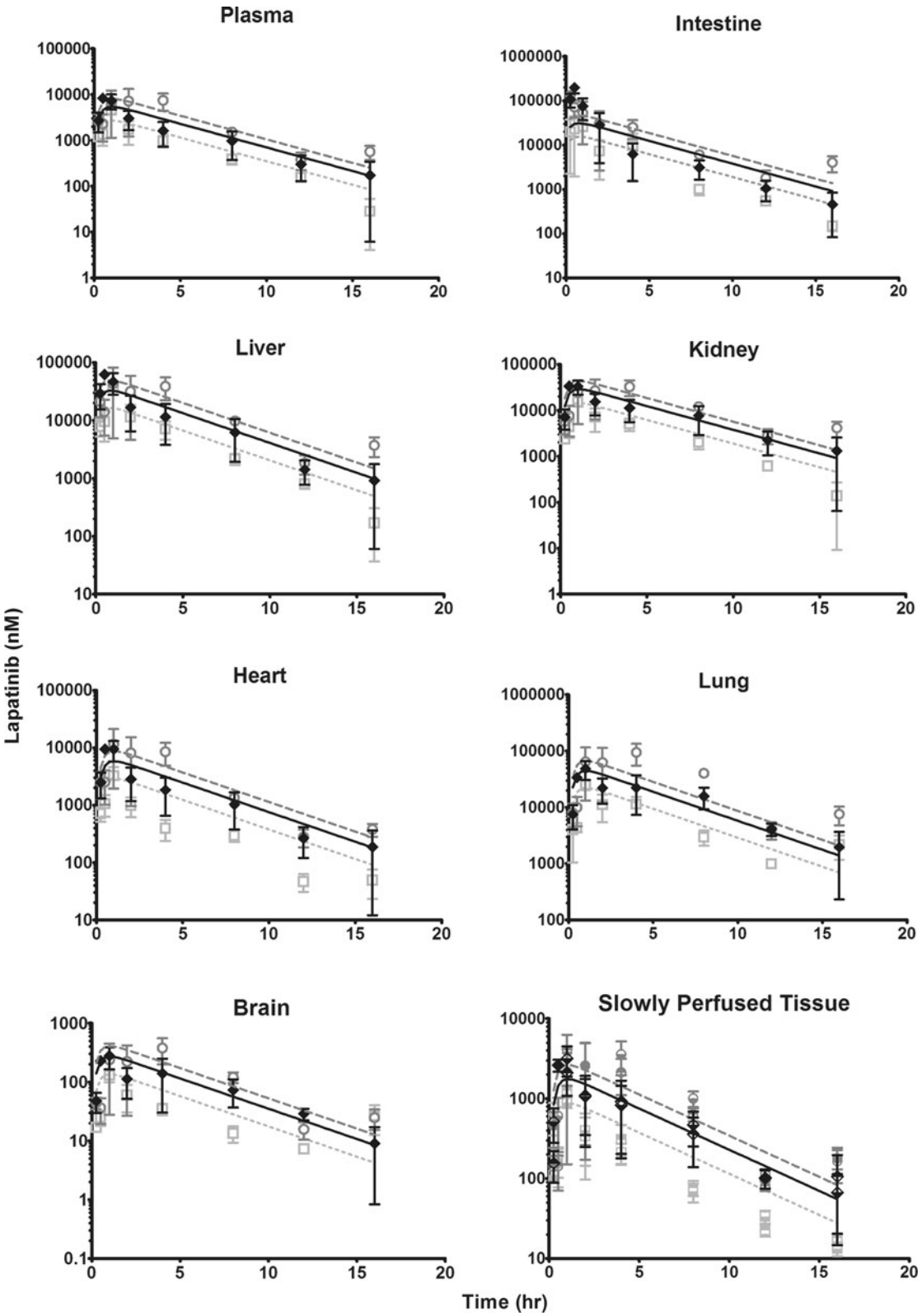
Plasma
Intestine
Liver
Kidney
Heart
Lung
Brain
Slowly Perfused Tissue
Lapatinib (nM)
Time (hr)

◀ **Fig. 2** Observed and model-simulated lapatinib concentrations in mouse plasma, intestine, liver, kidney, heart, lung, brain and slowly perfused tissue after oral gavage dosing of 30, 60 and 90 mg/kg. In all graphs except slowly perfused tissue, *open light gray squares*, *filled diamonds* and *open dark gray circles* represent the observed data from the 30, 60 and 90 mg/kg cohorts, respectively. In the slowly perfused tissue graph, the observed data from the 30 mg/kg dose cohort is represented by the *upper half-filled light gray squares* (adipose tissue) and *lower half-filled light gray squares* (muscle tissue); the observed data from the 60 mg/kg dose cohort is represented by *upper half-filled black diamonds* (adipose tissue) and *lower half-filled black diamonds* (muscle tissue); and the observed data from the 90 mg/kg dose cohort is represented by *upper half-filled dark gray circles* (adipose tissue) and *lower half-filled dark gray circles* (muscle tissue). For all observed data, error bars symbolize the standard error of the mean (SEM). *Light gray dotted lines*, *solid black lines*, and *dark gray dashed lines* represent model simulations for the 30, 60 and 90 mg/kg dose cohorts, respectively

Tissue:plasma partition coefficients were determined by parameter estimation, optimizing the fit for the observed plasma and tissue concentrations from the mouse 60 mg/kg dose cohort. These fitted values were compared with values calculated as detailed in Chen and Gross [44] using our experimental data (Online Resource 1). For these calculations, we used our concentration–time data from the mouse 60 mg/kg dose study and considered the terminal elimination phase to include the 4, 8, 12 and 16 h time points. The tissue:plasma partition coefficients were calculated as C_T^0/C_P^0, where C_T^0 and C_P^0 are the tissue and plasma intercepts (initial concentrations), respectively, from the concentration–time curves of the terminal elimination phase on a semilogarithmic plot. After the partition coefficients were determined, the values had to be adjusted because when we measured the plasma concentrations via LC/MS/MS, we analyzed both bound and unbound drug in the plasma. Thus, to correct the partition coefficients so they reflected only the unbound drug available for tissue uptake (1 % unbound), we multiplied the calculated value by 100. The Chen and Gross method [44] was applicable for the determination of kidney, lung and slowly perfused tissue (adipose and muscle were used as representative slowly perfused tissues) partition coefficients. However, for brain and heart partition coefficients, we were unable to utilize this method because the criteria for implementation of this equation were not met for these two tissues (K/Q was not $\ll 1$, where K is the organ clearance and Q is the blood flow). Additionally, for liver and intestine partition coefficients, Chen and Gross [44] describes unique equations, which we could not use because we did not have the values for all necessary variables. Therefore, because we were only able to determine three of the seven tissue partition coefficients using the Chen and Gross equations [44], we chose to estimate all partition coefficients by fitting these parameters to the model. For kidney, lung and slowly perfused tissue partition coefficients, the fitted values were 37, 7 and 12 % different than the calculated values, respectively. For brain, heart, liver and intestine partition coefficients, the fitted values were 10, 42, 29 and 16 % different than the calculated values, respectively.

The first-order rate constants for absorption from intestinal lumen and hepatic metabolism were determined by parameter estimation. For the mouse model, the fit was optimized for the observed plasma and tissue concentrations from the mouse 60 mg/kg dose cohort. For the human model, the fit was optimized for the observed plasma concentrations from a single 100 mg dose study conducted by GlaxoSmithKline in healthy subjects ($n = 21$).

The first-order rate constant for intestinal metabolism was estimated as a constant percentage of hepatic metabolism based on the ratio of total liver:intestinal CYP3A, the major cytochrome P450 enzyme sub-family responsible for lapatinib metabolism [1]. In mice, the mean quantity of immunoreactive CYP3A is 2.24 and 0.64 pmol/mg microsomal protein in liver and intestinal microsomes, respectively [45]. The total amount of microsomal protein in a 20 g mouse liver (5.49 % body weight [19] = 1.098 g) and small intestine is 38.9 mg (35.4 mg hepatic microsomal protein/g liver [46] × 1.098 g) and 2.67 mg [47], respectively. Accordingly, the total amount of CYP3A in a 20 g mouse liver and small intestine is 87.136 and 1.709 pmol, respectively. As a result, we concluded that the first-order rate constant for intestinal metabolism in mice is 2 % that of liver metabolism. In humans, total hepatic and small intestine (duodenum, jejunum and ileum) CYP3A was calculated to be 5,490 and 70.5 nmol, respectively [48]. Therefore, we represented the first-order rate constant for human intestinal metabolism as 1.3 % that of liver metabolism. This ratio held true for the microsomal intrinsic clearance of midazolam, a CYP3A-specific substrate, which was 15800 mL/min and 213.7 mL/min (or 1.35 %) in human liver and small intestine, respectively [48].

Table 1 lists all parameter values for both the mouse and human PBPK models.

The rate of change of the amount of drug in a generic storage tissue compartment mass balance equation is as follows:

$$\frac{dA_T}{dt} = Q_T \times (C_A - C_{VT})$$

where A_T is the amount of drug in the tissue compartment, t is time, Q_T is the blood flow to the tissue compartment, C_A is the arterial blood drug concentration entering the tissue compartment and C_{VT} is the venous blood drug concentration exiting the tissue compartment. Assuming venous equilibration, the drug concentration in the venous blood is:

$$C_{VT} = C_T/P_T$$

where C_T is the concentration of drug in the tissue compartment and P_T is the tissue:plasma partition coefficient.

Assuming the volume of the tissue (V_T) is constant, the drug concentration in the tissue is:

$$\frac{dC_T}{dt} = Q_T \times (C_A - C_{VT})/V_T$$

For metabolizing tissues (liver and intestine), the rate of change of the amount of drug metabolized (A_M) is as follows:

$$\frac{dA_M}{dt} = k \times C_{VT} \times V_T$$

where k is a first-order rate constant.

Computer simulation

For PBPK modeling, acslX Libero version 3.0.2.1 (The AEgis Technologies Group, Inc.) was used.

Pharmacokinetic analysis

Pharmacokinetic parameters were calculated using noncompartmental modeling performed with Microsoft Excel and standard equations for noncompartmental analysis.

Data analysis

The predictive capability of the model was evaluated by calculating the prediction error (PE%) as follows [20, 21]:

$$PE\% = \frac{Value_{predicted} - Value_{measured}}{Value_{measured}} \times 100$$

As a measure of the precision of the prediction, the median absolute prediction error (MAPE%) was calculated as follows:

$$MAPE\% = median(|PE\%1|,|PE\%2|, \ldots |PE\%n|)$$

As a measure of the bias of the prediction, the median prediction error (MPE%) was calculated as follows:

$$MPE\% = median(PE\%1, PE\%2, \ldots PE\%n)$$

Sensitivity analysis

A normalized sensitivity analysis was performed as described in Loccisano et al. [22] to assess the influence of each PBPK model parameter on the simulated plasma area under the concentration–time curve (AUC) for both the mouse and human models. Briefly, sensitivity coefficients were calculated with the original parameters and for those resulting from a 1 % change in each parameter value. The following equation was used to calculate the normalized sensitivity coefficient (SC):

$$SC = \frac{(A - B)/B}{(C - D)/D}$$

where A is the AUC resulting from the 1 % increase in the parameter value, B is the AUC resulting from the original parameter value, C is the parameter value increased by 1 % and D is the original parameter value.

Results

Lapatinib pharmacokinetics and model simulations in mice

A time course tissue distribution study of lapatinib was conducted in female FVB mice. Plasma and tissue concentrations were measured after single oral doses of 30, 60 and 90 mg/kg at 0.25, 0.5, 1, 2, 4, 8, 12 and 16 h post drug administration. These time points were chosen for sacrifice to provide multiple samplings during each pharmacokinetic phase (absorption, distribution and elimination).

The mouse PBPK model development was based on the concentration–time data from the 60 mg/kg dose cohort; partition coefficients and first-order rate constants were determined by parameter estimation, optimizing the fit for the observed plasma and tissue concentrations from this study. The concentration–time profiles of lapatinib in plasma, intestine, liver, kidney, heart, lung, slowly perfused tissue and brain and the resulting PBPK model simulations are shown in Fig. 2. For all tissues except intestine, the PBPK model simulations closely mirrored the observed data.

The model-predicted intestine concentrations for the first four time points (0.25, 0.5, 1 and 2 h) are significantly lower than the actual data. We suspect that the observed data is not an accurate measurement of the drug concentration in the intestinal epithelium. Instead, the measured values reflect both the lapatinib in the intestinal epithelium and unabsorbed lapatinib in the proximal intestinal lumen. As an attempt to circumvent this anticipated problem, we flushed the intestinal lumen with saline immediately after tissue collection; however, we still noted yellow aggregates of undissolved lapatinib within the lumen (resulting from administration of the drug as a suspension via oral gavage). Thus, the measured drug concentrations in the intestine are likely inflated due to the lapatinib suspension in the proximal intestinal lumen. After approximately 3 h, the model simulation accurately reflects the observed values. It is probable that the lapatinib suspension has moved through the intestinal lumen by this time, as the intestinal transit time in a mouse is approximately 3 h. Therefore, at these

Table 2 Observed and model-simulated lapatinib pharmacokinetic (PK) parameters in mice[a]

PK parameter	Dose		Plasma	Intestine	Liver	Kidney	Heart	Lung	Brain	Slowly perfused
$AUC_{0-16\ h}$ (nM × h)[b]	30	Observed	12,008	79,885	84,946	50,440	7,156	92,409	440.8	2,738
		Simulated	13,972	78,143	83,505	74,392	15,022	114,792	698.6	4,544
		Ratio	0.86	1.02	1.02	0.68	0.48	0.81	0.63	0.60
	60	Observed	24,052	235,114	157,288	137,624	26,545	233,760	1,315	9,519
		Simulated	27,944	156,284	167,010	148,784	30,044	229,583	1,397	9,087
		Ratio	0.86	1.50	0.94	0.92	0.88	1.02	0.94	1.05
	90	Observed	48,230	259,808	261,237	227,184	55,179	623,277	2,261	18,930
		Simulated	41,916	234,426	250,515	223,176	45,066	344,375	2,096	13,631
		Ratio	1.15	1.11	1.04	1.02	1.22	1.81	1.08	1.39
CL (L/h)[c]	30	Observed	0.09	0.01	0.01	0.02	0.14	0.01	2.34	0.38
		Simulated	0.07	0.01	0.01	0.01	0.07	0.01	1.48	0.23
		Ratio	1.16	0.98	0.98	1.47	2.10	1.24	1.58	1.66
	60	Observed	0.09	0.01	0.01	0.02	0.08	0.01	1.57	0.22
		Simulated	0.07	0.01	0.01	0.01	0.07	0.01	1.48	0.23
		Ratio	1.16	0.66	1.06	1.08	1.13	0.98	1.06	0.95
	90	Observed	0.06	0.01	0.01	0.01	0.06	0.005	1.37	0.16
		Simulated	0.08	0.03	0.01	0.01	0.07	0.01	1.48	0.22
		Ratio	0.78	0.45	0.96	0.98	0.79	0.55	0.93	0.73
$t_{1/2}$ (h)[d]	30	Observed	2.73	2.79	2.48	2.53	2.59	2.39	3.70	3.88
		Simulated	2.99	2.96	2.95	3.00	2.99	2.99	2.99	2.99
		Ratio	0.91	0.94	0.84	0.84	0.87	0.80	1.24	1.30
	60	Observed	3.42	3.05	2.75	3.57	3.05	3.04	3.12	2.57
		Simulated	2.99	2.96	2.95	3.00	2.99	2.99	2.99	2.99
		Ratio	1.14	1.03	0.93	1.19	1.02	1.02	1.04	0.86
	90	Observed	2.36	2.55	1.91	2.51	2.32	1.72	1.76	1.55
		Simulated	2.99	2.96	2.95	3.00	2.99	2.99	2.99	2.99
		Ratio	0.79	0.86	0.65	0.83	0.78	0.58	0.59	0.52

[a] PK parameters were calculated using noncompartmental modeling

[b] $AUC_{0-16\ h}$ is the area under the concentration–time curve from 0 to 16 h

[c] CL is clearance

[d] $t_{1/2}$ is the half-life for elimination as calculated from linear regression of the terminal elimination phase

later time points, the measured drug is presumably only lapatinib that has been absorbed into the intestinal epithelium.

After developing the mouse PBPK model with the 60 mg/kg dose cohort as a training set, we employed the other two dose cohorts (30 and 90 mg/kg) as test sets. The concentration–time data and the corresponding model simulations for these dose cohorts are also presented in Fig. 2. Again, the model simulations approximated the observed data with the exception of the early time points in the intestine, likely a result of the same phenomenon as described previously for the 60 mg/kg dose cohort.

The area under the concentration–time curve from 0 to 16 h ($AUC_{0-16\ h}$), clearance (CL) and elimination half-life ($t_{1/2}$) were calculated for both the observed and simulated data using noncompartmental analysis (Table 2). Lapatinib exhibits linear pharmacokinetics in all tissues within the 30–90 mg/kg dose range, as evidenced by a dose-dependent increase in $AUC_{0-16\ h}$ and constant CL (Fig. 3). To compare the actual and predicted data, we determined the ratio of the observed to model-predicted values (Table 2). The mean $AUC_{0-16\ h}$ ratio for all tissues was 1.00 and the range was 0.48 (heart from the 30 mg/kg dose cohort) to 1.81 (lung from the 90 mg/kg dose cohort), indicating that our model-predicted drug exposures reasonably mimicked the observed exposure for all tissues analyzed. As for CL, the model predictions also emulated the actual data; all ratios were between 0.45 (intestine from the 90 mg/kg dose cohort) and 2.10 (heart from the 30 mg/kg dose cohort), with the average ratio being 1.06. Lastly, all $t_{1/2}$ ratios were within the range of 0.52 (slowly perfused tissue from the 90 mg/kg dose cohort) and 1.24 (brain from the 30 mg/kg dose cohort), with an average ratio of 0.90. Overall, the PK

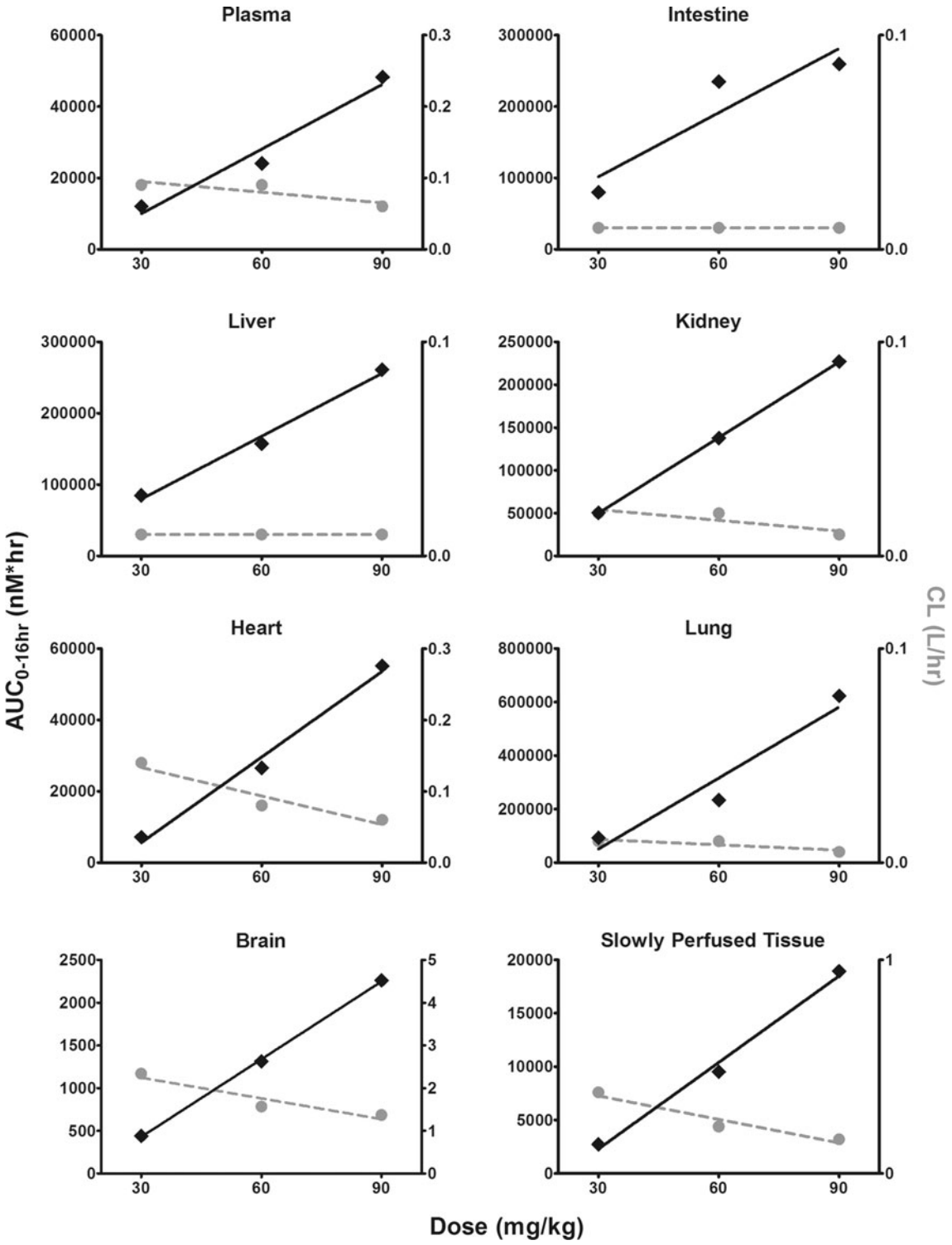

Fig. 3 Area under the concentration–time curve calculated from 0 to 16 h ($AUC_{0–16\ h}$) and clearance (CL) for the mouse 30, 60 and 90 mg/kg dose cohorts in plasma, intestine, liver, kidney, heart, lung, brain and slowly perfused tissue. $AUC_{0–16\ h}$ is presented on the *left y* axis and is represented by the *solid black diamonds*, with the corresponding linear regression trendline shown as the *solid black line*. CL is presented on the *right y* axis and is represented by the *solid gray circles* with the corresponding linear regression trendline shown as the *dashed gray line*. Both $AUC_{0–16\ h}$ and CL were determined by noncompartmental analysis

Table 3 Predictive performance for mouse PBPK model

	Concentrations		AUC^{a}_{0-16h}		$t^{b}_{1/2}$	
	MPE%[c]	MAPE%[d]	MPE%[c]	MAPE%[d]	MPE%[c]	MAPE%[d]
Plasma	28.53	43.36	16.18	16.18	9.57	12.64
Intestine	−8.40	68.10	9.77	−9.77	6.09	6.09
Liver	23.57	51.03	4.10	−1.70	19.11	19.11
Kidney	45.40	52.90	8.11	8.11	18.57	18.57
Heart	52.81	73.34	18.33	13.18	15.41	15.41
Lung	4.45	59.25	24.22	−1.79	25.14	25.14
Slowly perfused	28.77	47.40	27.99	−4.53	16.24	22.96
Brain	53.30	63.65	7.30	6.24	−4.29	19.16

[a] $AUC_{0-16\ h}$ is the area under the concentration–time curve from 0 to 16 h

[b] $t_{1/2}$ is the half-life for elimination as calculated from linear regression of the terminal elimination phase

[c] MPE% is the median prediction error, which is a measure of the bias of the prediction

[d] MAPE% is the median absolute prediction error, which is a measure of the precision of the prediction

parameters derived from the PBPK model simulations accurately mirrored the observed mouse data.

To further assess the predictive performance of the mouse model, we calculated the median prediction error (MPE%) and the median absolute prediction error (MAPE%) for the concentrations, $AUCs_{0-16\ h}$ and half-lives as measures of the bias and precision of the simulations, respectively (Table 3). Of these three variables, the concentrations were the most poorly predicted, with a mean MPE% of 28.6 and a mean MAPE% of 57.4. Although these prediction error assessments are not optimal, they are not surprising considering the large degree of variability in the data (mean concentration coefficient of variation of 78.6 %), likely due to the variable absorption of lapatinib when administered to unfasted animals. $AUC_{0-16\ h}$ and $t_{1/2}$ prediction errors were substantially better than the concentration prediction errors, feasibly because these parameters are derived from the cumulation of the concentration values and thus, the error of the individual points is muted. For $AUC_{0-16\ h}$, the average MPE% was 14.5 and the average MAPE% was 3.2. The MPE% for plasma and all tissue $AUCs_{0-16\ h}$ was less than 28.0 and the MAPE% was less than 16.2. Regarding half-life, the average MPE% was 13.2 and the average MAPE% was 17.4, with no individual plasma or tissue MPE% and MAPE% being more than ±25.2 and 25.2 %, respectively.

Lapatinib pharmacokinetics and model simulations in humans

The mouse PBPK model developed using the 60 mg/kg dose cohort was scaled to humans by using human parameters for tissue volumes and tissue blood flows and fitting the first-order rate constants for absorption and liver metabolism to the observed plasma concentrations from a single 100 mg dose study conducted by GlaxoSmithKline in healthy subjects ($n = 21$) (Table 1). The first-order rate constant for intestinal metabolism was set as 1.3 % that of liver metabolism as explained previously.

The concentration–time profiles of lapatinib in actual human plasma and the resulting PBPK model simulation are shown in Fig. 4a. The PBPK model prediction closely parallels the observed plasma concentration data. The MPE% and MAPE% for the lapatinib concentrations were −8.17 and 11.69, respectively. Regarding the actual and simulated plasma pharmacokinetic parameters, $AUCs_{0-60\ h}$ were 2,698 and 2,409 nM × h, CLs were 63.8 and 71.4 L/h and half-lives were 9.5 and 10.0 h, respectively. The $AUCs_{0-60\ h}$ for plasma and all tissues in the model are shown in Table 4. From largest to smallest, exposure to lapatinib ranked as follows: intestine, lung, liver, kidney, heart, plasma, slowly perfused tissue and brain.

Clinically, the recommended dose of lapatinib is 1,250 or 1,500 mg orally once daily continuously with either capecitabine (for advanced or metastatic breast cancer) or letrozole (for hormone receptor positive, HER2 positive metastatic breast cancer), respectively [1]. Thus, we modified our original model to incorporate multiple dosing of lapatinib. The resulting simulations of 1,250 and 1,500 mg doses of lapatinib q24 h for 8 days are shown in Fig. 4b. The steady-state area under the concentration–time curves calculated within the dosing interval from 0 to 24 h (AUC_{τ}) for plasma and all tissues in the model are shown in Table 4.

To further assess the predictive performance of the human model, we were not able to accrue concentration–time data for any other subjects/patients so we compared our model-predicted AUC, half-life, maximum concentration (C_{max}) and time of maximum concentration (T_{max}) values with those found in the literature for both healthy subjects [4, 24] and patients with solid tumors [5–13, 15].

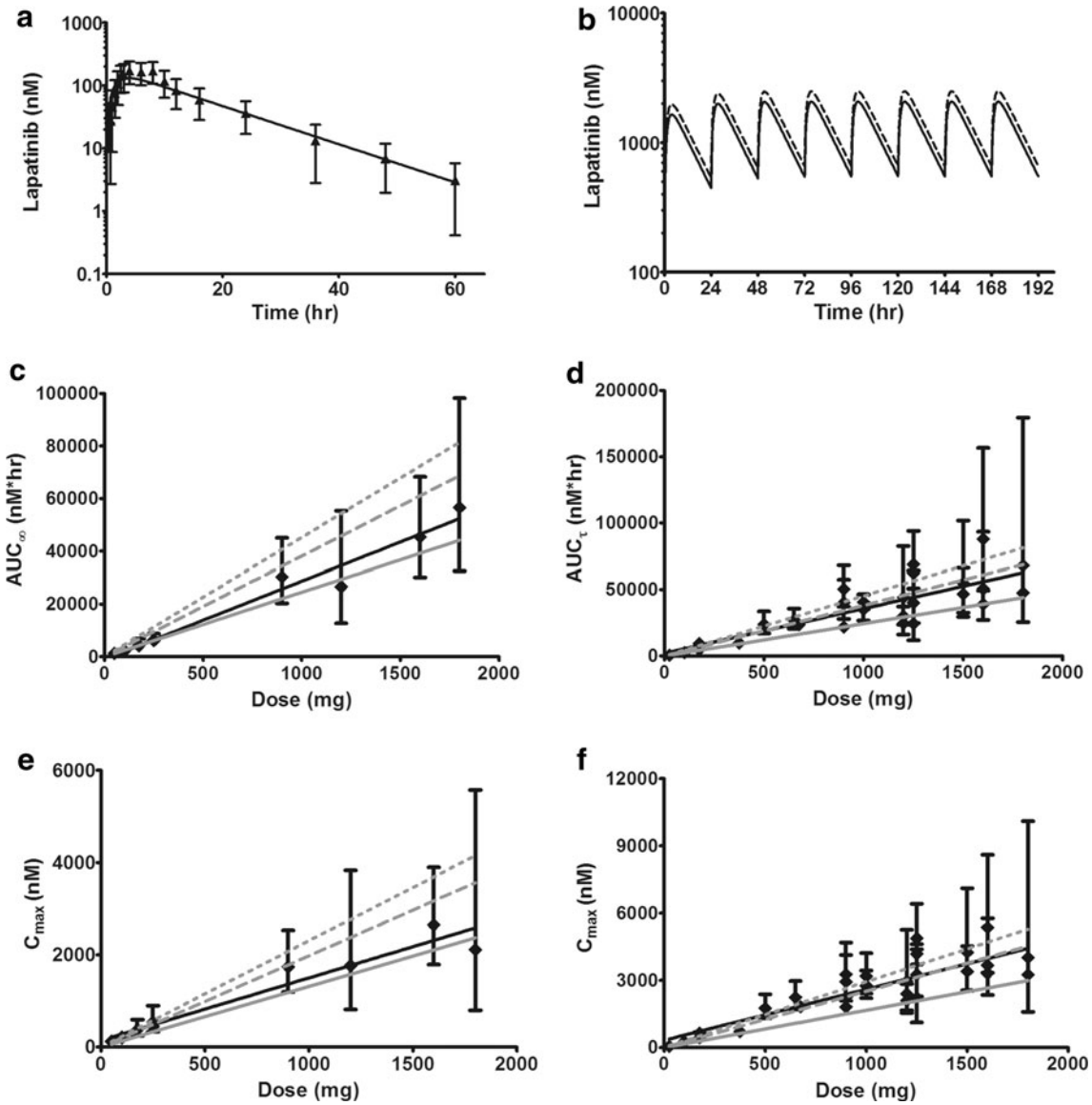

Fig. 4 Observed and model-simulated lapatinib concentrations, area under the concentration–time curve (AUC) and maximum concentration (C_{max}) in human plasma. **a** Single oral dose of 100 mg. *Filled black triangles* represent the observed data with *error bars* symbolizing the standard deviation (SD). The *solid black line* represents the model simulation. **b** Multiple doses (q24 h) for 8 days. *Solid black line* represents the model simulation for daily dosing of 1,250 mg. *Dashed black line* represents the model simulation for daily dosing of 1,500 mg. **c** After a single dose of lapatinib, *solid black diamonds* represent observed $AUCs_{\infty}$ (calculated from time 0 to infinity) with *error bars* symbolizing the 95 % confidence intervals and the *solid black line* is the corresponding linear regression trendline. The *solid gray line* represents the model-predicted $AUCs_{\infty}$. The *dashed gray line* represents simulated $AUCs_{\infty}$ from the model with moderate hepatic impairment. The *dotted gray line* represents simulated $AUCs_{\infty}$ from the model with severe hepatic impairment. **d** After multiple doses (q24 h) of lapatinib, *solid black diamonds* represent observed steady-state $AUCs_{\tau}$ (calculated within the dosing interval from time 0 to 24 h) with *error bars* symbolizing the 95 % confidence intervals and the *solid black line* is the corresponding linear regression trendline. The *solid gray line* represents the model-predicted $AUCs_{\infty}$. The *dashed gray line* represents simulated $AUCs_{\tau}$ from the model with moderate hepatic impairment. The *dotted gray line* represents simulated $AUCs_{\tau}$ from the model with severe hepatic impairment. **e** After a single dose of lapatinib, *solid black diamonds* represent observed C_{max} with *error bars* symbolizing the 95 % confidence intervals and the *black line* is the corresponding linear regression trendline. The *solid gray line* represents the model-predicted C_{max}. The *dashed gray line* represents simulated C_{max} from the model with moderate hepatic impairment. The *dotted gray lines* represents simulated C_{max} from the model with severe hepatic impairment. **f** After multiple doses (q24 h) of lapatinib, *solid black diamonds* represent observed C_{max} with *error bars* symbolizing the 95 % confidence intervals and the *solid black line* is the corresponding linear regression trendline. The *solid gray line* represents the model-predicted C_{max}. The *dashed gray line* represents simulated C_{max} from the model with moderate hepatic impairment. The *dotted gray line* represents simulated C_{max} from the model with severe hepatic impairment

Table 4 Human tissue AUCs for single and multiple (q24 h) lapatinib doses

	100 mg single dose $AUC^{a}_{0-60\ h}$ (nM × h)	1,250 mg multiple dose q24 h AUC^{b}_{τ} (nM × h)	1,500 mg multiple dose q24 h AUC^{b}_{τ} (nM × h)
Plasma	2,409	30,631	36,757
Intestine	21,884	277,286	332,744
Liver	14,470	183,723	220,468
Kidney	12,817	162,959	195,550
Heart	2,590	32,929	39,514
Lung	19,792	251,637	301,964
Brain	121	1,532	1,838
Slowly perfused	783	9,955	11,946

[a] $AUC_{0-60\ h}$ is the area under the concentration–time curve from 0 to 60 h

[b] AUC_{τ} is the steady-state area under the concentration–time curve within the dosing interval (0–24 h)

The results along with the subject/patient characteristics (disease state, fasted or not fasted when administered lapatinib, liver function and age) are presented in Table 5 (single dose lapatinib) and Tables 6, 7 (multiple dose lapatinib). Graphically, observed and predicted AUCs are depicted in Fig. 4c, d. For the single dose comparison, all of the prediction errors were less than ±27.2 %, with a MPE% of 0.29 and a MAPE% of 7.7. The single dose prediction errors were smaller for the area under the concentration–time curve calculated from time 0 to infinity ($AUCs_{\infty}$) of healthy subjects (MPE% of 1.5 and MAPE% of 2.5, $n = 6$ studies) than for the $AUCs_{\infty}$ of patients with solid tumors (MPE% of −17.8 and MAPE% of 17.8, $n = 4$ studies), which was not surprising given that our model was developed with data from healthy subjects who presumably cleared (metabolized) lapatinib more efficiently than the patients with advanced solid malignancies, as they were both younger and had normal liver function. Thus, our model tended to underpredict the AUC_{∞} for the patients with solid tumors, as indicated by the negative value of the MPE%. For the multiple dose lapatinib study, the prediction errors were larger, with a MPE% of −29.9 and a MAPE% of 29.9. Again, the negative MPE% was the result of our model simulations underpredicting lapatinib exposure, likely due to impaired hepatic function related to the age and disease state of the test population ($n = 24$ studies with cancer patients and only three studies with healthy subjects) versus the healthy training population used to develop the PBPK model.

Previously, lapatinib pharmacokinetics were assessed in subjects with moderate or severe hepatic impairment (Child-Pugh scores of 7–9, or greater than 9, respectively) and in 8 healthy control subjects; after a single oral dose of 100 mg, the lapatinib AUC increased approximately 56 and 85 % in subjects with moderate and severe hepatic impairment, respectively [25]. To imitate this liver dysfunction in our model, we decreased the first-order rate constant for liver metabolism by 35 and 45 % and, accordingly, achieved AUC increases of 56 and 85 %, respectively. Decreased liver metabolism of this magnitude has been observed in aged patients; a review of 16 cytochrome P450 (CYP) 3A substrates showed an average 37.2 % reduction in the clearance of these substrates by elderly versus young volunteers or patients [26]. The resulting AUC predictions from our modified model are graphed in Fig. 4c, d. The $AUCs_{\infty}$ resulting from hepatic impairment in the single dose studies both overpredicted exposure, conceivably because 60 % of the studies were done in healthy subjects. In contrast, the moderately impaired liver function simulation more correctly reflected the observed $AUCs_{\tau}$ from the multiple dose lapatinib clinical trials in which 86 % of the studies were done in cancer patients. Thus, decreasing the liver metabolism in our model improves the lapatinib exposure predictions for cancer patients.

In addition to actual and simulated human lapatinib exposures, we also wanted to evaluate concentration–time curve shape parameters. Accordingly, we compared observed and predicted half-life, C_{max} and T_{max} (Tables 8, 9, 10). For single dose lapatinib, the model-predicted and mean observed ($n = 10$ studies) half-lives were 10.0 and 10.3 h, respectively. For multiple dose lapatinib, the model predicted and mean observed ($n = 6$ studies) half-lives were 10.2 and 16.6 h, respectively. Overall, half-life MPE% was −8.1 and MAPE% was 28.1. In healthy subjects, the model overpredicted the half-life in 78 % of the studies (MPE% of 14.6) and in cancer patients, the model underpredicted the half-life in all studies (MPE% of −38.0).

For single dose lapatinib, our model-predicted T_{max} to be at 3.75 h post administration and the average observed T_{max} was 3.7 h. The MPE% and MAPE% were −6.3 and 9.6, respectively. For multiple dose lapatinib, our model-predicted steady-state T_{max} was 3.5 h and the mean observed T_{max} was 3.5 h. The MPE% and MAPE% were 1.6 and 14.6, respectively.

Regarding C_{max}, the actual values versus our model-simulated values are graphically shown in Fig. 4e, f. The single dose predictions directly paralleled the actual C_{max} (MPE% and MAPE% of −28.8 and 28.8, respectively). For the multiple dose predictions, our model underestimated steady-state C_{max} (MPE% and MAPE% of −33.9 and 33.9, respectively). However, when we decreased liver metabolism to mimic hepatic impairment (as we did with AUC), the predicted steady-state C_{max} for moderate liver dysfunction closely mirrored the observed data.

Table 5 Single dose lapatinib observed and predicted human AUC_∞ and subject characteristics

Dose (mg)	Observed AUC_∞ (nM × h)	Predicted AUC_∞ (nM × h)	AUC_∞ PE%[c]	Subjects	Food	Bilirubin[d]	AST[d]	ALT[d]	Age (years)[e]	Reference
50	1,170 (756–1,817)[a]	1,225	4.7	Healthy	Fasted	Normal	Normal	Normal	22 (18–53)	[4]
100	2,096 (1,492–2,941)[a]	2,450	16.9	Healthy	Fasted	Normal	Normal	Normal	22 (18–53)	[4]
100	2,459 (2,062–2,933)[b]	2,450	−0.4	Healthy	Not fasted	Normal	Normal	Normal	28 (20–47)	[14]
175	4,206 (2,588–6,834)[a]	4,288	1.9	Healthy	Fasted	Normal	Normal	Normal	22 (18–53)	[4]
250	6,313 (4,550–8,758)[a]	6,126	−3.0	Healthy	Fasted	Normal	Normal	Normal	22 (18–53)	[4]
250	6,068 (4,970–7,411)[b]	6,126	1.0	Healthy	Not fasted	Normal	Normal	Normal	29 (20–48)	[14]
900	30,250 (20,328–45,011)[a]	22,054	−27.1	Cancer	Fasted	≤1.5× ULN	≤2.5× ULN	≤2.5× ULN	60 (37–73)	[13]
1,200	26,574 (12,753–55,375)[a]	29,405	10.7	Cancer	Fasted	≤1.5× ULN	≤2.5× ULN	≤2.5× ULN	60 (37–73)	[13]
1,600	45,367 (30,150–68,263)[a]	39,207	−13.6	Cancer	Fasted	≤1.5× ULN	≤2.5× ULN	≤2.5× ULN	60 (37–73)	[13]
1,800	56,519 (32,499–98,293)[a]	44,108	−22.0	Cancer	Fasted	≤1.5× ULN	≤2.5× ULN	≤2.5× ULN	60 (37–73)	[13]

[a] AUC_∞ is the geometric mean (95 % confidence interval) of the area under the concentration–time curve calculated from time 0 to infinity

[b] AUC_∞ is the geometric mean (range) of the area under the concentration–time curve calculated from time 0 to infinity

[c] PE% is the prediction error

[d] Bilirubin, aspartate transaminase (AST) and alanine transaminase (ALT) are measures of liver function. ULN is upper limit of normal

[e] Median age (range)

Overall, our PBPK model properly predicted lapatinib pharmacokinetic parameters from actual populations. As our model was developed with data from healthy subjects, the predictions were better for studies which were conducted in healthy subjects versus patients with solid tumors. To improve our model simulations for cancer patients, we altered our liver metabolism parameter to reflect hepatic impairment resulting from disease and/or age. With this modification, the model more precisely reproduced actual AUCs and C_{max} from patients with solid tumors.

Sensitivity analysis

The normalized sensitivity coefficients for the mouse (60 mg/kg dose) and human (100 mg dose) PBPK models with respect to plasma AUC are shown in Fig. 5. Only parameters with sensitivity coefficients greater than 0.1 are shown. In both models, no normalized sensitivity coefficient was greater than ±1, indicating that there are no amplified parameter errors.

Discussion

Physiologically based pharmacokinetic models have been developed for numerous antineoplastic agents including methotrexate [27, 28], cisplatin [29], actinomycin-D [30], 5-fluorouracil [31], capecitabine [32], 1-β-D-arabinofuranosylcytosine [33], adriamycin [34–36], topotecan [37] and docetaxel [38]. The need for these types of pharmacokinetic models for chemotherapeutics is great because of the challenges presented by this class of pharmaceutical compounds, specifically the narrow therapeutic index which is governed by drug distribution in the body. With PBPK modeling, the dynamics of drug distribution can be predicted using basic information on physiochemical properties, transport, biotransformation and excretion, thus leading to a better understanding of target tissue exposure resulting in either a therapeutic or toxic effect.

We have successfully developed a first-generation PBPK model for the dual EGFR/HER2 tyrosine kinase inhibitor lapatinib. This drug is a mere decade old and has only been approved by the FDA for the treatment of breast cancer since 2007. Consequently, the intricacies of the pharmacokinetics are still being elucidated. To our knowledge, the details of mouse tissue distribution of lapatinib have been limited to plasma and brain [39, 40] whereas, in humans, only plasma concentrations have been determined [3–15]. The tissue distribution of [^{14}C] lapatinib was resolved by whole-body autoradiography in rats with detectable amounts quantified in the blood, brain, cerebrospinal fluid, harderian gland, heart, kidney, liver and muscle [41]. Our mouse data

Table 6 Multiple dose lapatinib (25–1,200 mg) observed and predicted human AUC_τ and subject characteristics

Dose (mg)	Observed AUC_τ (nM × h)[a]	Predicted AUC_τ (nM × h)	AUC_τ PE%[b]	Subjects	Food	Bilirubin[c]	AST[c]	ALT[c]	Age (years)[d]	Reference
25	515 (329–809)	613	19.1	Healthy	Fasted	Normal	Normal	Normal	22 (19–38)	[4]
100	25,68 (1,594–4,137)	2,450	−4.6	Healthy	Fasted	Normal	Normal	Normal	22 (19–38)	[4]
175	4,869 (3,313–7,154)	4,288	−11.9	Healthy	Fasted	Normal	Normal	Normal	22 (19–38)	[4]
175	9,431	4,288	−54.5	Cancer	Fasted	≤2 mg/dL	≤3.0× ULN	≤3.0× ULN	61 (25–80)	[15]
375	9,878	9,189	−7.0	Cancer	Fasted	≤2 mg/dL	≤3.0× ULN	≤3.0× ULN	62 (25–81)	[15]
500	23,922 (17,107–33,731)	12,252	−48.8	Cancer	Not fasted	≤2 mg/dL	≤3.0× ULN	≤3.0× ULN	56 (28–74)	[5]
650	27,020 (20,480–35,797)	15,928	−41.1	Cancer	Not fasted	≤2 mg/dL	≤3.0× ULN	≤3.0× ULN	60 (37–82)	[5]
675	23,578	16,540	−29.8	Cancer	Fasted	≤2 mg/dL	≤3.0× ULN	≤3.0× ULN	63 (25–82)	[15]
900	21,857	22,054	0.9	Cancer	Fasted	≤2 mg/dL	≤3.0× ULN	≤3.0× ULN	64 (25–83)	[15]
900	40,099 (28,052–57,481)	22,054	−45.0	Cancer	Not fasted	≤2 mg/dL	≤3.0× ULN	≤3.0× ULN	57 (34–82)	[5]
900	50,377 (37,204–68,217)	22,054	−56.2	Cancer	Fasted	≤1.5× ULN	≤2.5× ULN	≤2.5× ULN	60 (37–73)	[13]
1,000	40,615 (35,452–46,639)	24,504	−39.7	Cancer	Not fasted	≤2 mg/dL	≤3.0× ULN	≤3.0× ULN	53 (43–59)	[5]
1,000	35,280 (26,847–46,295)	24,504	−30.5	Cancer	Fasted	Adequate	Adequate	Adequate	53 (30–80)	[9]
1,200	24,610 (16,212–37,518)	29,405	19.5	Cancer	Not fasted	≤2 mg/dL	≤3.0× ULN	≤3.0× ULN	54 (37–67)	[5]
1,200	44,195 (23,626–82,673)	29,405	−33.5	Cancer	Fasted	≤1.5× ULN	≤2.5× ULN	≤2.5× ULN	60 (37–73)	[13]
1,200	29,773	29,405	−1.2	Cancer	Fasted	≤2 mg/dL	≤3.0× ULN	≤3.0× ULN	65 (25–84)	[15]

[a] AUC_τ is the geometric mean (95 % confidence interval) of the steady-state area under the concentration–time curve calculated within the dosing interval (0–24 h)

[b] PE% is the prediction error

[c] Bilirubin, aspartate transaminase (AST) and alanine transaminase (ALT) are measures of liver function. ULN is upper limit of normal

[d] Median age (range)

Table 7 Multiple dose lapatinib (1,250–1,800 mg) observed and predicted human AUC_τ and subject characteristics

Dose (mg)	Observed AUC_τ (nM × h)	Predicted AUC_τ (nM × h)	AUC_τ PE%[c]	Subjects	Food	Bilirubin[d]	AST[d]	ALT[d]	Age (years)[e]	Reference
1,250	62,300 (40,271–96,376)[a]	30,631	−50.8	Cancer	Not fasted	≤1.5 mg/dL	≤2.0× ULN	≤2.0× ULN	58.3 (2–79)	[7]
1,250	68,840 (50,425–94,138)[b]	30,631	−55.5	Cancer	Not fasted	Significant dysfunction excluded			58 (34–78)	[8]
1,250	24,438 (11,789–50,941)[b]	30,631	25.3	Cancer	Fasted	≤1.5 mg/dL	≤2.0× ULN	≤2.0× ULN	59 (19–74)	[10]
1,250	40,099 (24,954–64,193)[b]	30,631	−23.6	Cancer	Not fasted	≤2.0× ULN	≤5.0× ULN	≤5.0× ULN	57.5 (33–74)	[12]
1,500	46,639 (32,699–66,430)[b]	36,757	−21.2	Cancer	Not fasted	≤1.5 mg/dL	≤2.0× ULN	≤2.0× ULN	59.5 (39–73)	[6]
1,500	54,900 (29,601–101,833)[b]	36,757	−33.0	Cancer	Fasted	≤1.5 mg/dL	≤3.0× ULN	≤3.0× ULN	57 (31–73)	[11]
1,600	50,597 (27,364–93,450)[b]	39,207	−22.5	Cancer	Not fasted	≤2.0 mg/dL	≤3.0× ULN	≤3.0× ULN	55 (38–70)	[5]
1,600	87,941 (49,348–156,717)[b]	39,207	−55.4	Cancer	Fasted	≤1.5× ULN	≤2.5 × ULN	≤2.5× ULN	60 (37–73)	[13]
1,600	39,067[b]	39,207	0.4	Cancer	Fasted	≤2.0 mg/dL	≤3.0× ULN	≤3.0× ULN	66 (25–85)	[15]
1,800	47,671[b]	44,108	−7.5	Cancer	Fasted	≤2.0 mg/dL	≤3.0× ULN	≤3.0× ULN	67 (25–86)	[15]
1,800	67,895 (25,658–179,656)[b]	44,108	−35.0	Cancer	Fasted	≤1.5× ULN	≤2.5 × ULN	≤2.5× ULN	60 (37–73)	[13]

[a] AUC_τ is the mean (90 % confidence interval) of the steady-state area under the concentration–time curve calculated within the dosing interval (0–24 h)

[b] AUC_τ is the geometric mean (95 % confidence interval) of the steady-state area under the concentration–time curve calculated within the dosing interval (0–24 h)

[c] PE% is the prediction error

[d] Bilirubin, aspartate transaminase (AST) and alanine transaminase (ALT) are measures of liver function. ULN is upper limit of normal

[e] Median age (range)

Table 8 Single dose lapatinib observed and predicted human half-life ($t_{1/2}$), maximum concentration (C_{max}) and time of maximum concentration (T_{max})

Dose (mg)	Observed $t_{1/2}$ (h)	Predicted $t_{1/2}$ (h)	$T_{1/2}$ PE%[c]	Observed C_{max} (nM)	Predicted C_{max} (nM)	C_{max} PE%[c]	Observed T_{max} (h)	Predicted T_{max} (h)	T_{max} PE%[c]	Reference
50	6.0[a] (4.8–7.5)	10.0	66.7	124 (88–177)[d]	66	−46.7	3.0 (2.0–6.0)[f]	3.75	25.0	[4]
100	6.3[a] (5.6–7.0)	10.0	58.7	213 (148–308)[d]	132	−38.1	4.0 (2.5–5.9)[f]	3.75	−6.3	[4]
100	9.6[a] (8.5–10.7)	10.0	4.2	198 (174–224)[e]	132	−33.3	4.0 (2.5–8.0)[f]	3.75	−6.3	[14]
175	8.2[a] (6.7–9.9)	10.0	22.0	380 (241–599)[d]	231	−39.3	3.0 (2.0–4.0)[f]	3.75	25.0	[4]
250	8.8[a] (6.6–11.7)	10.0	13.6	546 (330–902)[d]	329	−39.7	4.0 (3.0–6.0)[f]	3.75	−6.3	[4]
250	10.2[a] (9.24–11.3)	10.0	−2.0	449 (360–563)[e]	329	−26.8	4.0 (2.5–6.0)[f]	3.75	−6.3	[14]
900	12.9[b] (10.1–18.3)	10.0	−22.5	1,740 (1,194–2,533)[d]	1,185	−31.9	4.0 (2.0–6.0)[g]	3.75	−6.3	[13]
1,200	11.5[b] (10.1–19.5)	10.0	−13.0	1,767 (816–3,833)[d]	1,581	−10.5	3.5 (2.1–6.0)[g]	3.75	7.1	[13]
1,600	13.9[b] (9.6–18.0)	10.0	−28.1	2,647 (1,793–3,903)[d]	2,107	−20.4	4.0 (2.0–8.0)[g]	3.75	−6.3	[13]
1,800	15.7[b] (11.0–133.1)	10.0	−36.3	2,112 (800–5,579)[d]	2,371	12.3	3.9 (3.0–8.0)[g]	3.75	−3.8	[13]

[a] $t_{1/2}$ is the terminal half-life geometric mean (95 % confidence interval)

[b] $t_{1/2}$ is the terminal half-life median (95 % confidence interval)

[c] PE% is the prediction error

[d] Is the geometric mean (95 % confidence interval) of C_{max}

[e] Is the geometric mean (range) of C_{max}

[f] Is the median (range) of T_{max}

[g] Is the median (95 % confidence interval) of T_{max}

demonstrated tissue:blood concentration ratios that were comparable to those presented by Polli et al. [41], indicating that lapatinib exhibits similar distribution dynamics in these two rodents. Considering the autoradiography data [41] and the work presented herein, we now have a comprehensive assessment of the biodistribution of lapatinib in rats and mice.

By incorporating the mouse tissue distribution data into a PBPK model, we were able to effectively predict lapatinib concentrations in mouse plasma, brain, heart, lung, kidney, intestine, liver and slowly perfused tissue after oral doses of 30, 60 and 90 mg/kg. Subsequently, by taking into account interspecies differences in physiology and physiochemistry, we extrapolated this PBPK model to humans. To validate the human model, we were only able to compare our model simulations with observed plasma lapatinib concentrations and pharmacokinetic parameters, as there is no data in the literature regarding human tissue levels. Our model correctly predicted plasma exposure [23], C_{max}, T_{max} and half-life following single doses of lapatinib ranging from 50 to 1,800 mg and following multiple doses of lapatinib ranging from 25 to 1,800 mg. After taking the clinical trial subject/patient characteristics into consideration, it was evident that our model predictions were more accurate for healthy subjects than for patients with solid tumors (whose AUCs and C_{max} were consistently underpredicted). This was not surprising given that our human PBPK model was developed with data from healthy subjects. In addition to the absence or presence of solid malignancies, the other major biological differences between these two populations were age and liver function. Both most likely contribute to hepatic impairment which results in a decrease in lapatinib clearance via metabolism and a subsequent increase in tissue exposure. When we altered our PBPK model to mimic hepatic impairment by decreasing the first-order rate constant for liver metabolism, the simulations for moderate hepatic impairment (incorporated as a 35 % decrease in liver metabolism) closely reflected the observed AUC and C_{max}

Table 9 Multiple dose lapatinib (25–1,200 mg) observed and predicted human half-life ($t_{1/2}$), maximum concentration (C_{max}) and time of maximum concentration (T_{max})

Dose (mg)	Observed $t_{1/2}$ (h)	Predicted $t_{1/2}$ (h)	$t_{1/2}$ PE%[c]	Observed C^{d}_{max} (nM)	Predicted C_{max} (nM)	C_{max} PE%[c]	Observed T_{max} (h)	Predicted T_{max} (h)	T_{max} PE%[c]	Reference
25	7.9[a] (6.4–9.8)	10.2	29.1	55 (38–81)	42	−23.7	2.7 (2.5–4.0)[e]	3.5	29.6	[4]
100	8.9[a] (6.1–12.9)	10.2	14.6	251 (150–420)	166	−33.9	3.0 (2.0–6.0)[e]	3.5	16.7	[4]
175	11.1[a] (7.3–16.8)	10.2	−8.1	429 (270–678)	290	−32.3	4.0 (3.0–6.0)[e]	3.5	−12.5	[4]
175	ND	10.2	NA	637	290	−54.5	ND	3.5	NA	[15]
375	ND	10.2	NA	706	622	−11.8	ND	3.5	NA	[15]
500	ND	10.2	NA	1,755 (1,308–2,375)	830	−52.7	ND	3.5	NA	[5]
650	ND	10.2	NA	2,237 (1,687–2,960)	1,078	−51.8	ND	3.5	NA	[5]
675	ND	10.2	NA	1,824	1,120	−38.6	ND	3.5	NA	[15]
900	ND	10.2	NA	1,807	1,493	−17.4	ND	3.5	NA	[15]
900	ND	10.2	NA	2,926 (2,082–4,130)	1,493	−49.0	ND	3.5	NA	[5]
900	23.1[b] (9.8–38.2)	10.2	−55.8	3,261 (2,270–4,683)	1,493	−54.2	4.0 (3.0–6.0)[f]	3.5	−12.5	[13]
1,000	ND	10.2	NA	3,184 (2,409–4,216)	1,659	−47.9	ND	3.5	NA	[5]
1,000	ND	10.2	NA	2,754 (2,203–3,442)	1,659	−39.8	ND	3.5	NA	[9]
1,200	ND	10.2	NA	2,100 (1,549–2,840)	1,990	−5.2	ND	3.5	NA	[5]
1,200	16.9[b] (15.1–34.3)	10.2	−39.6	2,952 (1,661–5,246)	1,990	−32.6	3.6 (3.0–7.9)[f]	3.5	−2.8	[13]
1,200	ND	10.2	NA	2,392	1,990	−16.8	ND	3.5	NA	[15]

ND not determined, *NA* not applicable

[a] $t_{1/2}$ is the terminal half-life geometric mean (95 % confidence interval)

[b] $t_{1/2}$ is the terminal half-life median (95 % confidence interval)

[c] PE% is the prediction error

[d] Is the geometric mean (95 % confidence interval) of C_{max}

[e] Is the median (range) of T_{max}

[f] Is the median (95 % confidence interval) of T_{max}

Table 10 Multiple dose lapatinib (1,250–1,800 mg) observed and predicted human half-life ($t_{1/2}$), maximum concentration (C_{max}) and time of maximum concentration (T_{max})

Dose (mg)	Observed $t_{1/2}$ (h)[a]	Predicted $t_{1/2}$ (h)	$t_{1/2}$ PE%[b]	Observed $C^{\S}_{max}$ (nM)	Predicted C_{max} (nM)	C_{max} PE%[b]	Observed T_{max} (h)	Predicted T_{max} (h)	T_{max} PE%[b]	Reference
1,250	ND	10.2	NA	4,182 (2,702–6,488)[c]	2,073	−50.4	3.5 (2.0–10)[e]	3.5	0	[7]
1,250	ND	10.2	NA	4,870 (3,700–6,419)[d]	2,073	−57.4	ND	3.5	NA	[8]
1,250	ND	10.2	NA	2,220 (1,119–4,389)[d]	2,073	−6.6	3.0 (1.5–8.0)[f]	3.5	16.7	[10]
1,250	ND	10.2	NA	3,253 (2,289–4,612)[d]	2,073	−36.3	3.0 (2.6–8.0)[f]	3.5	16.7	[12]
1,500	ND	10.2	NA	3,390 (2,547–4,526)[d]	2,488	−26.6	3.4 (0.0–6.0)[f]	3.5	3.2	[6]
1,500	ND	10.2	NA	4,251 (2,530–7,108)[d]	2,488	−41.5	3.0 (0.0–12.2)[f]	3.5	16.7	[11]
1,600	ND	10.2	NA	3,666 (2,341–5,765)[d]	2,654	−27.6	ND	3.5	NA	[5]
1,600	26.2 (12.9–48.3)	10.2	−61.1	5,354 (3,334–8,598)[d]	2,654	−50.4	5.1 (0.9–8.0)[g]	3.5	−31.4	[13]
1,600	ND	10.2	NA	3,304[d]	2,654	−19.7	ND	3.5	NA	[15]
1,800	ND	10.2	NA	3,253[d]	2,986	−8.2	ND	3.5	NA	[15]
1,800	21.8 (18.5–104.5)	10.2	−53.2	4,015 (1,595–10,102)[d]	2,986	−25.6	3.9 (3.0–7.9)[g]	3.5	−10.3	[13]

ND not determined, *NA* not applicable

[a] $t_{1/2}$ is the terminal half-life median (95 % confidence interval)

[b] PE% is the prediction error

[c] Is the mean (90 % confidence interval) of C_{max}

[d] Is the geometric mean (95 % confidence interval) of C_{max}

[e] Is the median (90 % confidence interval) of T_{max}

[f] Is the median (range) of T_{max}

[g] Is the median (95 % confidence interval) of T_{max}

in cancer patients. Thus, our model can not only predict lapatinib plasma pharmacokinetics in healthy subjects but, with a minor metabolic alteration, can also predict the pharmacokinetics of this drug in the plasma of patients with solid malignancies.

The human PBPK model additionally facilitates the estimation of tissue levels of lapatinib. There is incredible utility in this application of the model, as it is not feasible to collect actual tissue concentration data from humans. Based on the adverse reactions to lapatinib observed in clinical trials, we can speculate as to the organ distribution of this drug. It is probable that the heart, liver, intestine and lung are exposed to significant levels of lapatinib as patients administered this compound have experienced decreased left ventricular ejection fraction, QT prolongation, hepatotoxicity, diarrhea and interstitial lung disease/pneumonitis. From largest to smallest, our multiple dose (1,250 mg q24 h) model-predicted ratios of lapatinib tissue:plasma $AUCs_{\tau}$ were intestine (9.1), lung (8.2), liver (6.0), kidney (5.3), heart (1.1), slowly perfused tissue (0.3) and brain (0.05). Thus, for all organs in which adverse reactions to lapatinib have been noted, our model predicted tissue:plasma AUC ratios greater than 1, indicating substantial distribution into these tissues. Regarding brain, our model predicted low levels of lapatinib, which is consistent with the poor central nervous system (CNS) penetration observed in mice, owing to ABCB1- and ABCB2-mediated efflux [39]. Despite low lapatinib exposure in normal brain tissue, this drug has been shown to reduce the burden of metastatic breast cancer cells in the brains of mice [42] and have a modest CNS antitumor activity in human patients with brain metastases from HER2-positive breast cancer [43].

In summary, we have been able to successfully develop a PBPK model of lapatinib in mice, scale this model to humans and accurately predict the pharmacokinetics of this drug in human plasma over a wide range of doses. Additionally, our

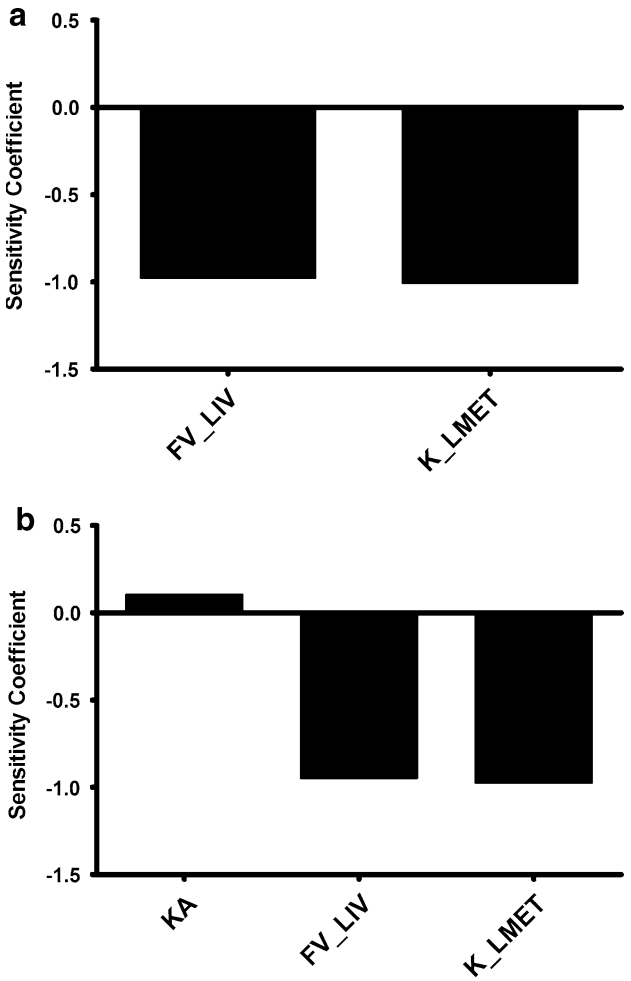

Fig. 5 Calculated sensitivity coefficients for PBPK model parameters with respect to plasma AUC for the (**a**) mouse model and (**b**) human single dose model. Only parameters with sensitivity coefficients >0.1 are shown. *FV_LIV* fractional volume of liver, *K_LMET* first-order rate constant for liver metabolism; and *KA* first-order rate constant for absorption from intestinal lumen

model also facilitated the estimation of various tissue exposures to lapatinib, which harmonize with the organ-specific toxicities documented in clinical trials. We acknowledge that this is a first-generation PBPK model which can be further improved with a greater understanding of lapatinib absorption, distribution, metabolism and excretion garnered from subsequent in vitro and in vivo studies. Moreover, our base model can be expanded to include other pharmacokinetic determinants, including efflux transporters, metabolite generation, combination dosing, etc., to make this PBPK model even more beneficial for the prediction of lapatinib disposition in both mouse and man.

Acknowledgments We are grateful to Jerry L. Campbell (Center for Human Health Assessment, The Hamer Institutes for Health Sciences, Research Triangle Park, Durham, NC, USA), Conrad Housand (The AEgis Technologies Group, Oshawa, ON, USA) and Robin McDougall (The AEgis Technologies Group, Oshawa, ON, USA) for all of their help and guidance with this project. This work was supported in part by Grant number W81XWH-09-1-0457 from the Department of Defense (DOD) Breast Cancer Research Program (BCRP) of the Office of the Congressionally Directed Medical Research Programs (CDMRP).

Conflict of interest The authors declare that they have no conflict of interest.

References

1. GlaxoSmithKline (2012) Tykerb prescribing information. http://us.gsk.com/products/assets/us_tykerb.pdf. Accessed 01 July 2012
2. www.clinicaltrials.gov
3. Gaul MD, Guo Y, Affleck K, Cockerill GS, Gilmer TM, Griffin RJ, Guntrip S, Keith BR, Knight WB, Mullin RJ, Murray DM, Rusnak DW, Smith K, Tadepalli S, Wood ER, Lackey K (2003) Discovery and biological evaluation of potent dual ErbB-2/EGFR tyrosine kinase inhibitors: 6-thiazolylquinazolines. Bioorg Med Chem Lett 13(4):637–640
4. Bence AK, Anderson EB, Halepota MA, Doukas MA, DeSimone PA, Davis GA, Smith DA, Koch KM, Stead AG, Mangum S, Bowen CJ, Spector NL, Hsieh S, Adams VR (2005) Phase I pharmacokinetic studies evaluating single and multiple doses of oral GW572016, a dual EGFR-ErbB2 inhibitor, in healthy subjects. Invest New Drugs 23(1):39–49
5. Burris HA III, Hurwitz HI, Dees EC, Dowlati A, Blackwell KL, O'Neil B, Marcom PK, Ellis MJ, Overmoyer B, Jones SF, Harris JL, Smith DA, Koch KM, Stead A, Mangum S, Spector NL (2005) Phase I safety, pharmacokinetics, and clinical activity study of lapatinib (GW572016), a reversible dual inhibitor of epidermal growth factor receptor tyrosine kinases, in heavily pretreated patients with metastatic carcinomas. J Clin Oncol 23(23):5305–5313
6. Siegel-Lakhai WS, Beijnen JH, Vervenne WL, Boot H, Keessen M, Versola M, Koch KM, Smith DA, Pandite L, Richel DJ, Schellens JH (2007) Phase I pharmacokinetic study of the safety and tolerability of lapatinib (GW572016) in combination with oxaliplatin/fluorouracil/leucovorin (FOLFOX4) in patients with solid tumors. Clin Cancer Res 13(15 Pt 1):4495–4502
7. Chu QS, Schwartz G, de Bono J, Smith DA, Koch KM, Versola MJ, Pandite L, Arya N, Curtright J, Fleming RA, Ho PT, Rowinsky EK (2007) Phase I and pharmacokinetic study of lapatinib in combination with capecitabine in patients with advanced solid malignancies. J Clin Oncol 25(24):3753–3758
8. Midgley RS, Kerr DJ, Flaherty KT, Stevenson JP, Pratap SE, Koch KM, Smith DA, Versola M, Fleming RA, Ward C, O'Dwyer PJ, Middleton MR (2007) A phase I and pharmacokinetic study of lapatinib in combination with infusional 5-fluorouracil, leucovorin and irinotecan. Ann Oncol 18(12):2025–2029
9. Storniolo AM, Pegram MD, Overmoyer B, Silverman P, Peacock NW, Jones SF, Loftiss J, Arya N, Koch KM, Paul E, Pandite L, Fleming RA, Lebowitz PF, Ho PT, Burris HA 3rd (2008) Phase I dose escalation and pharmacokinetic study of lapatinib in combination with trastuzumab in patients with advanced ErbB2-positive breast cancer. J Clin Oncol 26(20):3317–3323
10. LoRusso PM, Jones SF, Koch KM, Arya N, Fleming RA, Loftiss J, Pandite L, Gadgeel S, Weber BL, Burris HA III (2008) Phase I and pharmacokinetic study of lapatinib and docetaxel in patients with advanced cancer. J Clin Oncol 26(18):3051–3056
11. Chu QS, Cianfrocca ME, Goldstein LJ, Gale M, Murray N, Loftiss J, Arya N, Koch KM, Pandite L, Fleming RA, Paul E,

Rowinsky EK (2008) A phase I and pharmacokinetic study of lapatinib in combination with letrozole in patients with advanced cancer. Clin Cancer Res 14(14):4484–4490
12. Molina JR, Kaufmann SH, Reid JM, Rubin SD, Galvez-Peralta M, Friedman R, Flatten KS, Koch KM, Gilmer TM, Mullin RJ, Jewell RC, Felten SJ, Mandrekar S, Adjei AA, Erlichman C (2008) Evaluation of lapatinib and topotecan combination therapy: tissue culture, murine xenograft, and phase I clinical trial data. Clin Cancer Res 14(23):7900–7908
13. Nakagawa K, Minami H, Kanezaki M, Mukaiyama A, Minamide Y, Uejima H, Kurata T, Nogami T, Kawada K, Mukai H, Sasaki Y, Fukuoka M (2009) Phase I dose-escalation and pharmacokinetic trial of lapatinib (GW572016), a selective oral dual inhibitor of ErbB-1 and -2 tyrosine kinases, in Japanese patients with solid tumors. Jpn J Clin Oncol 39(2):116–123
14. Smith DA, Koch KM, Arya N, Bowen CJ, Herendeen JM, Beelen A (2009) Effects of ketoconazole and carbamazepine on lapatinib pharmacokinetics in healthy subjects. Br J Clin Pharmacol 67(4):421–426
15. Burris HA III, Taylor CW, Jones SF, Koch KM, Versola MJ, Arya N, Fleming RA, Smith DA, Pandite L, Spector N, Wilding G (2009) A phase I and pharmacokinetic study of oral lapatinib administered once or twice daily in patients with solid malignancies. Clin Cancer Res 15(21):6702–6708
16. Krishnan K, Loizou GD, Spendiff M, Lipscomb JC, Andersen ME (2010) PBPK modeling: a primer. In: Krishnan K, Andersen ME (eds) Quantitative modeling in toxicology, vol 17. Wiley, Chichester, p 485
17. Andersen ME, Yang RSH, Clewell HJ III, Reddy MB (2005) Introduction: a historical perspective of the development and applications of PBPK models. In: Reddy MB, Yang RSH, Clewell HJ III, Andersen ME (eds) Physiologically based pharmacokinetic modeling: science and applications, vol 19. Wiley-Interscience, Hoboken, p 420
18. Bai F, Freeman BB III, Fraga CH, Fouladi M, Stewart CF (2006) Determination of lapatinib (GW572016) in human plasma by liquid chromatography electrospray tandem mass spectrometry (LC-ESI-MS/MS). J Chromatogr B Analyt Technol Biomed Life Sci 831(1–2):169–175
19. Brown RP, Delp MD, Lindstedt SL, Rhomberg LR, Beliles RP (1997) Physiological parameter values for physiologically based pharmacokinetic models. Toxicol Ind Health 13(4):407–484
20. Sheiner LB, Beal SL (1981) Some suggestions for measuring predictive performance. J Pharmacokinet Biopharm 9(4):503–512
21. Wu G (1995) Calculating predictive performance: a user's note. Pharmacol Res 31(6):393–399
22. Loccisano AE, Campbell JL Jr, Butenhoff JL, Andersen ME, Clewell HJ III (2012) Comparison and evaluation of pharmacokinetics of PFOA and PFOS in the adult rat using a physiologically based pharmacokinetic model. Reprod Toxicol 33(4):452–467
23. Castellino S, O'Mara M, Koch K, Borts DJ, Bowers GD, MacLauchlin C (2012) Human metabolism of lapatinib, a dual kinase inhibitor: implications for hepatotoxicity. Drug Metab Dispos 40(1):139–150
24. Kwara A, Lartey M, Sagoe KW, Rzek NL, Court MH (2009) CYP2B6 (c.516G–>T) and CYP2A6 (*9B and/or *17) polymorphisms are independent predictors of efavirenz plasma concentrations in HIV-infected patients. Br J Clin Pharmacol 67(4):427–436
25. GlaxoSmithKline (2010) Tyverb prescribing information. http://www.ema.europa.eu/docs/en_GB/document_library/EPAR_-_Product_Information/human/000795/WC500044957.pdf. Accessed 01 July 2012
26. Cotreau MM, von Moltke LL, Greenblatt DJ (2005) The influence of age and sex on the clearance of cytochrome P450 3A substrates. Clin Pharmacokinet 44(1):33–60
27. Bischoff KB, Dedrick RL, Zaharko DS (1970) Preliminary model for methotrexate pharmacokinetics. J Pharm Sci 59(2):149–154
28. Bischoff KB, Dedrick RL, Zaharko DS, Longstreth JA (1971) Methotrexate pharmacokinetics. J Pharm Sci 60(8):1128–1133
29. Evans WE, Crom WR, Tsiatis A, Green AA, Hayes FA, Pratt CB (1982) Pharmacokinetic modeling of cisplatin disposition in children and adolescents with cancer. Cancer Chemother Pharmacol 10(1):22–26
30. Lutz RJ, Galbraith WM, Dedrick RL, Shrager R, Mellett LB (1977) A model for the kinetics of distribution of actinomycin-D in the beagle dog. J Pharmacol Exp Ther 200(3):469–478
31. Collins JM, Dedrick RL, King FG, Speyer JL, Myers CE (1980) Nonlinear pharmacokinetic models for 5-fluorouracil in man: intravenous and intraperitoneal routes. Clin Pharmacol Ther 28(2):235–246
32. Tsukamoto Y, Kato Y, Ura M, Horii I, Ishitsuka H, Kusuhara H, Sugiyama Y (2001) A physiologically based pharmacokinetic analysis of capecitabine, a triple prodrug of 5-FU, in humans: the mechanism for tumor-selective accumulation of 5-FU. Pharm Res 18(8):1190–1202
33. Dedrick RL, Forrester DD, Ho DH (1972) In vitro-in vivo correlation of drug metabolism—deamination of 1- -D-arabinofuranosylcytosine. Biochem Pharmacol 21(1):1–16
34. Harris PA, Gross JF (1975) Preliminary pharmacokinetic model for adriamycin (NSC-123127). Cancer Chemother Rep 59(4):819–825
35. Chan KK, Cohen JL, Gross JF, Himmelstein KJ, Bateman JR, Tsu-Lee Y, Marlis AS (1978) Prediction of adriamycin disposition in cancer patients using a physiologic, pharmacokinetic model. Cancer Treat Rep 62(8):1161–1171
36. Gustafson DL, Rastatter JC, Colombo T, Long ME (2002) Doxorubicin pharmacokinetics: macromolecule binding, metabolism, and excretion in the context of a physiologic model. J Pharm Sci 91(6):1488–1501
37. Sung C, Blaney SM, Cole DE, Balis FM, Dedrick RL (1994) A pharmacokinetic model of topotecan clearance from plasma and cerebrospinal fluid. Cancer Res 54(19):5118–5122
38. Bradshaw-Pierce EL, Eckhardt SG, Gustafson DL (2007) A physiologically based pharmacokinetic model of docetaxel disposition: from mouse to man. Clin Cancer Res 13(9):2768–2776
39. Polli JW, Olson KL, Chism JP, John-Williams LS, Yeager RL, Woodard SM, Otto V, Castellino S, Demby VE (2009) An unexpected synergist role of P-glycoprotein and breast cancer resistance protein on the central nervous system penetration of the tyrosine kinase inhibitor lapatinib (*N*-{3-chloro-4-[(3-fluorobenzyl)oxy]phenyl}-6-[5-({[2-(methylsulfonyl)ethyl]amino}methyl)-2-furyl]-4-quinazolinamine; GW572016). Drug Metab Dispos 37(2):439–442
40. Taskar KS, Rudraraju V, Mittapalli RK, Samala R, Thorsheim HR, Lockman J, Gril B, Hua E, Palmieri D, Polli JW, Castellino S, Rubin SD, Lockman PR, Steeg PS, Smith QR (2012) Lapatinib distribution in HER2 overexpressing experimental brain metastases of breast cancer. Pharm Res 29(3):770–781
41. Polli JW, Humphreys JE, Harmon KA, Castellino S, O'Mara MJ, Olson KL, John-Williams LS, Koch KM, Serabjit-Singh CJ (2008) The role of efflux and uptake transporters in [*N*-{3-chloro-4-[(3-fluorobenzyl)oxy]phenyl}-6-[5-({[2-(methylsulfonyl)ethyl]amino}methyl)-2-furyl]-4-quinazolinamine (GW572016, lapatinib) disposition and drug interactions. Drug Metab Dispos 36(4):695–701
42. Gril B, Palmieri D, Bronder JL, Herring JM, Vega-Valle E, Feigenbaum L, Liewehr DJ, Steinberg SM, Merino MJ, Rubin SD, Steeg PS (2008) Effect of lapatinib on the outgrowth of metastatic breast cancer cells to the brain. J Natl Cancer Inst 100(15):1092–1103
43. Lin NU, Dieras V, Paul D, Lossignol D, Christodoulou C, Stemmler HJ, Roche H, Liu MC, Greil R, Ciruelos E, Loibl S, Gori S, Wardley A, Yardley D, Brufsky A, Blum JL, Rubin SD,

Dharan B, Steplewski K, Zembryki D, Oliva C, Roychowdhury D, Paoletti P, Winer EP (2009) Multicenter phase II study of lapatinib in patients with brain metastases from HER2-positive breast cancer. Clin Cancer Res 15(4):1452–1459

44. Chen HS, Gross JF (1979) Estimation of tissue-to-plasma partition coefficients used in physiological pharmacokinetic models. J Pharmacokinet Biopharm 7(1):117–125
45. Perloff MD, Von Moltke LL, Greenblatt DJ (2003) Differential metabolism of midazolam in mouse liver and intestine microsomes: a comparison of cytochrome P450 activity and expression. Xenobiotica 33(4):365–377
46. Hietanen E, Vainio H (1973) Interspecies variations in small intestinal and hepatic drug hydroxylation and glucuronidation. Acta Pharmacol Toxicol (Copenh) 33(1):57–64
47. Zhang QY, Dunbar D, Kaminsky LS (2003) Characterization of mouse small intestinal cytochrome P450 expression. Drug Metab Dispos 31(11):1346–1351
48. Paine MF, Khalighi M, Fisher JM, Shen DD, Kunze KL, Marsh CL, Perkins JD, Thummel KE (1997) Characterization of interintestinal and intraintestinal variations in human CYP3A-dependent metabolism. J Pharmacol Exp Ther 283(3):1552–1562

Cancer Chemotherapy and Pharmacology

Co-administration of lapatinib increases exposure to docetaxel but not doxorubicin in the small intestine of mice

Journal:	*Cancer Chemotherapy and Pharmacology*
Manuscript ID:	CCP-13-0029
Manuscript Type:	Original Article
Date Submitted by the Author:	15-Jan-2013
Complete List of Authors:	Hudachek, Susan; Colorado State University, Clinical Sciences Gustafson, Daniel; Colorado State University, Clinical Sciences
Keywords:	Breast Cancer, Docetaxel, Doxorubicin, Lapatinib

Title: Co-administration of lapatinib increases exposure to docetaxel but not doxorubicin in the small intestine of mice

Authors: Susan F. Hudachek and Daniel L. Gustafson

Affiliations: Animal Cancer Center, Department of Clinical Sciences, Colorado State University, Fort Collins, Colorado

Corresponding Author:
Susan F Hudachek
Address: 1620 Campus Delivery, Fort Collins CO, 80523
Phone: (970) 297-4056
Email: Susan.Hudachek@colostate.edu

Conflicts of Interest: DISCLOSURES: NONE

Abstract:

Purpose: Combination therapy is increasingly utilized for the treatment of metastatic breast cancer. However, co-administration of drugs, particularly agents that are substrates for or inhibitors of p-glycoprotein, can result in increased tissue toxicity. Unfortunately, determining levels of chemotherapeutics in human tissues is challenging and plasma drug concentrations are not always indicative of tissue toxicokinetics or toxicodynamics, especially when tissue penetration is altered.

Methods: The aim of the work presented herein was to determine if concomitant administration of compounds currently being combined in clinical trials for metastatic breast cancer treatment alters plasma and tissue pharmacokinetics in mice if both agents are p-glycoprotein substrates and/or inhibitors. Accordingly, we investigated the pharmacokinetic interactions of the classic cytotoxics and p-glycoprotein substrates docetaxel and doxorubicin when given concurrently with the targeted agent and p-glycoprotein inhibitor lapatinib.

Results: Our time course plasma and tissue distribution studies showed that co-administration of lapatinib with doxorubicin did not appreciably alter the pharmacokinetics of this anthracycline in the plasma or six tissues evaluated in mice, presumably because, at doses relevant to human exposure, lapatinib inhibition of p-glycoprotein did not significantly alter doxorubicin transport out of these tissue compartments.

Conclusions: However, combining lapatinib with docetaxel dramatically increased intestinal exposure to this chemotherapeutic, which has clinical implications for enhancing gastrointestinal toxicity. The significant lapatinib-docetaxel interaction is likely CYP3A4-mediated, suggesting that caution should be taken when this combination is administered, particularly to patients with compromised CYP3A activity, and recipients should be closely monitored for enhanced toxicity, particularly for adverse effects on the intestine.

Introduction:

The treatment of metastatic breast cancer is increasingly turning towards the use of combination therapy to optimize clinical outcomes [1-3]. Although additive or synergistic activity of agents is clearly advantageous for enhancing efficacy, a concurrent increase in toxicity may also result from the combination. The latter is particularly likely when the co-administered compounds are substrates for or inhibitors of ATP-binding cassette (ABC) transporters, which have a critical role in protecting cells from xenobiotics.

One of the best characterized ABC transporters is P-glycoprotein (PGP), discovered in 1976 [4]. Consistent with its role as a toxin efflux pump, PGP is highly expressed on the apical surface of epithelial cells with excretory roles, such as cells lining the colon, small intestine, pancreatic ductules, bile ductules, kidney proximal tubules and the adrenal gland [5,6]. The transporter is also located on the endothelial cells of the blood-brain barrier [7], the blood-testis barrier [8] and the blood-mammary tissue barrier [9]. Impairing the ability of PGP to export drugs out of these tissues, either by direct or competitive inhibition, could result in increased intracellular drug concentrations and, accordingly, increased tissue toxicity.

Data regarding human tissue levels of chemotherapeutics is sparse and unfortunately, plasma drug concentrations are not always indicative of the drug's concentration in tissues, especially when tissue penetration is altered. In mice, the disconnect between plasma and tissue pharmacokinetics has been observed when a PGP substrate was administered to mdr1a (-/-) mice [10] and when two PGP substrates were administered in combination [11]. Concerning the PGP substrate doxorubicin, the latter paper concluded that "monitoring of plasma levels of doxorubicin, when used in combination with another drug that is a PGP substrate, will not reflect actual pharmacokinetic changes occurring in other tissues". Thus, identifying whether the co-administration of compounds will result in increased tissue exposure and consequent enhanced toxicity based on an agent's plasma profile alone is problematic.

To address tissue-specific drug exposure resulting from combination therapy, we conducted studies in mice. The aim of the work presented herein was to determine if the co-administration of compounds commonly combined for metastatic breast cancer treatment alters plasma and tissue pharmacokinetics if both agents are PGP substrates and/or inhibitors. Accordingly, we investigated the pharmacokinetic interactions of the classic cytotoxics and PGP substrates docetaxel and doxorubicin when given concomitantly with the targeted agent and PGP inhibitor lapatinib, as both combinations are being explored clinically for the treatment of metastatic breast cancer. There is precedent to suggest that drug-drug interactions involving PGP could be significant for these combinations; *in vitro* studies have shown that lapatinib increased the intracellular accumulation of docetaxel 4.2-fold and doxorubicin 3.6-fold in the ABCB1-overexpressing DLKP-A [12] and MCF7/adr [13] cell lines, respectively. By understanding the plasma and tissue dynamics of these combination therapies in mice, we can then correspondingly dose adjust in humans to mitigate potential increases in toxicity so that the benefit of treatment outweighs the burden.

Materials and Methods:

Chemicals

Docetaxel (Winthrop U.S.) was acquired from the University of Colorado Hospital Pharmacy. Doxorubicin was acquired from the Colorado State University Veterinary Teaching Hospital Pharmacy. Lapatinib (GW572016) and GW572016AH were generously provided by GlaxoSmithKline. Hydroxypropyl methylcellulose, Tween® 80 and daunorubicin were purchased from Sigma-Aldrich. All other reagents were of analytical grade.

Animals

Five to six-week-old female FVB mice were purchased from Taconic. Animals were housed in polycarbonate cages and kept on a 12 hr light/dark cycle. Food and water were given *ad libitum*. Upon arrival, mice acclimated for a minimum of seven days prior to any experimentation.

All experimental procedures were approved by Colorado State University's Animal Care and Use Committee and the Department of Defense US Army Medical Research and Material Command (USAMRMC) Animal Care and Use Review Office (ACURO).

Lapatinib pharmacokinetic study

A time course distribution study of lapatinib was conducted. Lapatinib was formulated as a suspension of 12 mg/mL in 0.5% hydroxypropyl methylcellulose: 0.1% Tween® 80 in Milli-Q water and administered via intraperitoneal injection as a bolus dose of 60 mg/kg. Lapatinib was dosed every 3 hours for a total of 5 doses (q3hr × 5). Subsequently, three mice were sacrificed at each post-dose C_{max} (determined from previous studies to be 1 hr post-dose) and C_{min} (3 hrs post-dose). For the fifth dose, we only sacrificed mice at the C_{max}. All sacrifices were done by cardiac stick exsanguination under isoflurane anesthesia. Plasma was immediately collected, frozen in liquid nitrogen and stored at -80°C until analysis.

Docetaxel pharmacokinetic study

A time course distribution study of docetaxel with both single dose and multiple dose lapatinib was conducted. Docetaxel was acquired as an initial solution of 20 mg/mL in 50/50 (v/v) ratio polysorbate 80/dehydrated alcohol, further diluted to a solution of 0.6 mg/mL in 0.9% sodium chloride and administered via intravenous tail vein injection as a single bolus dose of 3 mg/kg. Lapatinib was formulated as a suspension of 12 mg/mL in 0.5% hydroxypropyl methylcellulose: 0.1% Tween® 80 in Milli-Q water and administered via intraperitoneal injection

as a bolus dose of 60 mg/kg. Vehicle was 0.5% hydroxypropyl methylcellulose: 0.1% Tween® 80 in Milli-Q water.

For the combination docetaxel and single dose lapatinib study, docetaxel was injected one hour after the single lapatinib or vehicle administration. Subsequently, three mice were sacrificed at 1, 2, 4, 8 and 12 hr post docetaxel injection. For the combination docetaxel and multiple dose lapatinib study, lapatinib or vehicle was dosed q3hr × 5. Docetaxel was injected one hour after the first lapatinib or vehicle dose. Subsequently, three mice were sacrificed at 4, 8 and 12 hrs post docetaxel injection. All sacrifices were done by cardiac stick exsanguination under isoflurane anesthesia. Plasma, brain, liver, proximal small intestine, kidney, heart, lung, muscle and adipose tissue were immediately collected, frozen in liquid nitrogen and stored at -80°C until analysis.

Doxorubicin pharmacokinetic study

A time course distribution study of doxorubicin with both single dose and multiple dose lapatinib was conducted. Doxorubicin was acquired as an initial solution of 2 mg/mL in 0.9% sodium chloride, further diluted to a solution of 1.2 mg/mL in 0.9% sodium chloride and administered via intravenous tail vein injection as a single bolus dose of 6 mg/kg. Lapatinib and vehicle were formulated and administered as for docetaxel studies.

For the combination doxorubicin and single dose lapatinib study, doxorubicin was injected one hour after the single lapatinib or vehicle administration. Subsequently, three mice were sacrificed at 1, 2, 4, 8, 12, 24 and 48 hrs post doxorubicin injection. For the combination doxorubicin and multiple dose lapatinib study, lapatinib or vehicle was dosed q3hr × 5. Doxorubicin was injected one hour after the first lapatinib or vehicle dose. Subsequently, three mice were sacrificed at 4, 8, 12, 24 and 48 hr post doxorubicin injection. Sacrifices, tissue collection and storage were done as for docetaxel studies.

Lapatinib high-pressure liquid chromatography-tandem mass spectrometry analysis

Analysis of lapatinib in plasma was done using high-pressure liquid chromatography-tandem mass spectrometry (LC/MS/MS) analysis based on the method of Bai et al. [14], modified as follows. Briefly, lapatinib was extracted from plasma by adding 210 uL of acetonitrile and 10 uL of internal standard (17.2 pmol GW572016AH) to 100 uL of unknown sample plasma, vortexing for 10 min and centrifuging at 18,000 x g for 10 min at 4°C. An aliquot of 20 uL of the supernatant was injected into the LC/MS/MS system for analysis. Standards and quality control samples were prepared in mouse plasma and analyzed as described above.

The HPLC system consisted of an Agilent 1200 Series binary pump SL, vacuum degasser, thermostatted column compartment SL (Agilent Technologies, Santa Clara, CA, USA) and a CTC Analytics HTC PAL System autosampler (Leap Technologies, Carrboro, NC, USA). The HPLC column was a Waters Sunfire C8 column (4.6 × 50 mm I.D., 2.5 µm bead size) (Waters Corporation, Milford, MA, USA) protected by a SecurityGuard™ C18 cartridge (4 × 2.0 mm I.D.) (Phenomenex, Torrance, CA, USA) and maintained at room temperature. The mobile phase consisted of an aqueous component (A) of 20mM ammonium formate in MilliQ water, pH 2.2 (with formic acid), and an organic component (B) of acetonitrile with 1% formic acid. The 3.5 min run consisted of the following linear gradient elution: 95% A and 5% B at 0 min, 95% A and 5% B at 0.25 min, 25% A and 75% B at 0.35 min, 25% A and 75% B at 3.0 min, 95% A and 5% B at 3.1 min and 95% A and 5% B at 3.5 min. The system operated at a flow-rate of 0.75 mL/min.

Mass spectrometric detection was performed on an API 3200™ triple quadrupole instrument (Applied Biosystems Inc, Foster City, CA, USA) using multiple reaction monitoring (MRM). Ions were generated in positive ionization mode using an electrospray interface. Lapatinib compound-dependent parameters were as follows: declustering potential (DP): 60 V;

entrance potential (EP): 10 V; collision cell entrance potential (CEP): 21 V; collision energy (CE): 51 V and collision cell exit potential (CXP): 5.8 V. GW572016AH (internal standard) compound-dependent parameters were as follows: DP: 67 V; EP: 7.5 V; CEP: 23 V; CE: 49 V and CXP: 5.5 V. Source-dependent parameters were as follows: nebulizer gas (GS1): 50 psi; auxiliary (turbo) gas (GS2): 60 psi; turbo gas temperature (TEM): 500°C; curtain gas [15]: 10 psi; collision-activated dissociation gas (nitrogen) (CAD): 6 psi; ionspray voltage (IS): 5000 V and interface heater (IH): 500°C. Peak areas ratios obtained from MRM of lapatinib (*m/z* 581 → 365.1) and GW572016AH (*m/z* 587 → 367) were used for quantification.

Docetaxel high-pressure liquid chromatography-tandem mass spectrometry analysis

Analysis of docetaxel in plasma and tissues was done using high-pressure liquid chromatography-tandem mass spectrometry (HPLC/MS/MS) analysis based on a method previously developed in our laboratory [16,17], modified as follows. Briefly, docetaxel was extracted from plasma by adding 1000 uL of ethyl acetate to 100 uL of unknown sample plasma, vortexing for 10 min and centrifuging at 18,000 x g for 10 min at 4°C. 800 uL of the organic phase was collected and evaporated to dryness using a rotary evaporator. Dried samples were reconstituted in 200 uL of 80/20 0.1% formic acid in water/acetonitrile, vortexed for 10 min and centrifuged at 18,000 x g for 10 min at 4°C. An aliquot of 60 uL of the supernatant was injected into the LC/MS/MS system for analysis. Tissues were homogenized at 100 mg/mL in water and 100 uL of the homogenates was extracted using the method for plasma detailed above. Standards and quality control samples were prepared in the appropriate matrix and analyzed as described above.

The HPLC and autosampler systems were the same as used with lapatinib. The HPLC column was a Waters Sunfire C8 column (2.1 × 150 mm I.D., 5.0 µm bead size) (Waters Corporation, Milford, MA, USA) protected by a SecurityGuard™ C18 cartridge (4 × 2.0 mm I.D.)

(Phenomenex, Torrance, CA, USA) and maintained at room temperature. The mobile phase consisted of an aqueous component (A) of 0.1% formic acid in MilliQ water and an organic component (B) of acetonitrile. The 4.0 min run consisted of the following linear gradient elution: 50% A and 50% B at 0 min, 50% A and 50% B at 0.5 min, 2% A and 98% B at 1.25 min, 2% A and 98% B at 3.0 min, 50% A and 50% B at 3.5 min and 50% A and 50% B at 4.0 min. The system operated at a flow-rate of 0.5 mL/min.

The mass spectrometric system was the same as used with lapatinib. Docetaxel compound-dependent parameters were as follows: DP: 21 V; EP: 4.5 V; CEP: 71 V; CE: 23 V and CXP: 3.5 V. Source-dependent parameters were as follows: GS1: 40 psi; GS2: 60 psi; TEM: 400°C; CUR: 30 psi; CAD: 2 psi; IS: 4500 V and IH: 500°C. Peak areas ratios obtained from MRM of docetaxel (*m/z* 808.5 → 226) were used for quantification.

Doxorubicin high-pressure liquid chromatography (HPLC)-fluorescence analysis

Analysis of doxorubicin in plasma and tissues was done using HPLC-fluorescence analysis based on a method previously developed in our laboratory [18,19], modified as follows. Briefly, doxorubicin was extracted from plasma by adding 600 uL of methanol and 10 uL of internal standard (1000 ng/mL daunorubicin) to 100 uL of unknown sample plasma, vortexing for 10 min, adding 250 uL of 12 mM phosphoric acid, vortexing for 10 min and centrifuging at 18,000 x g for 10 min at 4°C. An aliquot of 100 uL of the supernatant was injected into the HPLC system for analysis. Tissues were homogenized at 100 mg/mL in water and 100 uL of the homogenates was extracted using the method for plasma detailed above. Standards and quality control samples were prepared in the appropriate matrix and analyzed as described above.

The HPLC system consisted of a Shimadzu prominence LC-20AD binary pump, prominence DGU-20A_3 vacuum degasser, prominence CTO-20A column oven, prominence SIL-20AC auto sampler, prominence CBM-20A communications bus module and an RF-10A_{XL}

fluorescence detector with excitation and emission wavelengths set at 480 and 580 nm, respectively (Shimadzu, Columbia, MD, USA). The HPLC column was a Waters Sunfire C18 column (4.6 × 50 mm I.D., 2.5 µm bead size) (Waters Corporation, Milford, MA, USA) protected by a SecurityGuard™ C18 cartridge (4 × 2.0 mm I.D.) (Phenomenex, Torrance, CA, USA) and maintained at room temperature. The mobile phase consisted of an aqueous component (A) of 15 mM sodium phosphate in MilliQ water, pH 2.2 (with orthophosphoric acid), and an organic component (B) of acetonitrile. The 7.5 min run consisted of the following linear gradient elution: 80% A and 20% B at 0 min, 80% A and 20% B at 1.5 min, 50% A and 50% B at 6.5 min, 80% A and 20% B at 7.0 min, and 80% A and 20% B at 7.5 min. The system operated at a flow-rate of 0.75 mL/min.

Pharmacokinetic Analysis

Pharmacokinetic parameters were calculated using noncompartmental modeling performed with Microsoft Excel and standard equations for noncompartmental analysis.

Statistical Analysis

Statistical analysis was performed using GraphPad Prism v5.01 (GraphPad Software, San Diego, California). For the comparison of concentration means, two-tailed unpaired *t*-tests were used.

Results:

Combination lapatinib and chemotherapy clinical trials

To determine the effect of lapatinib on the pharmacokinetics of multiple classes of chemotherapeutics in humans, we reviewed all phase I clinical trials to date that involved drugs administered in combination with lapatinib and included pharmacokinetic data. In these eight

clinical trials [20-25,15,26], the plasma pharmacokinetics of eleven drugs and metabolites were reported; only three of these compounds exhibited statistically significant alterations in pharmacokinetic parameters upon concomitant administration with lapatinib (Table 1). When dosed with lapatinib, the plasma area under the concentration-time curve [27] of SN-38 and topotecan increased by 45% and 18%, respectively. The authors of both studies suggested that the decreased clearance was likely due to the interaction of lapatinib with efflux transporters, particularly PGP. Lapatinib has been shown to be both a substrate for PGP and breast cancer resistance protein (BCRP) and an inhibitor of PGP, BRCP and organic anion transporting polypeptide 1B1 (OATP1B1) [28]. As an inhibitor, lapatinib could prevent PGP from transporting xenobiotics out of the cell, thus increasing exposure to compounds that are PGP substrates. As a substrate, lapatinib could act as a competitor for PGP efflux.

To determine if the other chemotherapeutics used in the clinical trials are PGP substrates, we utilized Althotas Virtual Laboratory [29]. The support vector machine (SVM) method predicted that 4 of the 10 compounds assessed are substrates of PGP (Table 1). Of these, two drugs (SN-38 and topotecan) exhibited an increase in exposure when given with lapatinib whereas two (irinotecan and docetaxel) did not.

To further investigate the relationship with PGP, we also used Althotas Virtual Laboratory [29] to calculate the docking energies of human PGP-ligand interactions. The lowest free energy of docking to PGP for each compound is presented in Table 1. In comparison, the lowest free energy of docking to PGP for lapatinib is -10.3 kcal/mol. The significance of these energies is unclear. The geometries of the human PGP-ligand interactions are shown in Supplementary Figures 1 and 2.

In the human clinical trials, although the plasma pharmacokinetics were altered for only 27.3% of the compounds evaluated, all combination regimens caused an increase in toxicity. In 6 of the trials, dose reduction [25,24,21,15,22] or the addition of pegfilgrastim [23] was

warranted. Thus, the plasma pharmacokinetic data was not indicative of tissue pharmacokinetics or toxicodynamics.

Currently, there are 114 breast cancer clinical trials involving concomitant lapatinib [30]. Of all trials, 69% (n = 79) involve another drug that is a PGP substrate (as determined by Althotas Virtual Laboratory [29]). Of these, 57% (n = 45) include a taxane (docetaxel or paclitaxel) and/or an anthracycline (doxorubicin or epirubicin) (Supplementary Spreadsheet 1). Hence, taxanes and anthracyclines are commonly administered with lapatinib for the treatment of breast cancer and are also PGP substrates. Therefore, we chose to further explore the plasma and tissue pharmacokinetics of docetaxel and doxorubicin when given in combination with lapatinib in mice.

Human equivalent dosing of lapatinib in mice

For the subsequent combination studies, our aim was to administer a dose of lapatinib to mice that would result in plasma exposure equivalent to the steady-state plasma exposure in humans when given the recommended dose of lapatinib (1250 mg/day). We determined that dosing mice intraperitoneally with 60 mg/kg lapatinib every 3 hours for a total of 5 doses resulted in maximum concentrations (C_{max}) and minimum concentrations (C_{min}) of lapatinib that were similar to human peak (2430 ng/mL at 4 hr) and trough levels (1000 ng/mL) (Figure 1A). Extrapolating the mouse steady-state concentrations (achieved after 5 doses) out to 24 hours, this dosing regimen resulted in an AUC of 39.9 μg/mL × hr which is comparable to both the calculated human AUC_{τ} of 41.2 μg/mL × hr (Figure 1B) and the observed human geometric mean AUC_{τ} of 36.2 μg/mL × hr [31]. Accordingly, we used this mouse dosing regimen for the following combination studies.

Combination lapatinib and docetaxel studies in mice

Two time course plasma and tissue distribution studies of combination lapatinib and docetaxel were conducted in female FVB mice, which were administered either a single or multiple (q3hr × 5) intraperitoneal 60 mg/kg doses of lapatinib. In both experiments, a single intravenous injection of 3 mg/kg docetaxel was given one hour after the first lapatinib dose. Samples were collected at 1, 2, 4, 8 and 12 hrs post docetaxel administration.

After a single dose of lapatinib, there was a statistically significant increase in the concentration of docetaxel in kidney at 1 hr (10.6%) and 12 hrs (18.3%), intestine at 2 hrs (72.4%) and adipose tissue at 8 hrs (41.1%) versus docetaxel following vehicle. After multiple doses of lapatinib, there was a statistically significant increase (versus vehicle) in the concentration of docetaxel in kidney at 8 hrs (25.5%), intestine at 4 hrs (19.4%) and 8 hrs (89.7%), muscle at 8 hrs (23.4%) and plasma at 8 hrs (21.8%) (Figure 2).

In terms of exposure, combination therapy resulted in >25% increases in intestine and adipose tissue (Table 2). In intestine, there was a 32.8% and 44.6% increase after single and multiple dose lapatinib, respectively. In adipose tissue, there was a 35.4% and a 25.2% increase after single and multiple dose lapatinib, respectively.

In addition to exposure, we also evaluated the effect of lapatinib on docetaxel concentration-time curve shape parameters by comparing half-life and C_{max} values (Supplementary Tables 1 and 2). For the former, half-lives differed by ±25% after multiple dose lapatinib in muscle (-42.5%) and brain (+144.0%). However, for terminal half-life calculations using nonlinear regression, our curve was comprised of only 3 time points (4, 8 and 12 hrs) and for the brain and muscle multiple dose lapatinib curves, the r square (weighted) goodness-of-fit values for the regression lines were suboptimal. Specifically, in muscle, the r square (weighted) values were 0.5740 and 0.6994 for docetaxel alone and combination lapatinib and docetaxel, respectively. In brain, the r square (weighted) values were 0.8515 and 0.5249 for docetaxel alone and combination lapatinib and docetaxel, respectively. Thus, the half-life calculations from

these curves are flawed and, as such, the differences are likely misrepresentations. Regarding C_{max} values, there were no statistically significant differences.

Plasma concentrations of lapatinib in the combination single dose lapatinib and docetaxel study and the multiple dose lapatinib and docetaxel study are shown in Figures 1C and 1D, respectively. In the single dose lapatinib and docetaxel study, the C_{max} (700 ng/mL) was below the human trough concentration. In the multiple dose lapatinib and docetaxel study, all three lapatinib concentrations measured were within the targeted range (between the human steady state C_{max} and C_{min} following the recommended dose of lapatinib (1250 mg/day)).

Combination lapatinib and doxorubicin studies in mice

Two time course plasma and tissue distribution studies of combination lapatinib and doxorubicin were conducted in female FVB mice, which were administered either a single or multiple (q3hr × 5) intraperitoneal 60 mg/kg doses of lapatinib. In both experiments, a single intravenous injection of 6 mg/kg doxorubicin was given one hour after the first lapatinib dose. Samples were collected at 1, 2, 4, 8, 12, 24 and 48 hrs post doxorubicin administration.

After a single dose of lapatinib, there was a statistically significant increase in the concentration of doxorubicin in adipose tissue at 4 hrs (65.5%) and a statistically significant decrease at 24 hrs (40.4%) versus doxorubicin following vehicle (Figure 3). There were no statistically significant differences in doxorubicin concentrations in plasma or tissues after multiple dose lapatinib versus vehicle. Doxorubicin levels in the brain could not be evaluated because all sample peaks were below our lower limit of quantitation (50 ng/g).

Pertaining to exposure, the only change greater than ±25% was a decrease in adipose tissue (26.0%) after multiple dose lapatinib. There was also a 46.2% decrease and a 28.6% increase in adipose tissue terminal half-lives (calculated from the 12, 24 and 48 hr time points) after single and multiple dose lapatinib, respectively. As with docetaxel, these half-lives are

likely distorted as the r square (weighted) values for these regression lines were substandard. As for C_{max} values, we found no statistically significant differences.

Plasma concentrations of lapatinib in the combination single dose lapatinib and doxorubicin study and the multiple dose lapatinib and doxorubicin study are shown in Figures 1E and 1F, respectively. In the single dose lapatinib and doxorubicin study, the C_{max} (553 ng/mL) was below the human trough concentration. In the multiple dose lapatinib and doxorubicin study, all three lapatinib concentrations measured during the multiple dosing period were within the targeted range (between the human steady state C_{max} and C_{min} following the recommended dose of lapatinib (1250 mg/day)).

Discussion:

Cytotoxic and biologic combinations for the treatment of metastatic breast cancer have been approved by the US Food and Drug Administration (FDA) and several investigational drug combinations are currently undergoing evaluation in clinical trials [1]. While there are clear advantages to combining therapies, there is also the potential disadvantage of increasing the toxicity burden to the patient with only moderate improvements in efficacy and benefit [2]. In our evaluation of eight clinical trials involving co-administration of lapatinib with cytotoxic agents, all combinations caused an increase in toxicity versus the regimen without lapatinib, indicating that concomitant administration increased tissue drug exposure beyond a tolerable level. However, plasma pharmacokinetics were altered for only 27.3% of the compounds evaluated, demonstrating that chemotherapeutic concentrations in plasma alone were not indicative of adverse drug-drug interactions in tissues.

Drug-drug interactions are often mediated by competition for or inhibition of efflux proteins. As lapatinib is both a substrate for and inhibitor of PGP [28], we combined this drug with cytotoxic agents that are PGP substrates and used clinically in conjunction with lapatinib for

the treatment of metastatic breast cancer. Our study of lapatinib and docetaxel in mice showed that co-administration resulted in intestinal docetaxel exposure increases of 32.8% and 44.6% after single dose and multiple dose lapatinib, respectively. Although we did not evaluate toxicodynamics because of the short duration of our pharmacokinetic studies (12 hrs), this amplified intestinal exposure likely would have clinical ramifications, as the gastrointestinal tract is a major site of reported docetaxel-related adverse events. In patients treated with docetaxel as a single agent for various tumor types (n = 2045), nausea (39%), diarrhea (39%) and vomiting (22%) were observed; other gastrointestinal events included anorexia, taste perversion, constipation, abdominal pain, gastrointestinal bleeding and esophagitis [32].

Regarding the increased docetaxel exposure in adipose tissue (35.4% and a 25.2% after single and multiple dose lapatinib, respectively), this may also have clinically significant consequences given that adipose tissue could theoretically serve as a reservoir of docetaxel (since many lipid-soluble drugs are stored in fat) and thereby contribute to the significant increases in plasma, kidney, muscle and intestine docetaxel concentrations at later time points (8 and 12 hrs).

In a phase I study of lapatinib and docetaxel in patients with advanced cancer, the plasma pharmacokinetics of both compounds in combination were not significantly different than the drug profiles when administered separately; however, there was an increase in toxicity [23]. Specifically, the drug-related adverse events reported by most patients were diarrhea (56%), rash (52%), fatigue (27%) and nausea (25%). The authors could not characterize the diarrhea, nausea or rash as specific to either lapatinib or docetaxel but, in light of the data from our mouse study, we can conjecture that the gastrointestinal toxicities were likely due to an increase in docetaxel exposure in the enterocytes. Neutropenia, a frequent toxicity associated with docetaxel, also occurred during the phase I trial and necessitated the addition of pegfilgrastin to

the dosing regimen. The authors suggest that lapatinib increased the sensitivity to this toxicity, possibly by inhibiting PGP-mediated efflux of docetaxel from bone marrow stem cells [23].

In contrast to docetaxel, lapatinib did not significantly alter the pharmacokinetics of doxorubicin in plasma or tissues commonly associated with doxorubicin-related toxicity, such as heart, intestine and liver [33]. However, increases in doxorubicin $AUC_{0\rightarrow 24hr}$ in these tissues (24% in heart, 65% in intestine and 339% in liver) and were observed in mice lacking mdr1a versus wild-type mice, implicating PGP as a causative factor in the alteration of doxorubicin pharmacokinetics in these tissues. This proposition is further support by additional rodent combination studies of doxorubicin with PGP inhibitors cyclosporin A [34,35] and SDZ PSC 833 [36], in which co-administration resulted in significant increases in tissue levels of doxorubicin. Thus, our study suggests that lapatinib is a weaker inhibitor of PGP than cyclosporin A and SDZ PSC 833. MDCKII-MDR1 monolayer efflux studies using 3H-digoxin as a probe substrate reported half maximal inhibitory concentrations of 3.9 [28] and 1.6 μM [37] for lapatinib and cyclosporin A, respectively, indicating that cyclosporin A is ~2.5 times more potent than lapatinib as a PGP inhibitor.

In addition to altering the pharmacokinetics of doxorubicin, cyclosporin A has also been shown to increase the plasma exposure of oral docetaxel 9-fold [38]. However, only a 3-fold increase was observed when docetaxel was administered per os to mdr1a/1b (-/-) mice compared to wild-type [39], suggesting that PGP inhibition was not the major factor accountable for the magnified systemic AUC when docetaxel was administered in combination with cyclosporin A. Alternatively, the increase in exposure was likely more resultant of competitive inhibition of cytochrome P450 enzymes by cyclosporin A, as both this immunosuppresant and docetaxel are substrates for CYP3A4 [40-42]. In mice, this is evidenced by a 12-fold plasma docetaxel exposure increase in cyp3a(-/-)versus wild-type mice after oral dosing [39]. Moreover,

after docetaxel dosing, the cyp3a(-/-) mice exhibited moderate toxicity in the small intestine whereas this was only mild in mrd1a/b(-/-) mice [39].

Further evidence that CYP3A metabolism plays a more important role than PGP-mediated efflux in docetaxel elimination comes from studies of intravenous injection of docetaxel in wild-type and mdr1a/b (-/-) mice, which resulted in no difference in systemic exposure to docetaxel [38]. Co-administration of cyclosporin A, however, increased plasma docetaxel AUC by 3-fold in both wild-type and mdr1a/b (-/-) mice [38], presumably due to the effect of cyclosporin A on docetaxel metabolism by CYP3A4.

Similar to cyclosporin A, lapatinib is not only an inhibitor of PGP but this targeted agent is also a CYP3A4 substrate and inhibitor [31,43]. As the latter, we propose that lapatinib competitively inhibits docetaxel intestinal metabolism by CYP3A4 and, consequently, is responsible for the considerable increase in docetaxel exposure that we observed in the small intestine of mice. A similar escalation was not seen in the liver because hepatic CYP3A is much more abundant than intestinal CYP3A, which is only ~2% of that in the liver [44-46]. Thus, these metabolic enzymes in the liver are not as susceptible to saturation as those in the small intestine. However, the importance of intestinal CYP3A metabolism of docetaxel should not be understated and is illustrated by a 16.6-fold versus a 2.2-fold decrease in docetaxel plasma exposure after oral administration to cyp3a (-/-) mice with human CYP3A4 in only the intestine or only the liver, respectively [47]. In contrast to docetaxel, a CYP3A4-mediated effect of lapatinib on doxorubicin exposure was not noted because this anthracycline is primarily metabolized to doxorubicinol by cytoplasmic aldo-keto and carbonyl reductases [48,49].

In conclusion, co-administration of lapatinib with doxorubicin did not appreciably alter the pharmacokinetics of this cytotoxic in the plasma or six tissues evaluated in mice, presumably because, at doses relevant to human exposure, lapatinib inhibition of PGP did not significantly alter doxorubicin export from these compartments and lapatinib inhibition of CYP3A4 was

inconsequential for doxorubicin metabolism to doxorubicinol. However, combining lapatinib with docetaxel dramatically increased intestinal exposure to this chemotherapeutic, which has clinical implications for enhancing gastrointestinal toxicity. The significant lapatinib-docetaxel interaction is likely CYP3A4-mediated and thus, our study suggests that caution should be taken when this combination is administered, particularly to patients with compromised CYP3A activity. As co-administration of these two agents is protocol for clinical trials that are either recruiting or active, we recommend closely monitoring the recipients of combined lapatinib and docetaxel for enhanced toxicity, particularly for adverse effects on the intestine.

Acknowledgements:

We are grateful to AJ Beaupre for performing all of the intravenous tail vein injections in both the docetaxel and doxorubicin mouse studies.

Grant Support: This work was supported in part by grant number W81XWH-09-1-0457 from the Department of Defense (DOD) Breast Cancer Research Program (BCRP) of the Office of the Congressionally Directed Medical Research Programs (CDMRP).

References:

1. Tkaczuk KH (2009) Review of the contemporary cytotoxic and biologic combinations available for the treatment of metastatic breast cancer. Clin Ther 31 Pt 2:2273-2289

2. Miles D, von Minckwitz G, Seidman AD (2002) Combination versus sequential single-agent therapy in metastatic breast cancer. Oncologist 7 Suppl 6:13-19

3. Cianfrocca M, Gradishar WJ (2007) Counterpoint: the argument for combination chemotherapy in the treatment of metastatic breast cancer. J Natl Compr Canc Netw 5 (8):673-675

4. Juliano RL, Ling V (1976) A surface glycoprotein modulating drug permeability in Chinese hamster ovary cell mutants. Biochim Biophys Acta 455 (1):152-162

5. Thiebaut F, Tsuruo T, Hamada H, Gottesman MM, Pastan I, Willingham MC (1987) Cellular localization of the multidrug-resistance gene product P-glycoprotein in normal human tissues. Proc Natl Acad Sci U S A 84 (21):7735-7738

6. Croop JM, Raymond M, Haber D, Devault A, Arceci RJ, Gros P, Housman DE (1989) The three mouse multidrug resistance (mdr) genes are expressed in a tissue-specific manner in normal mouse tissues. Mol Cell Biol 9 (3):1346-1350

7. Beaulieu E, Demeule M, Ghitescu L, Beliveau R (1997) P-glycoprotein is strongly expressed in the luminal membranes of the endothelium of blood vessels in the brain. Biochem J 326 (Pt 2):539-544

8. Melaine N, Lienard MO, Dorval I, Le Goascogne C, Lejeune H, Jegou B (2002) Multidrug resistance genes and p-glycoprotein in the testis of the rat, mouse, Guinea pig, and human. Biol Reprod 67 (6):1699-1707

9. Edwards JE, Alcorn J, Savolainen J, Anderson BD, McNamara PJ (2005) Role of P-glycoprotein in distribution of nelfinavir across the blood-mammary tissue barrier and blood-brain barrier. Antimicrob Agents Chemother 49 (4):1626-1628

10. van Asperen J, van Tellingen O, Tijssen F, Schinkel AH, Beijnen JH (1999) Increased accumulation of doxorubicin and doxorubicinol in cardiac tissue of mice lacking mdr1a P-glycoprotein. Br J Cancer 79 (1):108-113

11. Gustafson DL, Merz AL, Long ME (2005) Pharmacokinetics of combined doxorubicin and paclitaxel in mice. Cancer Lett 220 (2):161-169

12. Collins DM, Crown J, O'Donovan N, Devery A, O'Sullivan F, O'Driscoll L, Clynes M, O'Connor R Tyrosine kinase inhibitors potentiate the cytotoxicity of MDR-substrate anticancer agents independent of growth factor receptor status in lung cancer cell lines. Invest New Drugs 28 (4):433-444

13. Dai CL, Tiwari AK, Wu CP, Su XD, Wang SR, Liu DG, Ashby CR, Jr., Huang Y, Robey RW, Liang YJ, Chen LM, Shi CJ, Ambudkar SV, Chen ZS, Fu LW (2008) Lapatinib (Tykerb, GW572016) reverses multidrug resistance in cancer cells by inhibiting the activity of ATP-binding cassette subfamily B member 1 and G member 2. Cancer Res 68 (19):7905-7914

14. Bai F, Freeman BB, 3rd, Fraga CH, Fouladi M, Stewart CF (2006) Determination of lapatinib (GW572016) in human plasma by liquid chromatography electrospray tandem mass spectrometry (LC-ESI-MS/MS). J Chromatogr B Analyt Technol Biomed Life Sci 831 (1-2):169-175

15. Chu QS, Schwartz G, de Bono J, Smith DA, Koch KM, Versola MJ, Pandite L, Arya N, Curtright J, Fleming RA, Ho PT, Rowinsky EK (2007) Phase I and pharmacokinetic study of lapatinib in combination with capecitabine in patients with advanced solid malignancies. J Clin Oncol 25 (24):3753-3758

16. Bradshaw-Pierce EL, Eckhardt SG, Gustafson DL (2007) A physiologically based pharmacokinetic model of docetaxel disposition: from mouse to man. Clin Cancer Res 13 (9):2768-2776

17. Gustafson DL, Long ME, Zirrolli JA, Duncan MW, Holden SN, Pierson AS, Eckhardt SG (2003) Analysis of docetaxel pharmacokinetics in humans with the inclusion of later sampling time-points afforded by the use of a sensitive tandem LCMS assay. Cancer Chemother Pharmacol 52 (2):159-166

18. Gustafson DL, Rastatter JC, Colombo T, Long ME (2002) Doxorubicin pharmacokinetics: Macromolecule binding, metabolism, and excretion in the context of a physiologic model. J Pharm Sci 91 (6):1488-1501

19. de Jong J, Guerand WS, Schoofs PR, Bast A, van der Vijgh WJ (1991) Simple and sensitive quantification of anthracyclines in mouse atrial tissue using high-performance liquid chromatography and fluorescence detection. J Chromatogr 570 (1):209-216

20. Chu QS, Cianfrocca ME, Goldstein LJ, Gale M, Murray N, Loftiss J, Arya N, Koch KM, Pandite L, Fleming RA, Paul E, Rowinsky EK (2008) A phase I and pharmacokinetic study of lapatinib in combination with letrozole in patients with advanced cancer. Clin Cancer Res 14 (14):4484-4490

21. Molina JR, Kaufmann SH, Reid JM, Rubin SD, Galvez-Peralta M, Friedman R, Flatten KS, Koch KM, Gilmer TM, Mullin RJ, Jewell RC, Felten SJ, Mandrekar S, Adjei AA, Erlichman C (2008) Evaluation of lapatinib and topotecan combination therapy: tissue culture, murine xenograft, and phase I clinical trial data. Clin Cancer Res 14 (23):7900-7908

22. Kimball KJ, Numnum TM, Kirby TO, Zamboni WC, Estes JM, Barnes MN, Matei DE, Koch KM, Alvarez RD (2008) A phase I study of lapatinib in combination with carboplatin in women with platinum sensitive recurrent ovarian carcinoma. Gynecol Oncol 111 (1):95-101

23. LoRusso PM, Jones SF, Koch KM, Arya N, Fleming RA, Loftiss J, Pandite L, Gadgeel S, Weber BL, Burris HA, 3rd (2008) Phase I and pharmacokinetic study of lapatinib and docetaxel in patients with advanced cancer. J Clin Oncol 26 (18):3051-3056

24. Storniolo AM, Pegram MD, Overmoyer B, Silverman P, Peacock NW, Jones SF, Loftiss J, Arya N, Koch KM, Paul E, Pandite L, Fleming RA, Lebowitz PF, Ho PT, Burris HA, 3rd (2008) Phase I dose escalation and pharmacokinetic study of lapatinib in combination with trastuzumab in patients with advanced ErbB2-positive breast cancer. J Clin Oncol 26 (20):3317-3323

25. Midgley RS, Kerr DJ, Flaherty KT, Stevenson JP, Pratap SE, Koch KM, Smith DA, Versola M, Fleming RA, Ward C, O'Dwyer PJ, Middleton MR (2007) A phase I and pharmacokinetic study of lapatinib in combination with infusional 5-fluorouracil, leucovorin and irinotecan. Ann Oncol 18 (12):2025-2029

26. Siegel-Lakhai WS, Beijnen JH, Vervenne WL, Boot H, Keessen M, Versola M, Koch KM, Smith DA, Pandite L, Richel DJ, Schellens JH (2007) Phase I pharmacokinetic study of the safety and tolerability of lapatinib (GW572016) in combination with oxaliplatin/fluorouracil/leucovorin (FOLFOX4) in patients with solid tumors. Clin Cancer Res 13 (15 Pt 1):4495-4502

27. Castellino S, O'Mara M, Koch K, Borts DJ, Bowers GD, MacLauchlin C Human metabolism of lapatinib, a dual kinase inhibitor: implications for hepatotoxicity. Drug Metab Dispos 40 (1):139-150

28. Polli JW, Humphreys JE, Harmon KA, Castellino S, O'Mara MJ, Olson KL, John-Williams LS, Koch KM, Serabjit-Singh CJ (2008) The role of efflux and uptake transporters in [N-{3-chloro-4-[(3-fluorobenzyl)oxy]phenyl}-6-[5-({[2-(methylsulfonyl)ethyl]amino }methyl)-2-furyl]-4-quinazolinamine (GW572016, lapatinib) disposition and drug interactions. Drug Metab Dispos 36 (4):695-701

29. Bikadi Z, Hazai I, Malik D, Jemnitz K, Veres Z, Hari P, Ni Z, Loo TW, Clarke DM, Hazai E, Mao Q Predicting P-glycoprotein-mediated drug transport based on support vector machine and three-dimensional crystal structure of P-glycoprotein. PLoS One 6 (10):e25815

30. . www.clinicaltrials.gov.

31. GlaxoSmithKline (2012) Tykerb prescribing information. http://us.gsk.com/products/assets/us_tykerb.pdf.

32. Sanofi-Aventis (2011) Taxotere Product Mongraph. http://products.sanofi.ca/en/taxotere.pdf.

33. Pfizer (2012) Adriamycin Product Mongraph. http://www.pfizer.ca/en/our_products/products/monograph/150.

34. Bellamy WT, Peng YM, Odeleye A, Ellsworth L, Xu MJ, Grogan TM, Weinstein RS (1995) Cardiotoxicity in the SCID mouse following administration of doxorubicin and cyclosporin A. Anticancer Drugs 6 (6):736-743

35. Colombo T, Zucchetti M, D'Incalci M (1994) Cyclosporin A markedly changes the distribution of doxorubicin in mice and rats. J Pharmacol Exp Ther 269 (1):22-27

36. Gonzalez O, Colombo T, De Fusco M, Imperatori L, Zucchetti M, D'Incalci M (1995) Changes in doxorubicin distribution and toxicity in mice pretreated with the cyclosporin analogue SDZ PSC 833. Cancer Chemother Pharmacol 36 (4):335-340

37. Rautio J, Humphreys JE, Webster LO, Balakrishnan A, Keogh JP, Kunta JR, Serabjit-Singh CJ, Polli JW (2006) In vitro p-glycoprotein inhibition assays for assessment of clinical drug interaction potential of new drug candidates: a recommendation for probe substrates. Drug Metab Dispos 34 (5):786-792

38. Bardelmeijer HA, Ouwehand M, Buckle T, Huisman MT, Schellens JH, Beijnen JH, van Tellingen O (2002) Low systemic exposure of oral docetaxel in mice resulting from extensive first-pass metabolism is boosted by ritonavir. Cancer Res 62 (21):6158-6164

39. van Waterschoot RA, Lagas JS, Wagenaar E, van der Kruijssen CM, van Herwaarden AE, Song JY, Rooswinkel RW, van Tellingen O, Rosing H, Beijnen JH, Schinkel AH (2009) Absence of both cytochrome P450 3A and P-glycoprotein dramatically increases docetaxel oral bioavailability and risk of intestinal toxicity. Cancer Res 69 (23):8996-9002

40. Marre F, Sanderink GJ, de Sousa G, Gaillard C, Martinet M, Rahmani R (1996) Hepatic biotransformation of docetaxel (Taxotere) in vitro: involvement of the CYP3A subfamily in humans. Cancer Res 56 (6):1296-1302

41. Shou M, Martinet M, Korzekwa KR, Krausz KW, Gonzalez FJ, Gelboin HV (1998) Role of human cytochrome P450 3A4 and 3A5 in the metabolism of taxotere and its derivatives: enzyme specificity, interindividual distribution and metabolic contribution in human liver. Pharmacogenetics 8 (5):391-401

42. Niel N, Rechencq E, Muller A, Vidal JP, Escale R, Durand T, Girard JP, Rossi JC, Bonne C (1992) Synthesis and contractile activity of new pseudopeptido and thioaromatic analogues of leukotriene D4. Prostaglandins 43 (1):45-54

43. Teng WC, Oh JW, New LS, Wahlin MD, Nelson SD, Ho HK, Chan EC Mechanism-based inactivation of cytochrome P450 3A4 by lapatinib. Mol Pharmacol 78 (4):693-703

44. Perloff MD, Von Moltke LL, Greenblatt DJ (2003) Differential metabolism of midazolam in mouse liver and intestine microsomes: a comparison of cytochrome P450 activity and expression. Xenobiotica 33 (4):365-377

45. Hietanen E, Vainio H (1973) Interspecies variations in small intestinal and hepatic drug hydroxylation and glucuronidation. Acta Pharmacol Toxicol (Copenh) 33 (1):57-64

46. Paine MF, Khalighi M, Fisher JM, Shen DD, Kunze KL, Marsh CL, Perkins JD, Thummel KE (1997) Characterization of interintestinal and intraintestinal variations in human CYP3A-dependent metabolism. J Pharmacol Exp Ther 283 (3):1552-1562

47. van Herwaarden AE, Wagenaar E, van der Kruijssen CM, van Waterschoot RA, Smit JW, Song JY, van der Valk MA, van Tellingen O, van der Hoorn JW, Rosing H, Beijnen JH, Schinkel AH (2007) Knockout of cytochrome P450 3A yields new mouse models for understanding xenobiotic metabolism. J Clin Invest 117 (11):3583-3592

48. Robert J, Gianni L (1993) Pharmacokinetics and metabolism of anthracyclines. Cancer Surv 17:219-252

49. Loveless H, Arena E, Felsted RL, Bachur NR (1978) Comparative mammalian metabolism of adriamycin and daunorubicin. Cancer Res 38 (3):593-598

50. Andersen ME, Yang RSH, Clewell HJ, 3rd, Reddy MB (2005) Introduction: a historical perspective of the development and applications of PBPK models. In: Reddy MB, Yang RSH, Clewell HJ, 3rd, Andersen ME (eds) Physiologically based pharmacokinetic modeling : science and applications. Wiley-Interscience, Hoboken, N.J., pp xix, 420 p.

Figure Legend:

Figure 1: Lapatinib concentrations in mouse plasma. (A) Time course of maximum and minimum lapatinib concentrations after five 60 mg/kg intraperitoneal doses (at times 0, 3, 6, 9 and 12 hrs). Maximum and minimum concentrations were achieved 1 and 3 hrs post dose, respectively. Filled black diamonds represent mean concentrations and error bars represent standard deviations (n = 3). (B) Filled black diamonds and error bars as in (A). Open grey diamonds represent extrapolated maximum and minimum lapatinib concentrations with continued q3hr dosing after achievement of steady-state. Filled black circles represent human steady-state maximum (2430 ng/mL) and minimum (1000 ng/mL) concentrations (achieved 4 and 24 hrs post dose, respectively). (C) Time course of lapatinib concentrations after a single dose of 60 mg/kg intraperitoneal lapatinib administered at time -1 hr (arrow) followed by a single dose of 3 mg/kg intravenous docetaxel administered at time 0 hr. Filled black diamonds represent mean concentrations and error bars represent standard deviations (n = 3). (D) Time course of lapatinib concentrations after five 60 mg/kg intraperitoneal doses (at times -1, 2, 5, 8 and 11 hrs (arrows)) followed by a single dose of 3 mg/kg intravenous docetaxel administered at time 0 hr. Filled black diamonds represent mean concentrations and error bars represent

standard deviations (n = 3). (E) Time course of lapatinib concentrations after a single dose of 60 mg/kg intraperitoneal lapatinib administered at time -1 hr (arrow) followed by a single dose of 6 mg/kg intravenous doxorubicin administered at time 0 hr. Filled black diamonds represent mean concentrations and error bars represent standard deviations (n = 3). (F) Time course of lapatinib concentrations after five 60 mg/kg intraperitoneal doses (at times -1, 2, 5, 8 and 11 hrs (arrows)) followed by a single dose of 6 mg/kg intravenous doxorubicin administered at time 0 hr. Filled black diamonds represent mean concentrations and error bars represent standard deviations (n = 3). In all graphs, dashed lines represent the human steady-state maximum concentration (2430 ng/mL) and dotted lines represent the human steady-state minimum concentration (1000 ng/mL) after administration of the recommended dose of lapatinib (1250 mg/day).

Figure 2: Time courses of docetaxel concentrations in mouse plasma and tissues after a single dose of 3 mg/kg intravenous docetaxel administered at time 0 hr. For the single dose lapatinib study, one hour prior to docetaxel administration (at time -1 hr), mice were administered either single dose intraperitoneal vehicle (solid white bars) or single dose 60 mg/kg intraperitoneal lapatinib (horizontally striped bars). For the multiple dose lapatinib study, one hour prior to docetaxel administration (at time -1 hr) and again at times 2, 5, 8 and 11 hrs, mice were administered either intraperitoneal vehicle (solid black bars) or 60 mg/kg intraperitoneal lapatinib (diagonally striped bars). All bars represent mean concentrations and error bars represent standard deviations (n = 3). Asterisks represent statistically significance differences ($p < 0.05$).

Figure 3: Time courses of doxorubicin concentrations in mouse plasma and tissues after a single dose of 6 mg/kg intravenous doxorubicin administered at time 0 hr. For the single dose lapatinib study, one hour prior to doxorubicin administration (at time -1 hr), mice were

administered either single dose intraperitoneal vehicle (solid white bars) or single dose 60 mg/kg intraperitoneal lapatinib (horizontally striped bars). For the multiple dose lapatinib study, one hour prior to doxorubicin administration (at time -1 hr) and again at times 2, 5, 8 and 11 hrs, mice were administered either intraperitoneal vehicle (solid black bars) or 60 mg/kg intraperitoneal lapatinib (diagonally striped bars). All bars represent mean concentrations and error bars represent standard deviations (n = 3). Asterisks represent statistically significance differences ($p < 0.05$).

Supplementary Figure Legend:

Supplementary Figure 1: Docking geometry of P glycoprotein (PGP) and ligands. Docking geometry of PGP and (A) lapatinib, (B) irinotecan, (C) SN-38, (D) topotecan, (E) docetaxel and (F) doxorubicin. PGP cartoon rendering is grey. Ligands are represented as colored spheres. Atoms are carbon (green), hydrogen (grey), oxygen [50], nitrogen (blue), chlorine [20], fluorine (aqua) and sulfur (yellow).

Supplementary Figure 2: Docking geometry of P glycoprotein (PGP) interacting side chains and ligands. (A) lapatinib, (B) irinotecan, (C) SN-38, (D) topotecan, (E) docetaxel and (F) doxorubicin. PGP interacting side chains are rendering in a color ramp that goes from blue (at the N-terminus) to green to yellow (at the C-terminus). Ligands are represented as red spheres.

Table 1. Clinical, Pharmacokinetic and PGP Evaluation of Drugs Administered in Combination with Lapatinib in Phase I Clinical Trials

Clinical Trial	Drug	Number of Patients	Lapatinib Dose (mg/day)	Increased Toxicity	PK Parameter	Statistically Significant % Change[a]	PGP Substrate[b]	Docking Energy (kcal/mol)[c]	Ref
lapatinib + FOLFIRI	irinotecan	12	1250	Yes	AUC_{∞}, CL, V_{ss}	None	yes	-12.0	24
lapatinib + FOLFIRI	SN-38	12	1250	Yes	$AUC_{0\text{-}24hr}$	+44.9%	yes	-10.0	24
lapatinib + FOLFIRI	SN-38	12	1250	Yes	C_{max}	+27.0%	yes	-10.0	24
lapatinib + topotecan	topotecan	9	1250	Yes	$AUC_{0\text{-}24hr}$	+18.1%	yes	-9.4	20
lapatinib + topotecan	topotecan	9	1250	Yes	CL	-15.7%	yes	-9.4	20
lapatinib + topotecan	topotecan	9	1250	Yes	C_{max}, $t_{1/2}$, V_{ss}	None	yes	-9.4	20
lapatinib + docetaxel	docetaxel	8	1250	Yes	AUC_{∞}, CL, V_{ss}	None	yes	-9.2	22
lapatinib + letrozole	letrozole	8	1500	Yes	AUC_{τ}, C_{max}, T_{max}, C_{τ}	None	no	NA	19
lapatinib + capecitabine	capecitabine	19	1250	Yes	AUC_{τ}, C_{max}, T_{max}	None	no	NA	25
lapatinib + FOLFOX4	unbound platinum	17	1500	Yes	AUC, C_{max}, T_{max}, $t_{1/2}$, CL, V_{ss}	None	no	NA	26
lapatinib + FOLFIRI	5-fluorouracil	12	1250	Yes	C_{ss}	None	no	NA	24
lapatinib + capecitabine	5-fluorouracil	19	1250	Yes	AUC, T_{max}	None	no	NA	25
lapatinib + capecitabine	5-fluorouracil	19	1250	Yes	C_{max}	-20.6%	no	NA	25
lapatinib + FOLFOX4	5-fluorouracil	17	1500	Yes	C_{ave}, CL	None	no	NA	26
lapatinib + carboplatin	carboplatin	10	750	Yes	AUC	None	no	NA	21
lapatinib + capecitabine	α-fluoro-β-alanine	19	1250	Yes	AUC, C_{max}, T_{max}	None	no	NA	25
lapatinib + trastuzumab	trastuzumab	27	1000	Yes	$AUC_{0\text{-}24hr}$, C_{max}	None	NA[d]	NA[d]	23

Abbreviations: FOLFIRI, 5-fluorouracil, leucovorin and irinotecan; FOLFOX4, oxaliplatin, leucovorin and 5-fluorouracil; AUC, area under the concentration-time curve; $AUC_{0\text{-}24hr}$, area under the concentration-time curve from 0 to 24 hrs; AUC_{∞}, area under the concentration-time curve from 0 to infinity; AUC_{τ}, area under the concentration-time curve within a steady-state dosing interval; C_{max}, maximum concentration; C_{τ}, concentration at the end of a dosing interval; CL, clearance; C_{ss}, concentration at steady-state; C_{ave}, time-averaged concentration at steady-state; T_{max}, time of maximum concentration; $t_{1/2}$, half-life; V_{ss}, volume of distribution at steady-state; NA, not applicable.

[a]Percent (%) change was calculated as $100 \times \left(\left(Combination\,AUC \right) - \left(Single\,Agent\,AUC \right) \Big/ Single\,Agent\,AUC \right)$.

[b]PGP substrate determination of the ligand in column 2 was calculated with the support vector machine (SVM) method at http://pgp.althotas.com (21991360).

[c]Docking energy of ligand in column 2 with human PGP was calculated at http://pgp.althotas.com (21991360).

[d]Althotas (21991360) did not have information available regarding trastuzumab.

Table 2. Comparison of AUCs from Combination Lapatinib and Docetaxel Pharmacokinetic Studies in Mice

Sample	Single Dose Vehicle + Docetaxel $AUC_{0\text{-}12hr}$	Single Dose Lapatinib + Docetaxel $AUC_{0\text{-}12hr}$	% Change[e]	Multiple Dose Vehicle + Docetaxel $AUC_{4\text{-}12hr}$	Multiple Dose Lapatinib + Docetaxel $AUC_{4\text{-}12hr}$	% Change[c]
Lung[a]	15085	15442	+2.4%	9211	9987	+8.4%
Kidney[a]	12303	12974	+5.5%	5930	6964	+17.4%
Heart[a]	9989	9481	-5.1%	5601	5548	-0.9%
Muscle[a]	5283	4878	-7.7%	3084	3546	+15.0%
Intestine[a]	3511	4664	+32.8%	1957	2830	+44.6%
Liver[a]	3096	3471	+12.1%	1517	1668	+10.0%
Adipose[a]	1911	2587	+35.4%	1351	1691	+25.2%
Plasma[b]	378.6	423.2	+11.8%	179.5	185.3	+3.2%
Brain[a]	167.9	162	-3.5%	91.45	88.01	-3.8%

Abbreviations: $AUC_{0\text{-}12hr}$, area under the concentration-time curve from 0 to 12 hrs; $AUC_{4\text{-}12hr}$, area under the concentration-time curve from 4 to 12 hrs.
[a]Tissue AUC values are ng/g × hr.
[b]Plasma AUC values are ng/mL × hr.
[c]Percent (%) change was calculated as $100 \times \left(\left(Lapatinib + Docetaxel\ AUC \right) - \left(Vehicle + Docetaxel\ AUC \right) \Big/ Vehicle + Docetaxel\ AUC \right)$.

Table 3. Comparison of AUCs from Combination Lapatinib and Doxorubicin Pharmacokinetic Studies in Mice

Sample	Single Dose Vehicle + Doxorubicin $AUC_{0\text{-}48hr}$	Single Dose Lapatinib + Doxorubicin $AUC_{0\text{-}48hr}$	% Change[a]	Multiple Dose Vehicle + Doxorubicin $AUC_{4\text{-}48hr}$	Multiple Dose Lapatinib + Doxorubicin $AUC_{4\text{-}48hr}$	% Change[a]
Kidney[b]	238066	225903	-5.1%	194490	204623	+5.2%
Lung[b]	222640	211633	-4.9%	169515	175490	+3.5%
Liver[b]	126709	130778	+3.2%	78636	87168	+10.8%
Heart[b]	74829	71633	-4.3%	52493	52137	-0.7%
Intestine[b]	68936	62982	-8.6%	50136	58130	+15.9%
Adipose[b]	21058	17796	-15.5%	15555	11506	-26.0%
Plasma[c]	490.4	543.9	+10.9%	343.3	369.0	+7.5%

Abbreviations: $AUC_{0\text{-}48hr}$, area under the concentration-time curve from 0 to 48 hrs; $AUC_{4\text{-}48hr}$, area under the concentration-time curve from 4 to 48 hrs.

[a]Percent (%) change was calculated as $100 \times \left(\left(Lapatinib + Doxorubicin\,AUC \right) - \left(Vehicle + Doxorubicin\,AUC \right) \Big/ Vehicle + Doxorubicin\,AUC \right)$.

[b]Tissue AUC values are ng/g▪hr.

[c]Plasma AUC values are ng/mL▪hr.

Figure 1

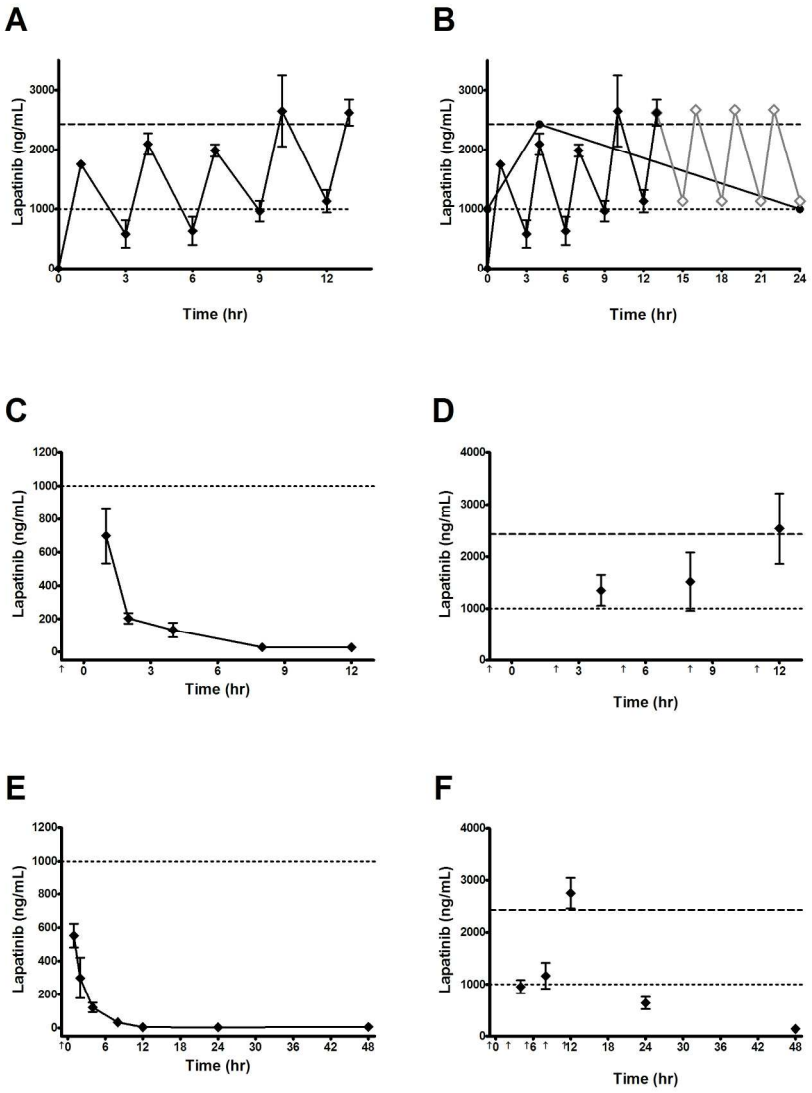

186x258mm (300 x 300 DPI)

Figure 2

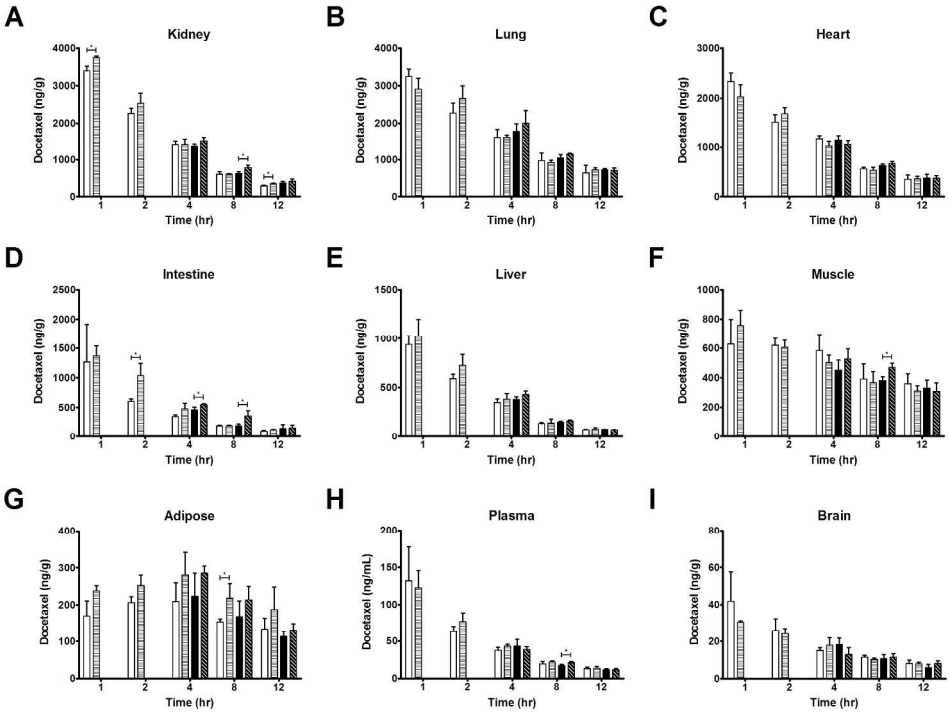

255x199mm (300 x 300 DPI)

Figure 3

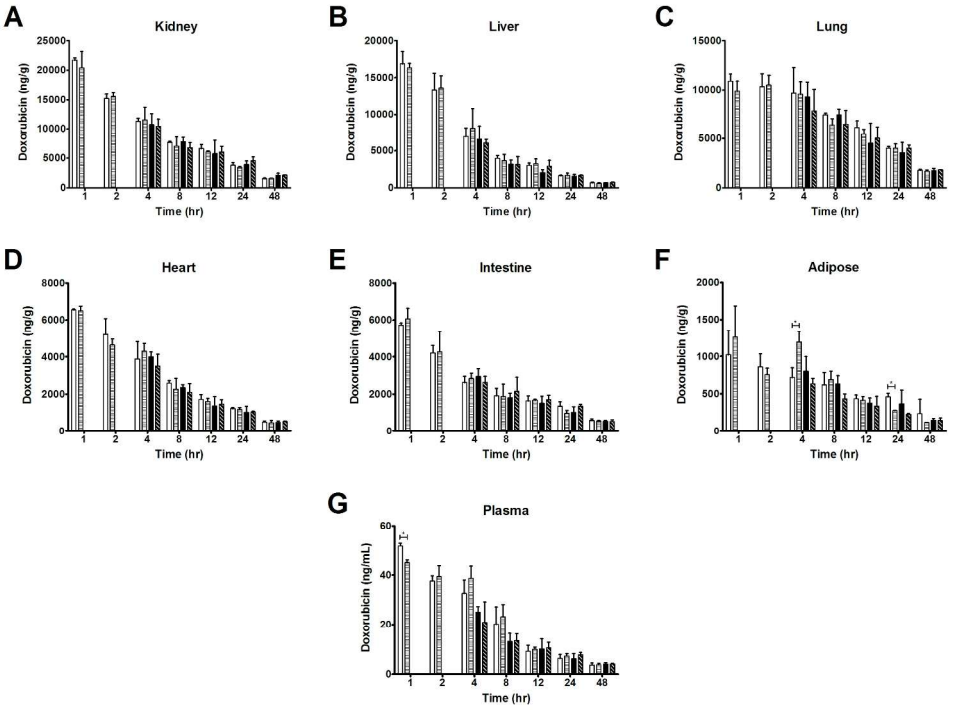

252x198mm (300 x 300 DPI)

Supplementary Table 1. Comparison of Half-lives from Combination Lapatinib and Docetaxel Pharmacokinetic Studies in Mice

Sample	Single Dose Vehicle + Docetaxel $t_{1/2}$	Single Dose Lapatinib + Docetaxel $t_{1/2}$	% Change[a]	Multiple Dose Vehicle + Docetaxel $t_{1/2}$	Multiple Dose Lapatinib + Docetaxel $t_{1/2}$	% Change[a]
Adipose	12.6 (7.0-66.0)	13.8 (6.5-∞)	+9.5%	8.2 (5.1-20.8)	7.2 (5.4-10.8)	-12.2%
Muscle	11.4 (6.2-70.0)	11.5 (7.4-26.1)	+0.9%	18.1 (10.2-81.6)	10.4 (6.8-22.0)	-42.5%
Brain	8.8 (6.1-16.2)	6.8 (4.9-11.0)	-22.7%	5 (3.7-7.7)	12.2 (6.5-94.7)	+144.0%
Lung	6.0 (4.1-10.8)	6.9 (5.5-9.1)	+15.0%	6.1 (5.1-7.5)	5.3 (4.4-6.6)	-13.1%
Plasma	5.2 (4.1-7.3)	4.9 (4.1-6.0)	-5.8%	4.3 (3.3-6.0)	4.6 (3.9-5.5)	+7.0%
Heart	4.5 (3.6-6.0)	5.3 (4.3-6.8)	+17.8%	4.9 (4.1-6.1)	6.1 (4.1-11.7)	+24.5%
Intestine	4.4 (3.8-5.3)	4.0 (3.3-5.2)	-9.1%	4.8 (3.2-9.9)	4.4 (3.2-6.9)	-8.3%
Liver	3.5 (3.1-4.2)	3.5 (2.8-4.9)	0.0%	3.4 (3.1-3.7)	3.1 (2.9-3.4)	-8.8%
Kidney	3.5 (3.2-3.9)	4.0 (3.4-4.7)	+14.3%	4.3 (3.7-5.0)	4.3 (3.8-5.1)	0.0%

Abbreviations: $t_{1/2}$, terminal half-life (95% confidence interval) in hr.

[a]Percent (%) change was calculated as $100 \times \left(\left(Lapatinib + Docetaxel\, t_{1/2} \right) - \left(Vehicle + Docetaxel\, t_{1/2} \right) \Big/ Vehicle + Docetaxel\, t_{1/2} \right)$.

Supplementary Table 2. Comparison of Maximum Concentrations from Combination Lapatinib and Docetaxel Pharmacokinetic Studies in Mice

Sample	Single Dose Vehicle + Docetaxel C_{max}	Single Dose Lapatinib + Docetaxel C_{max}	% Change[a]	Multiple Dose Vehicle + Docetaxel C_{max}[e]	Multiple Dose Lapatinib + Docetaxel C_{max}[e]	% Change[a]
Kidney[b]	3396.7 (130.1)[d]	3756.7 (35.1)[d]	+10.6%	1350.0 (60.8)	1500.0 (121.2)	+11.1%
Lung[b]	3250.0 (194.7)[d]	2913.3 (284.3)[d]	-10.4%	1786.7 (200.1)	2000.0 (340.4)	+11.9%
Heart[b]	2336.7 (172.1)[d]	2033.3 (240.1)[d]	-13.0%	1163.3 (86.2)	1053.3 (76.4)	-9.5%
Intestine[b]	1268.7 (647.7)[d]	1366.7 (171.6)[d]	+7.7%	458.3 (47.5)	547.3 (18.6)	+19.4%
Liver[b]	938.0 (94.6)[d]	1025.3 (171.4)[d]	+9.3%	381.7 (25.8)	431.0 (35.5)	+12.9%
Muscle[b]	628.3 (170.7)[d]	759.3 (102.0)[d]	+20.8%	450.0 (68.4)	526.3 (69.3)	+17.0%
Adipose[b]	209.3 (50.5)[e]	280.3 (61.1)[e]	+33.9%	223.3 (62.1)	285.7 (19.2)	-27.9%
Plasma[c]	132.0 (45.5)[d]	122.3 (23.1)[d]	-7.3%	43.2 (9.1)	38.7 (3.9)	-10.4%
Brain[b]	42.0 (15.5)[d]	30.7 (0.8)[d]	-26.9%	18.2 (3.5)	12.9 (3.7)	-29.1%

Abberviations: C_{max}, maximum concentration (standard deviation).

[a]Percent (%) change was calculated as $100 \times \left(\left(Lapatinib + Docetaxel C_{\max} \right) - \left(Vehicle + Docetaxel C_{\max} \right) \Big/ Vehicle + Docetaxel C_{\max} \right)$.

[b]Tissue C_{max} values are ng/g.
[c]Plasma C_{max} values are ng/mL.
[d]C_{max} was at 1 hr.
[e]C_{max} was at 4 hr.

Supplementary Table 3. Comparison of Half-lives from Combination Lapatinib and Doxorubicin Pharmacokinetic Studies in Mice

Sample	Single Dose Vehicle + Doxorubicin $t_{1/2}$	Single Dose Lapatinib + Doxorubicin $t_{1/2}$	% Change[a]	Multiple Dose Vehicle + Doxorubicin $t_{1/2}$	Multiple Dose Lapatinib + Doxorubicin $t_{1/2}$	% Change[a]
Adipose	37.0 (16.6-∞)	19.9 (18.2-22.0)	-46.2%	23.4 (13.4-94.0)	30.1 (18.8-75.4)	+28.6%
Plasma	27.3 (18.4-52.5)	25.3 (20.4-33.1)	-7.3%	29.3 (17.1-102)	26.2 (20.6-36.0)	-10.6%
Intestine	23.6 (17.9-34.4)	23.0 (19.0-29.3)	-2.5	24.9 (17.3-44.6)	21.0 (17.2-27.1)	-15.7%
Heart	20.1 (17.1-24.2)	19.9 (16.0-26.6)	-1.0%	23.6 (15.5-49.2)	24.8 (20.9-30.4)	+5.1%
Lung	20.0 (18.1-22.4)	20.7 (18.0-24.3)	+3.5%	25.3 (16.1-59.5)	24.0 (19.0-32.3)	-5.1%
Kidney	17.4 (15.4-20.0)	19.2 (17.4-21.4)	+10.3%	25.3 (17.4-46.4)	24.0 (19.7-30.6)	-5.1%
Liver	16.9 (14.8-19.8)	15.1 (12.6-18.9)	-10.7%	21.8 (17.3-29.4)	18.5 (15.1-24.0)	-15.1%

Abbreviations: $t_{1/2}$, terminal half-life (95% confidence interval) in hr.

[a]Percent (%) change was calculated as $100 \times \left(\left(Lapatinib + Doxorubicin t_{1/2} \right) - \left(Vehicle + Doxorubicin t_{1/2} \right) \Big/ Vehicle + Doxorubicin t_{1/2} \right)$.

Supplementary Table 4. Comparison of Maximum Concentrations from Combination Lapatinib and Doxorubicin Pharmacokinetic Studies in Mice

Sample	Single Dose Vehicle + Doxorubicin C_{max}	Single Dose Lapatinib + Doxorubicin C_{max}	% Change[a]	Multiple Dose Vehicle + Doxorubicin C_{max}[e]	Multiple Dose Lapatinib + Doxorubicin C_{max}[e]	% Change[a]
Kidney[b]	21710.1 (385.9)[d]	20422.4 (2733.6)[d]	-5.9%	10749.4 (1891.6)	10486.4 (1217.8)	-2.4%
Liver[b]	16855.7 (1658.0)[d]	16343.8 (582.4)[d]	-3.0%	6553.3 (1862.7)	6045.4 (513.0)	-7.8%
Lung[b]	10893.6 (703.2)[d]	9871.9 (1006.4)[d]	-9.4%	9316.9 (1483.6)	7856.1 (2192.4)	-15.7%
Heart[b]	6546.8 (48.5)[d]	6490.2 (260.6)[d]	-0.9%	3995.0 (263.5)	3495.2 (641.3)	-12.5%
Intestine[b]	5726.7 (106.1)[d]	6072.6 (562.8)[d]	+6.0%	2944.0 (416.3)	2629.5 (320.3)	-10.7%
Adipose[b]	1021.4 (326.1)[e]	1259.0 (427.0)[e]	+23.3%	802.0 (194.6)	635.4 (69.8)	-20.8%
Plasma[c]	51.7 (1.1)[d]	45.0 (1.1)[d]	-13.0%	25.1 (2.3)	20.8 (8.3)	-17.1%

Abberviations: C_{max}, maximum concentration (standard deviation).

[a]Percent (%) change was calculated as $100 \times \left(\left(Lapatinib + Docetaxel C_{\max} \right) - \left(Vehicle + Docetaxel C_{\max} \right) \Big/ Vehicle + Docetaxel C_{\max} \right)$.

[b]Tissue C_{max} values are ng/g.
[c]Plasma C_{max} values are ng/mL.
[d]C_{max} was at 1 hr.
[e]C_{max} was at 4 hr.

Supplementary Figure 1

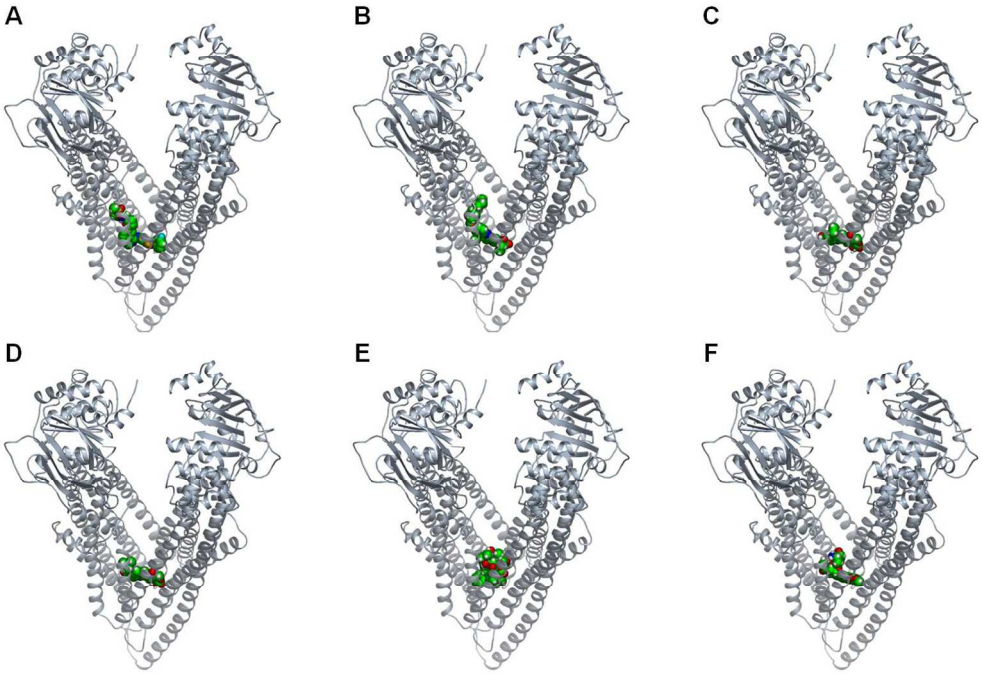

255x188mm (150 x 150 DPI)

Supplementary Figure 2

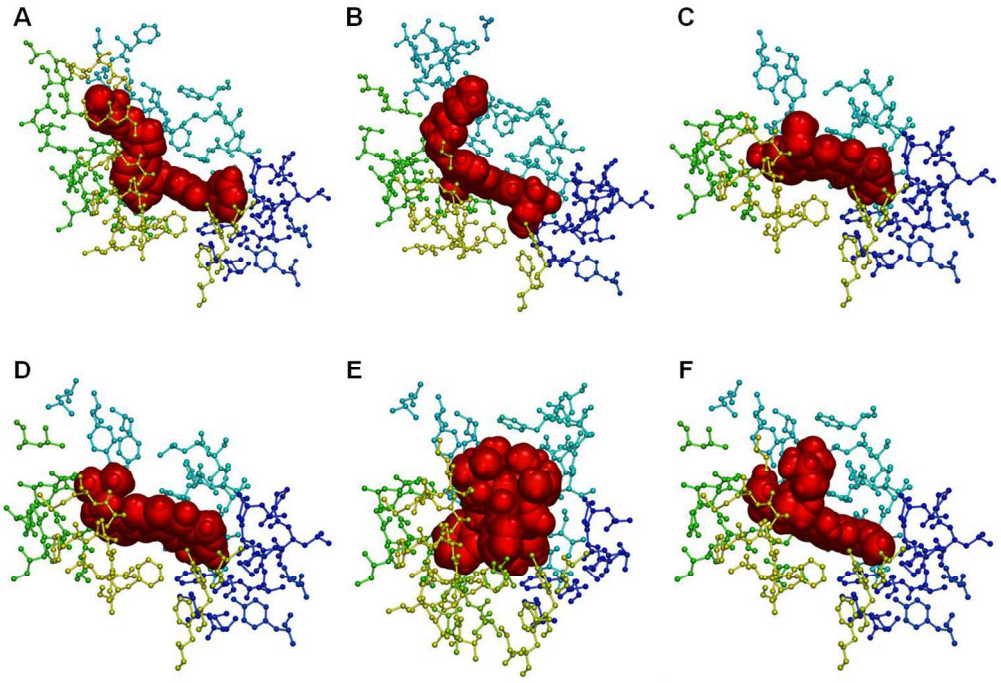

248x182mm (150 x 150 DPI)

Title	Recruitment	Study Results	PGP Substrate	Drug		Docking Energy	Interventions
Safety Study of AMG 386 to Treat HER2-positive Locally Recurrent or Metastatic Breast Cance	Recruiting	No Results Available	NO				Drug: AMG 386|Drug: Capecitabine|Drug: Lapatinib|Drug: Paclitaxel|Drug: Trastuzumab
Capecitabine (Xeloda) and Lapatinib (Tykerb) as First-line Therapy in HER2/Neu-positive Breast Cance	Active, not recruiting	No Results Available	NO				Drug: Capecitabine|Drug: Lapatinib
Continued HER2 Suppression With Lapatinib Plus Trastuzumab Versus Trastuzumab Alone	Recruiting	No Results Available	NO				Drug: Lapatinib|Biological: Trastuzumab
A Phase Ib/II Study of BEZ235 and Trastuzumab in Patients With HER2-positive Breast Cancer Who Failed Prior to Trastuzumab	Recruiting	No Results Available	NO				Drug: BEZ235|Drug: Trastuzumab|Drug: Lapatinib|Drug: Capecitabine
GW572016 Combined With Trastuzumab For The Treatment Of Previously Trastuzumab-Treated Breast Cancer	Completed	No Results Available	NO				Drug: Lapatinib
Lapatinib in Combination With Trastuzumab in Patients With HER2-Positive, Metastatic Breast Cancer	Recruiting	No Results Available	NO				Drug: Lapatinib|Drug: Herceptin
Lapatinib in Combination With Capecitabine in Japanese Patients With Metastatic Breast Cancer	Completed	Has Results	NO				Drug: Lapatinib|Drug: Capecitabine
ELBA: Exemestane and Lapatinib in Advanced Breast Cancer	Withdrawn	No Results Available	NO				Drug: Exemestane|Drug: Lapatinib
Lapatinib Plus Capecitabine Versus Trastuzumab Plus Capecitabine in ErbB2 (HER2) Positive Metastatic Breast Cancer	Recruiting	No Results Available	NO				Drug: Capecitabine|Drug: Lapatinib|Drug: Trastuzumab
Capecitabine and Lapatinib With or Without Cixutumumab in Treating Patients With Previously Treated HER2-Positive Stage IIIB, Stage IIIC, or Stage IV Breast Cancer	Active, not recruiting	No Results Available	NO				Drug: Cixutumumab|Drug: Capecitabine|Drug: Lapatinib ditosylate
Vorinostat and Lapatinib in Advanced Solid Tumors and Advanced Breast Cancer to Evaluate Response and Biomarkers	Recruiting	No Results Available	NO				Drug: Vorinostat|Drug: Lapatinib
Letrozole In Combination With Lapatinib In Neoadjuvant Treatment Of Early Breast Cancer	Recruiting	No Results Available	NO				Drug: Lapatinib|Drug: Letrozole
PhII Neo-Adjuvant Letrozole & Lapatinib in Pts w/HER2+ & Hormone Receptor+ Operable Breast CA SPORE	Terminated	Has Results	NO				Drug: Lapatinib ditosylate|Drug: Letrozole
Capecitabine (XELODA) With Or Without Lapatinib (GW572016) For Women With Refractory Advanced or Metastatic Breast Cancer	Completed	No Results Available	NO				Drug: Capecitabine|Drug: Lapatinib
Lapatinib Ditosylate and Capecitabine in Treating Patients With Stage IV Breast Cancer and Brain Metastases	Recruiting	No Results Available	NO				Drug: Capecitabine|Drug: Lapatinib ditosylate
Novel Capecitabine Dosing Schedule in Combination With Lapatinib, Based on the Norton-Simon Mathematical Method in Patients With HER2 Overexpressed/Amplified, Trastuzumab (Herceptin) -Refractory, Metastatic Breast Cance	Active, not recruiting	No Results Available	NO				Drug: Capecitabine|Drug: Lapatinib
Lapatinib and Temozolomide for the Treatment of Progressive Brain Disease in HER-2 Positive Breast Cance	Active, not recruiting	No Results Available	NO				Drug: Lapatinib|Drug: Temozolomide
Neoadjuvant Combined Endocrine and HER2 Target Therapy in Postmenopausal Women With ER and Her2 Positive Breast Cancer	Recruiting	No Results Available	NO				Drug: Letrozole|Drug: Lapatinib
Evaluating Lapatinib + Capecitabine in Patients Aged 70 and Over With HER2 Metastatic Breast Cancer	Active, not recruiting	No Results Available	NO				Drug: Lapatinib|Drug: Capecitabine
An Open-Label Study of Trastuzumab Emtansine (T-DM1) vs Capecitabine+Lapatinib in Patients With HER2-Positive Locally Advanced or Metastatic Breast Cancer (EMILIA	Recruiting	No Results Available	NO				Drug: Trastuzumab|Drug: Emtansine|Drug: Lapatinib|Drug: Capecitabine
Tolerability of the Combination of Lapatinib and Trastuzumab in Adults Age 60 or Older With HER2 Positive Metastatic Breast Cancer	Recruiting	No Results Available	NO				Drug: Lapatinib|Drug: Trastuzumab
Lapatinib and Trastuzumab With or Without Endocrine Therapy	Active, not recruiting	Has Results	NO				Drug: Lapatinib|Drug: Trastuzumab|Drug: Endocrine
ALTTO (Adjuvant Lapatinib And/Or Trastuzumab Treatment Optimisation) Study: BIG 2-06/N063D	Active, not recruiting	No Results Available	NO				Drug: Lapatinib|Drug: Trastuzumab
Extension Study of Lapatinib Plus Herceptin With or Without Endocrine Therapy	Recruiting	No Results Available	NO				Drug: Herceptin|Drug: Lapatinib|Drug: Letrozole
Lapatinib With Trastuzumab in Treating Patients With HER2-Negative/HER2 Mutant Metastatic Breast Cancer	Not yet recruiting	No Results Available	NO				Drug: Lapatinib ditosylate|Drug: Trastuzumab
GW572016 and Trastuzumab in Treating Patients With Metastatic Breast Cancer That Overexpresses HER2/Neu	Completed	No Results Available	NO				Drug: Trastuzumab|Drug: Lapatinib ditosylate
Modulation of Response to Hormonal Therapy With Lapatinib and/or Metformin in Patients With Metastatic Breast Cancer	Recruiting	No Results Available	NO				Drug: Lapatinib|Drug: Metformin
Role of Early Versus Late Switch to Lapatinib-Capecitabine (TYCO	Recruiting	No Results Available	NO				Drug: Lapatinib|Drug: Capecitabine
Lapatinib +Capecitabine Treatment for Advanced Metastatic Breast Cancer in Women From China	Active, not recruiting	Has Results	NO				Drug: Lapatinib|Drug: Capecitabine
Study Comparing GW572016 And Letrozole Versus Letrozole In Subjects With Advanced Or Metastatic Breast Cancer	Active, not recruiting	Has Results	NO				Drug: Lapatinib|Drug: Letrozole
EAP (Expanded Access Protocol) Of Lapatinib Combined With Capecitabine In Metastatic Breast Cancer	Recruiting	No Results Available	NO				Drug: Lapatinib|Drug: Capecitabine
Lapatinib and Bevacizumab for Metastatic Breast Cancer	Active, not recruiting	Has Results	NO				Drug: Lapatinib|Drug: Bevacizumab
Study to Assess dHER2+AS15 Cancer Vaccine Given in Combination With Lapatinib to Patients With Metastatic Breast Cancer	Active, not recruiting	No Results Available	NO				Drug: dHER2 + AS15 ASCI|Drug: Lapatinib
Lapatinib In Combination With Trastuzumab Versus Lapatinib Monotherapy In Subjects With HER2-positive Metastatic Breast Cancer	Completed	Has Results	NO				Drug: Lapatinib|Drug: Trastuzumab
A Study to Compare the Safety and Efficacy of an Aromatase Inhibitor in Combination With Lapatinib, Trastuzumab or Both for the Treatment of Hormone Receptor Positive, HER2+ Metastatic Breast Cance	Recruiting	No Results Available	NO				Drug: Lapatinib|Drug: Trastuzumab|Drug: Aromatase inhibitor|Drug: lapatinib
Efficacy and Tolerability of Eribulin Plus Lapatinib in Patients With Metastatic Breast Cancer (E-VITA	Recruiting	No Results Available	YES	eribulin	-12.4		Drug: Lapatinib|Drug: Eribulin
Study To Examine The Effects Of Lapatinib On The Pharmacokinetics Of Digoxin In Subjects w/ ErbB2 Positive Breast Cancer	Completed	No Results Available	YES	digoxin	-11.5		Drug: Lapatinib|Drug: Digoxin
Study of Foretinib in Combination With Lapatinib in Patients With Metastatic Breast Cancer	Recruiting	No Results Available	YES	foretinib	-11.4		Drug: Foretinib|Drug: Lapatinib
Pazopanib Plus Lapatinib Compared To Lapatinib Alone In Subjects With Inflammatory Breast Cancer	Completed	Has Results	YES	pazopanib	-10.9		Drug: Lapatinib|Drug: Pazopanib
Pazopanib Plus Lapatinib Compared To Lapatinib Alone In Subjects With Advanced Or Metastatic Breast Cancer	Active, not recruiting	Has Results	YES	pazopanib	-10.9		Drug: Pazopanib|Drug: Lapatinib
Lapatinib Ditosylate and MK2206 in Treating Women With Metastatic Breast Cancer	Recruiting	No Results Available	YES	MK2206	-10.7		Drug: MK2206|Drug: Lapatinib ditosylate
MK2206 in Combination With Lapatinib Ditosylate in Patients With Advanced or Metastatic Solid Tumors or Breast Cancer	Not yet recruiting	No Results Available	YES	MK2206	-10.7		Drug: MK2206|Drug: Lapatinib ditosylate
A Study of MK2206 in Combination With Trastuzumab and Lapatinib for the Treatment of HER2+ Solid Tumors (2206-015)	Completed	No Results Available	YES	MK2206	-10.7		Drug: MK2206|Drug: Trastuzumab|Drug: Lapatinib
LBH589 in Combination With Capecitabine Plus/Minus (As) Lapatinib in Breast Cancer Patients	Active, not recruiting	No Results Available	YES	LBH589	-10.5		Drug: LBH589|Drug: Capecitabine|Drug: Lapatinib
Entinostat and Lapatinib Ditosylate in Patients With Locally Recurrent or Distant Relapsed Metastatic Breast Cancer Previously Treated With Trastuzumab	Recruiting	No Results Available	YES	entinostat	-10		Drug: Entinostat|Drug: Lapatinib ditosylate
Lapatinib and Tamoxifen in Treating Patients With Advanced or Metastatic Breast Cancer	Active, not recruiting	No Results Available	YES	tamoxifen	-9.7		Drug: Lapatinib ditosylate|Drug: Tamoxifen citrate
Lapatinib and Tamoxifen in Treating Patients With Locally Advanced or Metastatic Breast Cancer That Did Not Respond to Previous Tamoxifen	Active, not recruiting	No Results Available	YES	tamoxifen	-9.7		Drug: Lapatinib ditosylate|Drug: Tamoxifen citrate
AUY922 With Lapatinib and Letrozole for ER+ HER2+ Advanced Breast Cancer	Recruiting	No Results Available	YES	AUY922	-9.7		Drug: AUY922|Drug: Lapatinib|Drug: Letrozole
Lapatinib and Vinorelbine in Treating Women With HER2-Overexpressing Locally Advanced or Metastatic Breast Cancer	Recruiting	No Results Available	YES	vinorelbine	-9.6		Drug: Lapatinib ditosylate|Drug: Vinorelbine tartrate
A Study Evaluating the Efficacy and Safety of Lapatinib + Vinorelbine in ErbB2 Positive Metastatic Breast Cancer Patients	Recruiting	No Results Available	YES	vinorelbine	-9.6		Drug: Lapatinib|Drug: Vinorelbine
Vinorelbine Metronomic Plus Lapatinib for Overexpressing HER-2 Metastatic Breast Cance	Withdrawn	No Results Available	YES	vinorelbine	-9.6		Drug: Vinorelbine|Drug: Lapatinib
Lapatinib in Combination With Oral Vinorelbine for Metastatic Breast Cancer	Recruiting	No Results Available	YES	vinorelbine	-9.6		Drug: Lapatinib|Drug: Vinorelbine
Lapatinib + Vinorelbine in ErbB2 Overexpressing, First or Second Line Metastatic Breast Cancer Subjects	Active, not recruiting	No Results Available	YES	vinorelbine	-9.6		Drug: Lapatinib|Drug: Vinorelbine
Safety Study in Subjects With Metastatic Breast Cancer Who Progressed After Taxanes Treatment	Recruiting	No Results Available	YES	vinorelbine	-9.6		Drug: Lapatinib|Drug: Vinorelbine|Drug: Capecitabine|Drug: Gemcitabine
Lapatinib in Combination With Vinorelbine	Active, not recruiting	No Results Available	YES	vinorelbine	-9.6		Drug: Lapatinib|Drug: Vinorelbine
Dose Finding Study for Combination of Capecitabine, Lapatinib and Vinorelbine in Metastatic Breast Cancer	Recruiting	No Results Available	YES	vinorelbine	-9.6		Drug: Lapatinib|Drug: Capecitabine|Drug: Vinorelbine
Lapatinib in Combination With Vinorelbine	Active, not recruiting	No Results Available	YES	vinorelbine	-9.6		Drug: Vinorelbine|Drug: Lapatinib|Drug: Capecitabine
Safety and Efficacy of BKM120 and Lapatinib in HER2+/PI3K-activated, Trastuzumab-resistant Advanced Breast Cancer	Recruiting	No Results Available	YES	BKM120	-9.5		Drug: BKM120|Drug: Lapatinib
Phase I Study of Ixabepilone Plus Lapatinib With or Without Capecitabine in the Treatment of Human Epidermal Growth Factor Receptor 2 (HER2)-Positive Breast Cancer	Terminated	Has Results	YES	ixabepilone	-9.4		Drug: Ixabepilone|Drug: Lapatinib|Drug: Capecitabine
Brain Metastases In ErbB2-Positive Breast Cancer	Terminated	No Results Available	YES	topotecan	-9.4		Drug: Lapatinib|Drug: Capecitabine|Drug: Topotecan
APRICOT-B: Study to Evaluate Apricoxib in Combination With Lapatinib and Capecitabine in the Treatment of HER2/Neu+ Breast Cancer (TP2001-202)	Terminated	No Results Available	YES	apricoxib	-9.2		Drug: Apricoxib|Drug: Lapatinib|Drug: Capecitabine
Fulvestrant With or Without Lapatinib and/or Aromatase Inhibitor Therapy in Treating Postmenopausal Women With Metastatic Breast Cancer That Progressed After Previous Aromatase Inhibitor Therapy	Recruiting	No Results Available	YES	fulvestrant	-9.2		Drug: Anastrozole|Drug: Exemestane|Drug: Fulvestrant|Drug: Lapatinib ditosylate|Drug: Letrozole
Fulvestrant With or Without Lapatinib in Treating Postmenopausal Women With Stage III or Stage IV Breast Cancer That is Hormone Receptor-Positive	Active, not recruiting	No Results Available	YES	fulvestrant	-9.2		Drug: Lapatinib ditosylate|Drug: Fulvestrant
A Study of Lapatinib in Combination With Everolimus in Patients With Advanced, Triple Negative Breast Cancer	Recruiting	No Results Available	YES	everolimus	-9.1		Drug: Lapatinib|Drug: Everolimus
Study of How Well Letrozole Works in Combination With Lapatinib Followed by an Addition of Everolimus in Postmenopausal Women With Advanced Endocrine Resistant Breast Cancer	Recruiting	No Results Available	YES	everolimus	-9.1		Drug: Letrozole|Drug: Lapatinib|Drug: Everolimus
Lapatinib and RAD-001 for HER2 Positive Metastatic Breast Cancer	Recruiting	No Results Available	YES	RAD-001	-9.1		Drug: Lapatinib|Drug: RAD-001
Study Evaluating Neratinib Versus Lapatinib Plus Capecitabine For ErbB2 Positive Advanced Breast Cancer	Active, not recruiting	No Results Available	YES	neratinib	-9		Drug: Neratinib|Drug: Lapatinib|Drug: Capecitabine
Efficacy and Safety of BMS-690514 in Combination With Letrozole to Treat Metastatic Breast Cancer	Completed	No Results Available	YES	BMS-690514	-8.6		Drug: BMS-690514|Drug: Lapatinib|Drug: Letrozole
A Study to Examine the Effects of Esomeprazole on the Pharmacokinetics of Orally Administered Lapatinib in Subjects With Metastatic ErbB2 Positive Breast Cancer	Completed	No Results Available	YES	esomeprazole	-7.5		Drug: Lapatinib|Drug: Esomeprazole
Phase II Neoadjuvant in Inflammatory Breast Cancer	Active, not recruiting	No Results Available	YES	TAXANE OR ANTHRACYCLINE			Drug: Lapatinib|Drug: Paclitaxel|Drug: 5-Fluorouracil|Drug: Epirubicin|Drug: Cyclophosphamide
Study Of Lapatinib In Combination With Paclitaxel In The Treatment Of Newly Diagnosed Inflammatory Breast Cancer	Completed	No Results Available	YES	TAXANE OR ANTHRACYCLINE			Drug: Lapatinib|Drug: Paclitaxel
Abraxane and Lapatinib in Treating Patients With Stage I, Stage II, or Stage III Breast Cancer	Active, not recruiting	No Results Available	YES	TAXANE OR ANTHRACYCLINE			Drug: Lapatinib ditosylate|Drug: Paclitaxel
Lapatinib and Epirubicin in Treating Patients With Metastatic Breast Cancer	Active, not recruiting	No Results Available	YES	TAXANE OR ANTHRACYCLINE			Drug: Epirubicin hydrochloride|Drug: Lapatinib ditosylate
Phase I/II Study of Neoadjuvant Lapatinib in Breast Cancer	Recruiting	No Results Available	YES	TAXANE OR ANTHRACYCLINE			Drug: Docetaxel|Drug: Lapatinib|Drug: Trastuzumab
Docetaxel, Carboplatin, and Trastuzumab and/or Lapatinib in Treating Women With Stage I, Stage II, or Stage III Breast Cancer That Can Be Removed by Surgery	Recruiting	No Results Available	YES	TAXANE OR ANTHRACYCLINE			Drug: Trastuzumab|Drug: Carboplatin|Drug: Docetaxel|Drug: Lapatinib ditosylate
Lapatinib in Combination With Docetaxel in Patients With HER-2 Positive Advanced or Metastatic Breast Cancer	Recruiting	No Results Available	YES	TAXANE OR ANTHRACYCLINE			Drug: Lapatinib|Drug: Docetaxel
Lapatinib Combined With Paclitaxel For Patients With First-Line ErbB2-Amplified Metastatic Breast Cancer	Active, not recruiting	No Results Available	YES	TAXANE OR ANTHRACYCLINE			Drug: Lapatinib|Drug: Paclitaxel
Chemotherapy and Lapatinib or Trastuzumab in Treating Women With HER2/Neu-Positive Metastatic Breast Cancer	Active, not recruiting	No Results Available	YES	TAXANE OR ANTHRACYCLINE			Drug: Trastuzumab|Drug: Docetaxel|Drug: Lapatinib ditosylate|Drug: Paclitaxe
A Study of AC Followed by a Combination of Paclitaxel Plus Trastuzumab or Lapatinib or Both Given Before Surgery to Patients With Operable HER2 Positive Invasive Breast Cance	Active, not recruiting	No Results Available	YES	TAXANE OR ANTHRACYCLINE			Drug: Doxorubicin|Drug: Cyclophosphamide|Drug: Paclitaxel|Drug: Trastuzumab|Drug: Lapatinib
Paclitaxel and Trastuzumab With or Without Lapatinib in Treating Patients With Stage II or Stage III Breast Cancer That Can Be Removed by Surgery	Active, not recruiting	No Results Available	YES	TAXANE OR ANTHRACYCLINE			Drug: Trastuzumab|Drug: Lapatinib ditosylate|Drug: Paclitaxel
Paclitaxel With / Without GW572016 (Lapatinib) As First Line Therapy For Women With Advanced Or Metastatic Breast Cancer	Completed	No Results Available	YES	TAXANE OR ANTHRACYCLINE			Drug: Paclitaxel|Drug: Lapatinib
Lapatinib Plus Caelyx in Patients With Advanced Metastatic Breast Cancer Following Failure of Trastuzumab Therapy	Active, not recruiting	No Results Available	YES	TAXANE OR ANTHRACYCLINE			Drug: Doxorubicin hydrochloride|Drug: Lapatinib
A Phase III Trials Program Exploring the Integration of Bevacizumab, Everolimus (RAD001), and Lapatinib Into Current Neoadjuvant Chemotherapy Regimes for Primary Breast Cance	Active, not recruiting	No Results Available	YES	TAXANE OR ANTHRACYCLINE			Drug: Epirubicin|Drug: Cyclophosphamide|Drug: Docetaxel|Drug: Epirubicin|Drug: Bevacizumab|Drug: Paclitaxel|Drug: Everolimus|Drug: Trastuzumat
Lapatinib and Doxorubicin Hydrochloride Liposome in Treating Patients With Metastatic Breast Cancer	Active, not recruiting	No Results Available	YES	TAXANE OR ANTHRACYCLINE			Drug: Lapatinib ditosylate|Drug: Doxil
Docetaxel, Carboplatin, Trastuzumab, and Lapatinib in Treating Patients With Early Stage Breast Cancer	Completed	No Results Available	YES	TAXANE OR ANTHRACYCLINE			Drug: Trastuzumab|Drug: Carboplatin|Drug: Docetaxel|Drug: Lapatinib ditosylate
Study In Women And Men With Metastatic Breast Cancer That Have Overexpression Of ErbB2	Active, not recruiting	Has Results	YES	TAXANE OR ANTHRACYCLINE			Drug: Lapatinib|Drug: Paclitaxel
Lapatinib In Combination With Chemotherapy In Subjects With Relapsed Breast Cancer	Terminated	Has Results	YES	TAXANE OR ANTHRACYCLINE			Drug: Lapatinib|Drug: Capecitabine|Drug: Docetaxel|Drug: nab-Paclitaxe
Doxorubicin and Cyclophosphamide Followed by Paclitaxel, Trastuzumab, and Lapatinib in Treating Patients With HER2/Neu-Overexpressed Breast Cance	Active, not recruiting	No Results Available	YES	TAXANE OR ANTHRACYCLINE			Drug: Trastuzumab|Drug: Cyclophosphamide|Drug: Doxorubicin hydrochloride|Drug: Lapatinib ditosylate|Drug: Paclitaxe
Doxorubicin and Cyclophosphamide Followed By Trastuzumab, Paclitaxel, and Lapatinib in Treating Patients With Early-Stage HER2-Positive Breast Cancer That Has Been Removed By Surger	Completed	No Results Available	YES	TAXANE OR ANTHRACYCLINE			Drug: Trastuzumab|Drug: Cyclophosphamide|Drug: Doxorubicin hydrochloride|Drug: Lapatinib ditosylate|Drug: Paclitaxe
Phase II Neoadjuvant Doxorubicin and Cyclophosphamide -> Docetaxel With Lapatinib in Stage II/III Her2Neu+ Breast Cancer	Completed	No Results Available	YES	TAXANE OR ANTHRACYCLINE			Drug: Lapatinib|Drug: Doxorubicin|Drug: Cyclophosphamide|Drug: Docetaxel|Drug: Pegfilgrastim|Drug: Filgrastim|Drug: Dexamethasone|Drug: Trastuz
A Phase II Neo-adjuvant Study Assessing TCH (Docetaxel, Carboplatin and Trastuzumab), TCL (Docetaxel, Carboplatin and Lapatinib) and the Combination of TCHL (Docetaxel,Carboplatin, Trastuzumab and Lapatinib) in HER-2 Positive Breast Cancer Patient	Recruiting	No Results Available	YES	TAXANE OR ANTHRACYCLINE			Drug: Docetaxel|Drug: Carboplatin|Drug: Trastuzumab|Drug: Lapatinib
ErbB2 Positive Metastatic Breast Cancer	Recruiting	No Results Available	YES	TAXANE OR ANTHRACYCLINE			Drug: Lapatinib|Drug: Lipo-Dox
A Randomized Study of TH Versus THL in First Line Treatment of HER2-positive Metastatic Breast Cance	Recruiting	No Results Available	YES	TAXANE OR ANTHRACYCLINE			Drug: Trastuzumab|Drug: Paclitaxel|Drug: Lapatinib
Study of Preoperative Weekly Paclitaxel and Carboplatin With Lapatinib (TykerbA®) in Patients With ErbB2-Positive Stage I-III Breast Cancer	Recruiting	No Results Available	YES	TAXANE OR ANTHRACYCLINE			Drug: Paclitaxel|Drug: Carboplatin|Drug: Lapatinib
Lapatinib/Carboplatin/Paclitaxel in Previously Treated Ovarian or Breast Cancer Patients	Completed	No Results Available	YES	TAXANE OR ANTHRACYCLINE			Drug: Lapatinib|Drug: Carboplatin|Drug: Paclitaxel
Preoperative Chemotherapy With Paclitaxel, Gemcitabine, and Lapatinib (TykerbA®) (PGT	Completed	No Results Available	YES	TAXANE OR ANTHRACYCLINE			Drug: Paclitaxel|Drug: Gemcitabine|Drug: Lapatinib
Primary Chemotherapy in Patients With HER2-positive Early Breast Cancer	Recruiting	No Results Available	YES	TAXANE OR ANTHRACYCLINE			Drug: Lapatinib
DETECT III - A Multicenter, Phase III Study to Compare Standard Therapy +/- Lapatinib in HER2-ve MBC-Patients With HER2+ve CTCs	Recruiting	No Results Available	YES	TAXANE OR ANTHRACYCLINE			Drug: Docetaxel|Drug: Paclitaxel|Drug: Vinorelbine|Drug: Capecitabine|Drug: Doxorubicin|Drug: Anastrozole|Drug: Letrozole|Drug: Exemestane|Drug:
Trastuzumab Versus Lapatinib as Neoadjuvant Treatment for Her2+ Patients	Active, not recruiting	No Results Available	YES	TAXANE OR ANTHRACYCLINE			Drug: Epirubicin|Drug: Cyclophosphamide|Drug: Taxotere|Drug: Herceptin|Drug: Lapatinib
The Myocet/Lapatinib Study	Recruiting	No Results Available	YES	TAXANE OR ANTHRACYCLINE			Drug: Myocet|Drug: Lapatinib
Lapatinib and Paclitaxel in Treating Patients With Advanced Solid Tumors	Active, not recruiting	No Results Available	YES	TAXANE OR ANTHRACYCLINE			Drug: Lapatinib ditosylate|Drug: Paclitaxel
GW572016 With Docetaxel and Trastuzumab for the Treatment Of Untreated ErbB2 Over-Expressing Metastatic Breast Cancer	Active, not recruiting	No Results Available	YES	TAXANE OR ANTHRACYCLINE			Drug: Lapatinib|Drug: Docetaxel|Drug: Trastuzumab
ErbB2 Over-expressing Metastatic Breast Cancer Study Using Paclitaxel, Trastuzumab, and Lapatinib	Active, not recruiting	No Results Available	YES	TAXANE OR ANTHRACYCLINE			Drug: Lapatinib|Drug: Paclitaxel|Drug: Trastuzumab
Combination Of Lapatinib With Carboplatin, Paclitaxel and Trastuzumab in Metastatic Breast Cancer	Active, not recruiting	No Results Available	YES	TAXANE OR ANTHRACYCLINE			Drug: Lapatinib|Drug: Carboplatin|Drug: Trastuzumab|Drug: Paclitaxel
Lapatinib or Trastuzumab Given Prior to Surgery With Chemotherapy in Patients With Early Breast Cancer	Withdrawn	No Results Available	YES	TAXANE OR ANTHRACYCLINE			Drug: Lapatinib|Drug: Trastuzumab|Drug: Epirubicin|Drug: Cyclophosphamide|Drug: Paclitaxel
A Phase II, Randomized, Open-label Study of Lapatinib Plus Chemotherapy Versus Trastuzumab Plus Chemotherapy in HER2-positive and p95HER2-positive Metastatic Breast Cancer	Not yet recruiting	No Results Available	YES	TAXANE OR ANTHRACYCLINE			Drug: Lapatinib|Drug: Trastuzumab|Drug: Docetaxel|Drug: Paclitaxel|Drug: Vinorelbine
Neoadjuvant Study With Chemotherapy, Lapatinib And Trastuzumab In Breast Cancer	Completed	No Results Available	YES	TAXANE OR ANTHRACYCLINE			Drug: Lapatinib|Drug: Trastuzumab|Drug: Paclitaxel|Drug: Fluorouracil|Drug: Epidoxorubicin|Drug: Cyclophosphamide
Lapatinib +/- Trastuzumab In Addition To Standard Neoadjuvant Breast Cancer Therapy	Active, not recruiting	Has Results	YES	TAXANE OR ANTHRACYCLINE			Drug: Trastuzumab|Drug: Paclitaxel|Drug: FEC75|Drug: Lapatinib
Addition of Carboplatin to Neoadjuvant Therapy for Triple-negative and HER2-positive Early Breast Cance	Recruiting	No Results Available	YES	TAXANE OR ANTHRACYCLINE			Drug: Carboplatin|Drug: Paclitaxel|Drug: Doxorubicin|Drug: Trastuzumab|Drug: Bevacizumab|Drug:
Neo ALTTO (Neoadjuvant Lapatinib and/or Trastuzumab Treatment Optimisation) Study	Active, not recruiting	Has Results	YES	TAXANE OR ANTHRACYCLINE			Drug: Lapatinib|Drug: Trastuzumab|Drug: Paclitaxel
Phase II Lapatinib Plus Nab-Paclitaxel As First And Second Line Therapy In her2+ MBC	Active, not recruiting	Has Results	YES	TAXANE OR ANTHRACYCLINE			Drug: Lapatinib|Drug: nab-Paclitaxel
Phase I/II Study of Lapatinib in Combination With Paclitaxel as 1L Chemotherapy for ErbB2-positive MBC	Active, not recruiting	No Results Available	YES	TAXANE OR ANTHRACYCLINE			Drug: Lapatinib|Drug: Paclitaxel
Continuation Study of Lapatinib Monotherapy or Lapatinib in Combination With Other Anti-cancer Agents	Recruiting	No Results Available	YES	TAXANE OR ANTHRACYCLINE			Drug: Lapatinib|Drug: Paclitaxel|Drug: Letrozole|Drug: Capecitabine|Drug: Oxaliplatin|Drug: Gemcitabine|Drug: Docetaxel|Drug: Trastuzumab|Drug: Le
Pazopanib (VOTRIENT) Plus Paclitaxel (TAXOL), Pazopanib Plus Paclitaxel (TAXOL) Plus Carboplatin (PARAPLATIN), and Pazopanib Plus Paclitaxel (TAXOL) Plus Lapatinib (TYKERB	Completed	No Results Available	YES	TAXANE OR ANTHRACYCLINE			Drug: Pazopanib|Drug: Lapatinib|Drug: Paclitaxel|Drug: Carboplatin